Thomas Schwarzhuber, M.Sc.

Motion Cueing in Nonlinear Vehicle Dynamics Driving Simulation

DOCTORAL THESIS

to achieve the university degree of

Doctor technicae

submitted to

Graz University of Technology

Assessors:

Assoc.Prof. Dipl-Ing. Dr.techn. Arno Eichberger

Institute of Automotive Engineering
Graz University of Technology

Prof. Dr. Bengt Jacobson

Department of Mechanics and Maritime Sciences
Chalmers University of Technology

Graz, April 2022

Acknowledgement

This thesis was compiled during my time as a doctoral student at Graz University of Technology, Institute of Automotive Engineering, and the BMW AG where I have been working in the vehicle performance department of BMW M Motorsport. The following paragraphs are dedicated to the people to whom I would like to express my gratitude.

Sincere thanks go to Assoc.Prof. Dipl.-Ing. Dr.techn. Arno Eichberger who is leading the Vehicle Dynamics research area at TU Graz. Beyond excellent scientific guidance, the combination of technical advice and trust created an ideal academic environment and must therefore be highlighted. During the entire project and particularly in times of social distancing, I could greatly benefit from his network in the scientific community. It gave me the chance to work with Dr.rer.nat. Ioana Koglbauer whom I would like to thank for the invaluable support while designing my experimental studies.

I owe special thanks to Prof. Dr. Bengt Jacobson, leader of the vehicle dynamics group at Chalmers University of Technology, for serving as a second assessor and for his enriching involvement during the final months of the project.

The scientific research on which this work is based could not have been realised without the technical, financial and organisational resources of the BMW AG. My special thanks go to Dr.-Ing. Michael Graf and Dr.techn. Lukas Wörle who both initiated the project, took on the role of scientific supervision within the company and established working conditions of mutual trust and motivation. I am further grateful for the numerous discussions we have had, together with Dr.techn. Julian von Schleinitz, on fundamentals and great visions. I would also like to thank my colleagues at BMW M Motorsport and particularly the vehicle performance group for great interpersonal relations and for actively supporting my work despite a challenging daily business.

The great interest of my friends in this work led to many discussions which at this time have expanded my horizon. This contribution is hard to quantify but at least it was an invaluable boost of motivation on a personal level.

I am especially grateful to my family who have supported me by consistently being a source of new courage and strength. In combination with the freedom and flexibility needed, this was the fundamental basis to start and complete my doctorate. Last but not least, I would like to thank Annabella for contributing as my patient listener, inspiring motivator, relentless editor and, above all, beloved girlfriend.

Munich, April 2022 Thomas Schwarzhuber

AFFIDAVIT

I declare that I have authored this thesis independently, that I have not used other than the declared sources/resources, and that I have explicitly indicated all material which has been quoted either literally or by content from the sources used. The text document uploaded to TUGRAZonline is identical to the present doctoral thesis.

.....	.....
Date	Signature

Abstract

Driver in the loop (DiL) simulation shows high potential to reduce cost whilst increasing track performance in motorsport. An essential part of DiL simulators is the motion system which is controlled by a motion cueing algorithm (MCA). Its objective is to create a realistic motion sensation within the physical limitations of the system. Various performance indicators aiming to evaluate motion fidelity are established for road car applications and form the basis of optimal motion cueing. These techniques are not applicable to near-limit vehicle handling, because the varying importance of individual cues is disregarded. Hence, a lack of knowledge arises about which cues are most relevant and how to provide them with an MCA.

This work aims towards closing that gap by, as a first step, proposing two novel methods for MCA evaluation. The first method puts a special focus on how drivers anticipate near-limit vehicle behaviour in the BMW M Motorsport driving simulator. For professional racing drivers, there is a link between vehicle state anticipation and driving performance which is characterised by tire potential exploitation. An optimisation-based method is proposed which provides a distance concept between maximum vehicle capabilities and the vehicle potential exploited by a driver. The objective of the second method is to quantify the validity of driver-vehicle interaction by descriptive metrics. Subsequently, a model-based extension to a filter based MCA is proposed. It aims to replicate near-limit vehicle characteristics by means of yaw motion.

An experimental study is conducted at two DiL simulators with professional racing drivers. It demonstrates that behavioural validity increases with motion fidelity by up to 3.2%. The effect of physical fidelity related to the simulators' human machine interfaces is significantly higher (16%). Besides an increase of drivers' vehicle capability exploitation by 12% with increased motion fidelity, driving errors are reduced by 50%. In a second study, the comparison of professional and nonprofessional drivers identified diverging subjective MCA preferences. However, both groups performed closest to maximum capabilities with the same MCA. It is concluded that the relevance of motion cues is more dependent on the use case than on the driver. This research constitutes the basis for optimal motion cueing in nonlinear vehicle dynamics.

Kurzfassung

Der Einsatz von Fahrsimulatoren ermöglicht neben Zeit- und Kostenersparnis eine verbesserte Fahrer- und Fahrzeugperformance im Motorsportbereich. Ein wichtiger Teil von Fahrsimulatoren ist das Bewegungssystem, welches von einem Motion Cueing Algorithmus (MCA) angesteuert wird. Der MCA soll eine möglichst realitätsgetreue Bewegungswahrnehmung innerhalb des limitierten Bewegungsraumes erzeugen. Zur Bewertung der Wiedergabetreue von Bewegungsreizen gibt es Methoden, die für Anwendungen mit Straßenfahrzeugen entwickelt wurden. Diese Methoden bilden den Ausgangspunkt für MCAs, welche die Abweichung von Bewegungsreizen im Fahrsimulator gegenüber dem realen Fahrzeug numerisch minimieren. Im fahrdynamischen Grenzbereich finden solche MCAs kaum Anwendung, da die Relevanz einzelner Reize für die menschliche Wahrnehmung des Fahrzustands nicht berücksichtigt wird. Eine zentrale Forschungslücke stellt die mangelnde Kenntnis über die relative Bedeutung einzelner Bewegungsreize im fahrdynamischen Grenzbereich dar, sowie deren Abbildung durch einen MCA.
Für die Schließung dieser Forschungslücke werden zwei neuartige Methoden zur Bewertung von MCAs vorgestellt. Der Fokus liegt darauf, wie präzise Fahrer im BMW M Motorsport Fahrsimulator das Fahrzeugverhalten im fahrdynamischen Grenzbereich antizipieren. Diese Fertigkeit beeinflusst bei professionellen Rennfahrern die Performance, welche im Grenzbereich durch den Grad der Ausnutzung des Reifenpotentials charakterisiert wird. Die erste Bewertungsmethode liefert mittels numerischer Optimierung einen Distanzbegriff zwischen tatsächlicher und maximal möglicher Ausnutzung des Reifenpotentials. Die zweite Bewertungsmethode zielt auf die Quantifizierung der Validität von Fahrer-Fahrzeug-Interaktion ab und basiert auf deskriptiven Metriken. Im Verlauf der Arbeit wird ein Filter-basierter MCA vorgestellt, welcher modellbasiert unterschiedliche Signalanteile der Gierbewegung extrahieren und als Bewegungsreize abbilden kann.
Eine experimentelle Studie an zwei Fahrsimulatoren zeigt eine Steigerung der Validität von fahrverhaltensbasierten Ergebnissen um bis zu 3.2% bei professionellen Rennfahrern durch eine erhöhte Wiedergabetreue der Fahrzeugbewegung. Allerdings ist der Einfluss der physischen Realitätstreue von Mensch-Maschine-Schnittstellen mit einem Effekt von 16% signifikant größer. Eine erhöhte Wiedergabetreue der Fahrzeugbewegung lässt zwei professionelle Rennfahrer bis zu 12% mehr vom dynamischen Fahrzeugpotential auszunutzen und die Häufigkeit von Fahrfehlern wird um 50% reduziert. In einer zweiten Studie zeigt der Vergleich von professionellen und nicht professionellen Fahrern abweichende, subjektive Präferenzen einzelner MCAs, wohingegen beide Gruppen mit der gleichen Einstellung das Fahrzeugpotential am meisten ausnutzen. Daraus wird gefolgert, dass die Relevanz von Bewegungsreizen vorrangig vom Anwendungsfall abhängt. Die Arbeit liefert eine Grundlage für optimiertes Motion Cueing im fahrdynamischen Grenzbereich.

Contents

Abbreviations

AM amateur driver.

ANOVA analysis of variance.

CNS central nervous system.

CQ cockpit questionnaire.

CR continuous rating.

DAE differential algebraic equation.

DiL driver in the loop.

DiLS driver in the loop simulator.

DiLS$_{\mathrm{BMW}}$ BMW M Motorsport driver in the loop simulator.

DiLS$_{\mathrm{THRD}}$ third party driver in the loop simulator.

DoF degree of freedom.

ECG electrocardiogram.

GT grand touring.

HMI human machine interface.

HP high-pass.

HR heart rate.

HRV heart rate variability.

KPI key performance indicator.

LP low-pass.

LTI linear time-invariant.

MC motion cue.

MCA motion cueing algorithm.

MPC model predictive control.

MRG motion reference generator.

NASA National Aeronautics and Space Administration.

NASA-TLX NASA task load index.

OC optimal control.

OCP optimal control problem.

OP point of observation.

PANAS positive and negative affects schedule.

PBMC perception based motion cueing.

pdf probability density function.

PRO professional racing driver.

RMS root mean square.

RQ research question.

SD standard deviation.

SSQ simulator sickness questionnaire.

TPER tire potential exploitation rating.

VQ validity quantification.

WO washout.

Symbols

Parameters, Variables, Vectors and Matrices

$\boldsymbol{a}$	vector comprising a_x, a_y and a_z.
A_{HF}	area of high frequency steering corrections.
a_x	vehicle longitudinal acceleration.
a_y	vehicle lateral acceleration.
a_z	vehicle vertical acceleration.
AD	absolute difference.
α_i	tire slip angle.
b_i	half track width.
$B_{\max}$	max-brake point.
B_{no}	no-brake point.
B_{on}	on-brake point.
br_{dist}	baking torque distribution between front and rear axle.
br_{drv}	static baking torque distribution selected by the driver.
β	vehicle side slip angle.
$\dot{\beta}$	vehicle side slip gradient.
$c(k_2)$	linear function to compensate for the intensity impact of k_2.
CC	correlation coefficient.
D	damping coefficient of a HP filter.
DI	delay indicator.
δ	steering angle.
$\dot{\delta}$	time derivative of the steering angle.
δ_0	initial steering angle.
δ_i	tire steer angle (toe angle).
e^{abs}	absolute error.
e^{rel}	relative error.
ϵ_1	smoothing parameter.

ϵ_2	offset parameter.
f	probability density function obtained from the kernel density estimator.
$\boldsymbol{f}$	vector of equality constraints.
$f(s)$	specific force stimulus.
$\hat{f}(s)$	specific force percept.
$\hat{f}_b(x)$	kernel density estimator of the random variable x.
f_{tol}	optimisation stepsize tolerance.
$F_{x,i}$	longitudinal tire force.
$F_{x,\text{D}}$	longitudinal aerodynamic drag force.
$F_{y,i}$	lateral tire force.
$F_{y,\text{D}}$	lateral aerodynamic drag force.
$F_{z,i}$	vertical tire force.
g	arbitrary signal.
$G_{\text{o}}(s)$	transfer function of the otolith organ.
$G_{\text{HP}}(s)$	transfer function of a HP filter.
$G_{\text{lat}}(s)$	transfer function of optimal cueing filter for lateral acceleration.
$G_{\text{s}}(s)$	transfer function of the semicircular canals.
$G_{\text{yaw}}(s)$	transfer function of optimal yaw cueing filter.
γ_i	camber angle.
$\boldsymbol{h}$	vector of inequality constraints.
$H(f_1, f_2)$	hellinger distance between the pdfs f_1 and f_2.
θ	vehicle pitch angle.
i_{g}	engaged gear.
i_{Tot}	overall gear ratio between engine and tires.
J	cost function to obtain the TPM.
J_{zz}	moment of inertia around the vehicle's vertical axis.
K	global gain.
$k(x)$	gaussian kernel function.
k_1	gain on overall intensity of yaw motion reference model.
k_2	relative weight on $\dot{\beta}$ in yaw motion reference model.
κ_i	tire longitudinal slip ratio.
L	cost function to obtain the TPB.
l_{f}	CoG distance to the front axle.

l_r	CoG distance to the rear axle.
m	vehicle mass.
$M_{z,i}$	tire self-aligning torque.
n	number of elements or samples.
n_Engine	rotational speed of the engine.
p_Brk	brake pressure signal.
$\dot{p}_\mathrm{Brk}$	time derivative of the brake pressure signal.
r	pearson correlation coefficient.
r_i	tire radius.
r_swr	steering wheel reversal rate.
r_Thr	throttle pedal position signal.
$\dot{r}_\mathrm{Thr}$	time derivative of the throttle pedal position signal.
$\mathrm{R}(\tau)$	cross-correlation operator.
s	path coordinate.
S_in	turn-in point.
t	time.
$T_\mathrm{Engine,max}$	maximum engine torque.
T_f	sum of torques (driving / braking) at the front tires.
T_full	full-throttle point.
T_i	torque (driving / braking) at tire i.
t_Lap	lap time.
T_no	no-throttle point.
T_off	off-throttle point.
T_on	on-throttle point.
T_r	sum of torques (driving / braking) at the rear tires.
TPB	balance of tire potential margin KPI.
TPM	tire potential margin KPI.
τ	time constant.
v	vehicle velocity.
$\boldsymbol{v}_\mathrm{con}$	TPER optimisation constaints vector.
VI	validity indicator.
VI_sub	subscale validity indicator.
ϕ	vehicle roll angle.
x	random variable x.

$\boldsymbol{x}_{\text{in}}$	TPER optimisation input vector representing the initial vehicle state.
$\boldsymbol{x}_{\text{solv}}$	vector of variables manipulated by the TPER optimisation.
$\boldsymbol{y}$	TPER optimisation output vector.
ψ	vehicle yaw angle.
$\boldsymbol{\omega}$	vector comprising ω_x, ω_y and ω_z.
ω(s)	angular velocity stimulus.
$\hat{\omega}(s)$	angular velocity percept.
ω_{HP}	break frequency of a HP filter.
ω_{WO}	break frequency of a washout filter.
ω_x	vehicle roll rate, equivalent to $\dot{\phi}$.
$\dot{\omega}_x$	vehicle roll acceleration, equivalent to $\ddot{\phi}$.
ω_y	vehicle pitch rate, equivalent to $\dot{\theta}$.
$\dot{\omega}_y$	vehicle pitch acceleration, equivalent to $\ddot{\theta}$.
ω_z	vehicle yaw rate, equivalent to $\dot{\psi}$.
$\dot{\omega}_z$	vehicle yaw acceleration, equivalent to $\ddot{\psi}$.

Subscripts and Superscripts

a	axis, with a $\in \{\text{f}, \text{r}\}$.
Brk	brake related signal or metric.
d	DoF, with d $\in \{x, y, z, \phi, \theta, \psi\}$.
end	last sample of the respective signal.
ext	external disturbance.
f	front axis.
fl	reference to front left tire.
fr	reference to front right tire.
h	horizontal.
high	increased intensity by 25%.
i	tire reference, with $i \in \{1 = \text{fl}, 2 = \text{fr}, 3 = \text{rl}, 4 = \text{rr}\}$.
ID	metric identifier.
in	initial state.

k	single sample of the respective signal.
low	decreased intensity by 25%.
max	maximum value.
oc	vehicle CoG optimum.
ot	tire optimum.
p	corner phase, with $\mathrm{p} \in \{\mathrm{Entry}, \mathrm{Mid}, \mathrm{Exit}, \mathrm{All}\}$.
r	rear axis.
ref	reference signal.
rl	reference to rear left tire.
Rlt	temporal interrelation of throttle, brake and steering.
rr	reference to rear right tire.
s	simulator motion platform originated signal.
Str	steering related signal or metric.
sub	subscale, with $\mathrm{sub} \in \{\mathrm{Thr}, \mathrm{Brk}, \mathrm{Str}, \mathrm{Rlt}\}$.
t	tire coordinate system.
Thr	throttle related signal or metric.
v	vehicle model originated signal.
x	signal component parallel to or rotating around the x-axis of the respective coordinate system.
y	signal component parallel to or rotating around the y-axis of the respective coordinate system.
z	signal component parallel to or rotating around the z-axis of the respective coordinate system.
0	initial value.

1. Introduction

Accelerated by technological advances, driving simulation has evolved to be an indispensable tool for researchers and the automotive industry. One out of many key advantages is the prospect of obtaining valid results in a safe and cost-effective environment. Validity in this context is a complex subject. It relates to numerous properties of a driving simulator, such as its ability to provide accurate motion cues (MCs). The interrelation of validity and motion perception yields the question of which characteristics these MCs ideally contain while driving safety critical manoeuvres. A multitude of such scenarios is devoted to near-limit vehicle operation which is characterised by nonlinear vehicle dynamics. Thus, it appears as a natural consequence to examine the interaction of motion cueing and nonlinear vehicle dynamics.

The particular motivation of this work is described in this chapter, followed by preliminaries on human motion perception and driving simulation. The chapter is concluded with contributions of the thesis and an overview of its structure.

1.1. Motivation

Driving simulation applications are manifold and the same applies to the requirements put on a driving simulator system. In this regard, Fisher et al. (2011) provide a broad overview in section I-1 of [34]. Generally, a vehicle is modelled and simulated in a virtual environment. If the simulated vehicle is controlled by a human driver who receives sensory feedback, the system is referred to as driver in the loop (DiL) simulation. In the area of professional motorsport, DiL simulation is of particular importance. This marks the starting point of the present work conducted in cooperation with BMW M Motorsport.

Safety-related matters as well as time- and cost-effectiveness are of similar or potentially even higher importance as they are in road car applications. Despite increasing awareness of safety deficits, which for example led to the introduction of a secondary roll structure (halo) in 2018 for open-wheel racing series [31], motor racing remains a dangerous sport. Recently, an increasing focus of manufacturers, racing teams and governing organisers is on restricting budgets to compete in a racing series. This circumstance further emphasizes the aspect of time, as the teams' headcount is limited according to the budget and employees must work more time-efficiently. Even within the rather unique motorsport environment, use cases for a driver in the loop simulator (DiLS) are manifold. Driver training appears most obvious and is closely related to team training which involves the internalisation of processes and automatisms demanded for the race track. On the vehicle

side, the virtual development and setup evaluation are closely interrelated. In this regard, the fidelity of simulation models, cueing systems and human machine interfaces (HMIs) is of great importance. Inaccuracies in any of the systems may provoke misleading results which in turn affect driver and vehicle performance or even safety on track. Therefore, examining the validity of DiLS based results is a fundamental area of research that is rarely covered by literature for near-limit vehicle operation.

A part of the cueing system with a significant impact on drivers' perceived realism is the motion cueing algorithm (MCA). An MCA translates certain inertial signals of a simulated vehicle into simulator motion demands besides respecting the motion simulator's maximum capabilities. Maximum capabilities in this regard relate to the motion envelope or range of each degree of freedom (DoF), maximum (angular) velocity and maximum (angular) acceleration. A multitude of different MCAs have been introduced and studied since their first application around 1970 [87]. Relevant algorithms are reviewed and summarised by Casas et al. (2017) [14]. Most MCAs strive to minimise the incongruence of a simulated vehicle's inertial signals and the ones replicated by the motion simulator. This objective is based on the assumption that a driver's perceived motion fidelity is maximised if deviations between sensory stimuli are minimised. [51] In general terms, this assumption appears valid. However, for specific applications such as near-limit vehicle operation, this approach produces undesirable results due to the following observations:

- High sustained accelerations as they appear in motor racing yield very low scaling factors between vehicle reference and simulator motion. In a worst-case scenario, all MCs are below humans' perceptual thresholds which are introduced in the following section 1.2.
- Although driving a vehicle close to its maximum capabilities is a multisensory integration task, drivers explicitly extract only the most relevant cues to gauge grip availability. [59]
- The MCA is required to extract MCs from vehicle reference signals which provide information on vehicle stability and control characteristics. [86]

The latter two aspects conflict with a global objective of minimising the perceived motion incongruence and hence novel methodologies need to be examined.

1.2. Human Motion Perception

Human motion perception is based on four distinct sensory channels which are illustrated in Figure 1.1. This section covers an introduction to visual perception, auditory perception, somatosensory perception and vestibular perception. Although the first two aspects remain mostly unaffected from motion cueing they are important inputs to the multisensory integration in humans' central nervous system (CNS). Thereby, distinct stimuli are integrated according to each perception system's advantages which yields a statistically optimal motion estimation. [68] The following paragraphs describe each

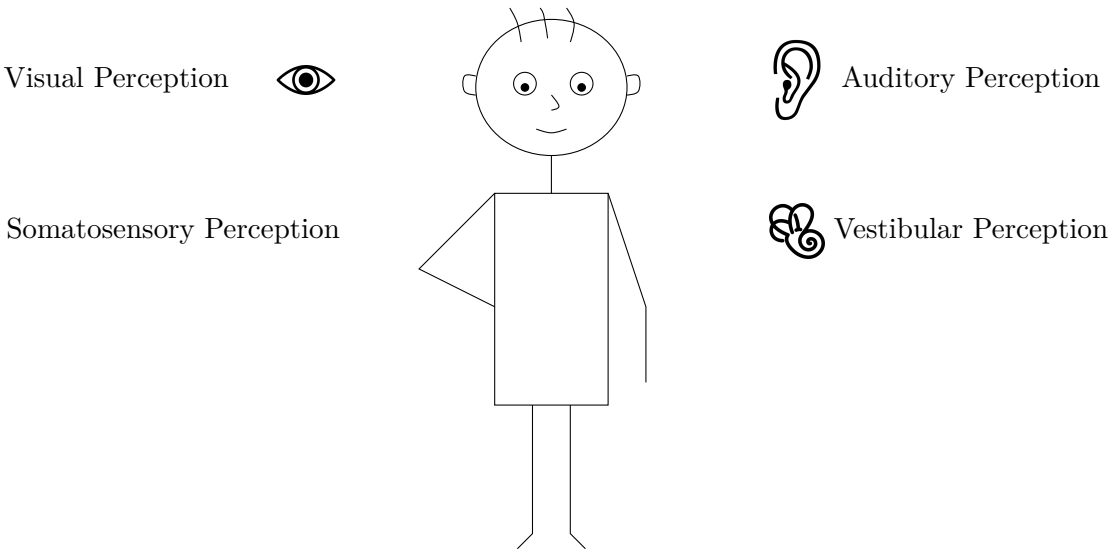

Figure 1.1.: Simplified visualisation of human motion perception channels.

perception channel separately. Subsequently, the multisensory integration task of driving a vehicle is detailed and a link to MCA evaluation is made by introducing different types of cueing errors.

Visual Perception

The visual system optically captures information about the environment and passes the information to the CNS for further processing. As a result, information about self-motion as well as humans' orientation relative to the gravitational vector are obtained. Visual perception on its own is incapable of differentiating between observed motion and self-motion. Position and velocity are perceived accurately by the visual system whereas accelerations are not. [106] For motorsport applications, this implies that visual perception is particularly important for self-motion perception in proximity to brake points or while cornering. During these manoeuvres, reference points are used the most by racing drivers. [59]

Auditory Perception

The main sources of auditory cues in motorsport DiL simulation are related to drivetrain sound as well as the vehicle's interaction with the surrounding environment. Wind, tire rolling or slipping and sound frequency contrasts due to doppler effects (i.e., while passing objects in the virtual environment) are the most relevant examples. The auditory motion perception is related to intensity cues and binaural cues. [100] The latter are created by differences of interaural time and level. Intensity cues in the context of auditory self-motion perception relate to a variation of sound pressure caused by a moving source.

Somatosensory Perception

The somatosensory system is not closely linked to a single organ which is the reason why Figure 1.1 lacks an illustrative symbol for this sensory channel. Somatosensory perception provides information on the relative position of body parts (proprioception) by multiple receptors such as muscles and joints. Another receptor is the skin whose sensation is referred to as haptics. [77] The stimuli are processed to obtain information on accelerations in car driving and DiL simulation. An illustrative example is related to a lane change manoeuvre at constant speed or a high-speed corner in motorsport applications. On the one hand, the pressure between the seat and the driver's skin changes and on the other hand the head tilts although muscles aim to stabilise its position. Another cueing method of DiL simulation sensed by the somatosensory system relates to steering force feedback. All these sensations are integrated with cues from the other sensory systems to an overall self-motion perception by the CNS. The somatosensory perception is affected by MCAs which is why Duc-An et al. (2019) [73] integrate a mathematical model of head-movement-based proprioception to an optimisation based MCA. Thereby, false proprioceptive cues are reduced compared to MCAs without proprioceptive models. More frequently, vestibular models are considered which are described in the following paragraph.

Vestibular Perception

The vestibular system comprises two macula organs named urticle and saccule as well as three semicircular canals in each of both inner ears. While semicircular canals are sensitive to rotational accelerations, the macula organs or more precisely otolith membranes on top of the macula organs, sense translational accelerations. [43] The sole processing of macula sensory signals does not enable human beings to distinguish between translational accelerations and gravitational accelerations. [6] An MCA technique named tilt coordination takes advantage of this phenomenon and is detailed in chapter 3. Besides the described deficiencies from a sensory perspective, the vestibular system can not detect stimuli below a certain intensity. This limit is referred to as the vestibular perception threshold which for example is studied by Hosman et al. (1978) [45]. For translational accelerations, thresholds are identified in a range of $0.014\,\mathrm{m\,s^{-2}}$ to $0.25\,\mathrm{m\,s^{-2}}$ and rotational velocity related perception thresholds between $0.1\,^\circ\,\mathrm{s^{-1}}$ and $3\,^\circ\,\mathrm{s^{-1}}$. [46] The vestibular perception thresholds are affected by several aspects such as the presence or absence of additional cues or mental task load [45]. Furthermore, a dependency on human expectation during an experimental study [9] and on stimulus frequency [37, 45] is identified. In driving simulation, MCAs make use of the thresholds for optimised handling of workspace limitations. An illustrative example is the re-centring or pre-positioning procedure below perceptual thresholds which technically increases the available workspace for an upcoming manoeuvre.

Despite the existence of finite element approaches to model the vestibular system [32], it is mostly represented by a linear time-invariant (LTI) system [112, 46, 32] in the context of flight and driving simulation with parameters of the models being identified empirically in experimental studies. The obtained mathematical representations describe

transfer characteristics from relevant physical stimuli of the respective organ to some quantity of subjective experience. [51] The output of such vestibular perception models is therefore referred to as percepts. Equation (1.1) describes the transfer characteristics of semicircular canals $G_{\mathrm{s}}(s)$ as proposed by Ormsby et al. (1977) [71] with $\hat{\omega}(s)$ being denoted to the perceived angular velocity and ω(s) to the physical angular velocity stimulus. Time constants of $\tau_{\mathrm{L}} = 18\,\mathrm{s}$ and $\tau_{\mathrm{A}} = 30\,\mathrm{s}$ complete the model parametrisation.

$$G_{\mathrm{s}}(s) = \frac{\hat{\omega}(s)}{\omega(s)} = \frac{\tau_{\mathrm{L}}\tau_{\mathrm{A}}s^2}{(1+\tau_{\mathrm{L}}s)(1+\tau_{\mathrm{A}}s)} \tag{1.1}$$

Houck et al. (2005) [46] propose the following LTI model for transfer characteristics of the otolith organ $G_{\mathrm{o}}(s)$ between the specific force percept $\hat{f}(s)$ and the specific force stimulus $f(s)$

$$G_{\mathrm{o}}(s) = \frac{\hat{f}(s)}{f(s)} = \frac{K\cdot(1+\tau_{\mathrm{A}}s)}{(1+\tau_{\mathrm{L}}s)(1+\tau_{\mathrm{S}}s)}. \tag{1.2}$$

The gain thereof is parametrised to K= 0.4 and the time constants are $\tau_{\mathrm{A}} = 10\,\mathrm{s}$, $\tau_{\mathrm{L}} = 5\,\mathrm{s}$ and $\tau_{\mathrm{S}} = 0.016\,\mathrm{s}$. Models of varying complexity are published where psychophysical methods are used for parameter identification. Thus, the identified models vary despite qualitatively similar transfer characteristics. [25] In driving simulation, models of vestibular perception are used to formulate a vestibular perception error. The error is defined as the difference between (simulated) vehicle percept and simulator percept. [102]

Multisensory Integration

Operating a vehicle is deemed a multisensory integration task. [59] In the context of motion sensation, this process is highly related to two sensory channels: visual perception and vestibular perception. How both are integrated for rotational motion is studied by Zacharias (1977) [112]. In an experimental study, a total of 14 participants are exposed to varying visual cues while completing the tracking task of nulling the perceived self-motion. A weighted dependence on both channels is found with vestibular cues being the dominant sensation above 0.05 Hz while visual cues dominate below the approximated threshold. This approximation is coherent with the time constants of the semicircular canals' transfer characteristics $G_{\mathrm{s}}(s)$. Another aspect of multisensory integration is related to visual-vestibular phase errors and the respective perception thresholds. Grant et al. (2007) [38] identify an average detection threshold of a phase error between visual and vestibular cues across nine participants at 57°. Less than half of this value is determined in the study of Jonik et al. (2011) [50] (22°) who use the previous results as a reference for comparable results. Both their studies reveal that phase error detection thresholds are not significantly dependent on stimulus frequency or amplitude. Therefore, human subjects are considered to detect phase errors rather than pure time delays. A practical aspect of these findings is the definition of coherence zones which allow the motion and visualisation system (see Figure 1.2) some synchronisation margin.

Sensory integration as such is well understood for normal driving conditions. However, there is little agreement for situations with conflicting sensory information, particularly under multimodal conditions. [68] Conflicting information between visual and vestibular cues is inevitable in DiL simulation. This statement holds for most applications but certainly for the area of motorsport. Hence, it is not fully understood how distinct cues are weighted internally by the driver to immerse in the simulated driving scenario.

Cueing Errors

Three types of cueing errors are described by Grant et al. (1995) [39]:

- Scaling Errors: The vehicle reference percept and the simulator percept share the same sign but the amplitude deviates. The extreme case of an amplitude equal to zero is referred to as a missing cue.
- False Cue: Either the vehicle reference percept and the simulator percept have opposite signs or the vehicle reference percept is equal to zero while the simulator percept is non-zero.
- Phase Errors: A phase distortion between vehicle reference percept and simulator percept. It may be argued that phase errors of signals below the perceptual threshold detailed in section 1.2 are neglected.

1.3. Driving Simulation Preliminaries

Despite the multitude of concepts and architectures it is feasible to arrange the subsystems of DiLS in a generally applicable system diagram. The basic interaction of driving simulation, cueing systems, physical surroundings of the driver and the driver her- or himself is illustrated in Figure 1.2. The driver controls a vehicle model mainly through the throttle pedal, brake pedal and steering wheel actuation. These inputs are processed by the vehicle model which in combination with an environment simulation adapts its internal states accordingly. Relevant states such as driving trajectory, engine speed, steering torque and inertial signals are passed to the cueing systems where simulation signals are translated into physical stimuli. Depending on the stimulus type, the cues do not affect the driver directly but propagate through an HMI. An illustrative example is the steering force feedback which is created by the steering cueing system but finally transferred to the driver by a physical steering wheel. The driver integrates the sensory information according to section 1.2 and performs another control action.

This section is devoted to information and definitions on driving simulation as such which are essential foundations for this thesis. Firstly, points of observation (OPs) within the DiL system diagram are defined, followed by the introduction to the BMW M Motorsport DiLS. Finally, theoretical models to describe a driving task are presented. Terminology of the latter and the first aspect are picked up for the description of the methods in chapter 2 and the DiL simulator's characteristics are considered in chapters 3 and 4.

Points of Observation

In the course of this work, multiple methods are discussed which aim to evaluate driver performance, cueing system fidelity or the validity of certain results. At this stage, four points of observation are introduced which facilitate the classification of such methods. The points are denoted by OP1, OP2, OP3 and OP4 and concern the following properties:

- OP1: Observations from the driver directly such as verbal, written or other subjective feedbacks. Physiological measurements at a driver's body belong to the same observation point.
- OP2: Control actions produced by a driver to operate a (simulated) vehicle. Activities such as throttle pedal, brake pedal and steering wheel actuation are captured.
- OP3: Outputs of the driving simulation such as vehicle speed, position and orientation are observed.
- OP4: Outputs of the cueing systems depict the fourth point of observation. In this work, the motion system's outputs are captured exlusively.

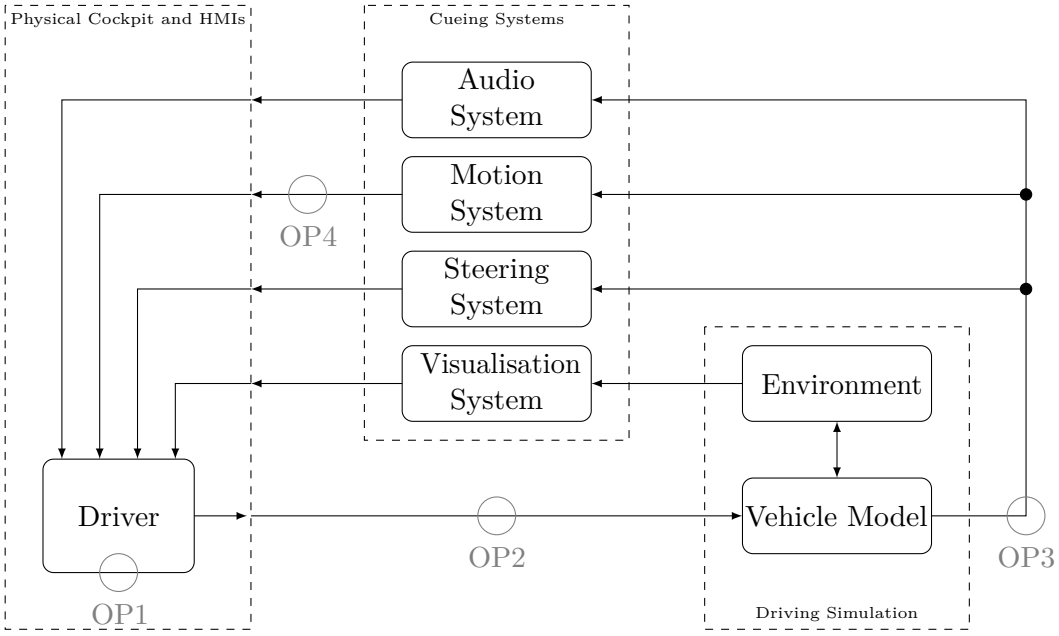

Figure 1.2.: Schematic of a DiLS on system level.
Typically a driver is surrounded by a physical cockpit including HMIs. The driver controls the underlying models of the driving simulation which comprise a virtual vehicle and a virtual environment. The driving simulation provides inputs to the cueing systems where auditory, vestibular, proprioceptive and visual cues are created and passed to the driver.

BMW M Motorsport Simulator

As stated by the motivation in section 1.1, this work is related to the DiLS of BMW M Motorsport located in Munich, Germany. This paragraph introduces the system following the suggestions of Wynne et al. (2019) [111] towards a standardised description of DiL simulators for increased comparability between DiLS studies. For that purpose, physical fidelity is described, followed by the individual cueing systems.
The physical simulator is shown in Figure 1.3. It comprises a touring car chassis which is an original race car chassis of the simulated vehicle with slight modifications for weight and mechanical integration purposes. It is attached on top of a four DoF motion platform. Three out of four DoFs are rendering angular velocities (i.e., roll rate $\dot{\phi} = \omega_x$, pitch rate $\dot{\theta} = \omega_y$ and yaw rate $\dot{\psi} = \omega_z$) and the residual DoF renders vertical translational acceleration $a_z = \ddot{z}$ (heave). The maximum capabilities of each DoF individually are listed in Table 1.1. The values are obtained from a system identification process conducted similar to the one described by Pitz (2017) [75]. The entire assembly is surrounded by a 210° curved screen. For visualisation and track modelling purposes, driving simulation software provided by rFpro [82] is in use. The graphics engine in combination with the projectors allows a frame rate of 120 Hz. Track models have a resolution of at least 1 cm in the horizontal plane and a vertical resolution of at least 1 mm for the texture of the road. [82] No traffic simulation is considered for this work as it is a disturbance factor for near-limit vehicle operation.
Another vital part of DiL simulators is the steering system. [98] At the BMW M Motorsport DiLS, torque feedback is provided by an electric motor which directly loads the steering wheel with a maximum of 48 N m [93].

Table 1.1.: Maximum capabilities of the BMW M Motorsport DiLS.

	range	**velocity**	**acceleration**
heave	0.3 m	0.3 m/s	17.6 m/s^2
pitch	0.24 rad	0.24 rad/s	9 rad/s^2
roll	0.24 rad	0.24 rad/s	9 rad/s^2
yaw	0.7 rad	0.46 rad/s	20 rad/s^2

The Driving Task

There is a multitude of approaches that qualitatively model human behaviour during their interaction with a technical system via HMIs. A general description is provided by Rasmussen (1983) [80], who considers three levels of human performance. On the lowest level of control, there is skill-based behaviour which relates to sensory-motor performance. As skill-based behaviour is executed unconsciously, a human person is not necessarily able to describe what sensory information is processed to achieve the given performance. The model's second level is devoted to rule-based behaviour, where actions are based on stored rules. An appropriate rule is selected consciously and therefore the perceptual basis of actions can usually be reported by the person. Despite the skill-based behaviour happening unconsciously, a distinction from rule-based behaviour is partially fuzzy as

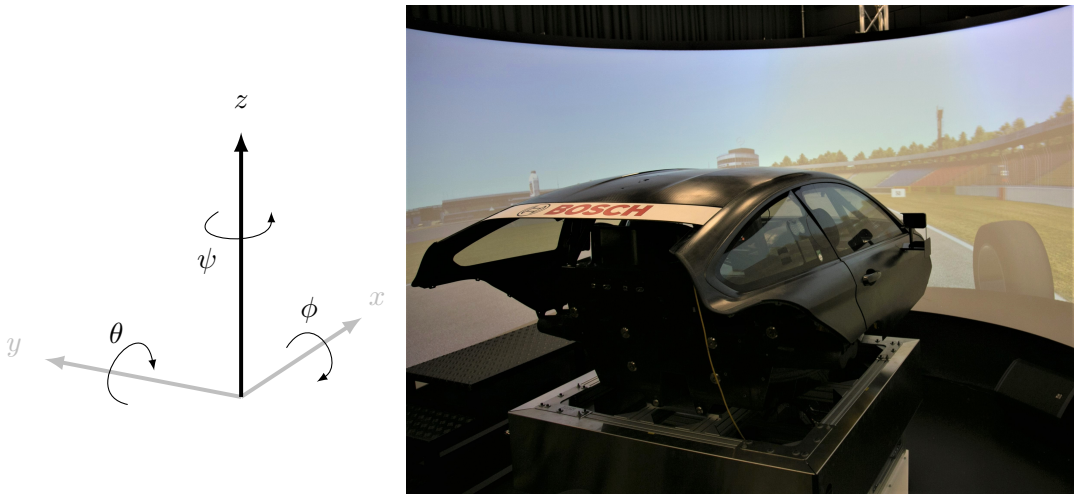

Figure 1.3.: Image of the BMW M Motorsport DiLS on the right and its motion system's coordinate system on the left side.
The axes denoting x and y are transparent as the four DoF system does not produce longitudinal translational motion (surge) and lateral translational motion (sway) but only translational MCs along the vertical axis (heave) which is denoted by z.

extensive training can result in a shift from rule- to skill-based behaviour. The highest of the proposed three levels is referred as knowledge-based behaviour. It is particularly relevant for unfamiliar situations, where no preliminary know-how and internal rules are available. [80]
Similar but more task-specific models are proposed for vehicle operation. Donges (1982) [23] differentiates the driving task into three levels. The highest level of Figure 1.4 describes the navigation task which yields a selection of route and timing. The process is mainly influenced by the road network. On that basis, a targeted trajectory is planned on the guidance level. The trajectory relies on road and traffic-related properties and results in reference variables for the driving line and speed. Both are processed towards stabilising motor routines (i.e., throttle pedal, brake pedal and steering wheel actuation) under consideration of the actual driving line and velocity. Particularly on the stabilisation level, a driver senses cues according to the perception mechanisms detailed in section 1.2, filters the cues for relevant features and applies some control action to the vehicle. This process is referred to as a closed-loop perception-reaction automatism. [23]
Another hierarchical model, described and reviewed by Michon (1985) [64], similarly considers three levels. The general mission planning relates to the highest level which is referred to as the strategic level. The manoeuvring level denotes the next lower level where tactical control action patterns are obtained. The actions of this level are considered to have time constants with a magnitude of a few seconds. In contrast, the control level relates to time constants in the range of milliseconds. At this lowest level of the model, automatic action patterns are produced.

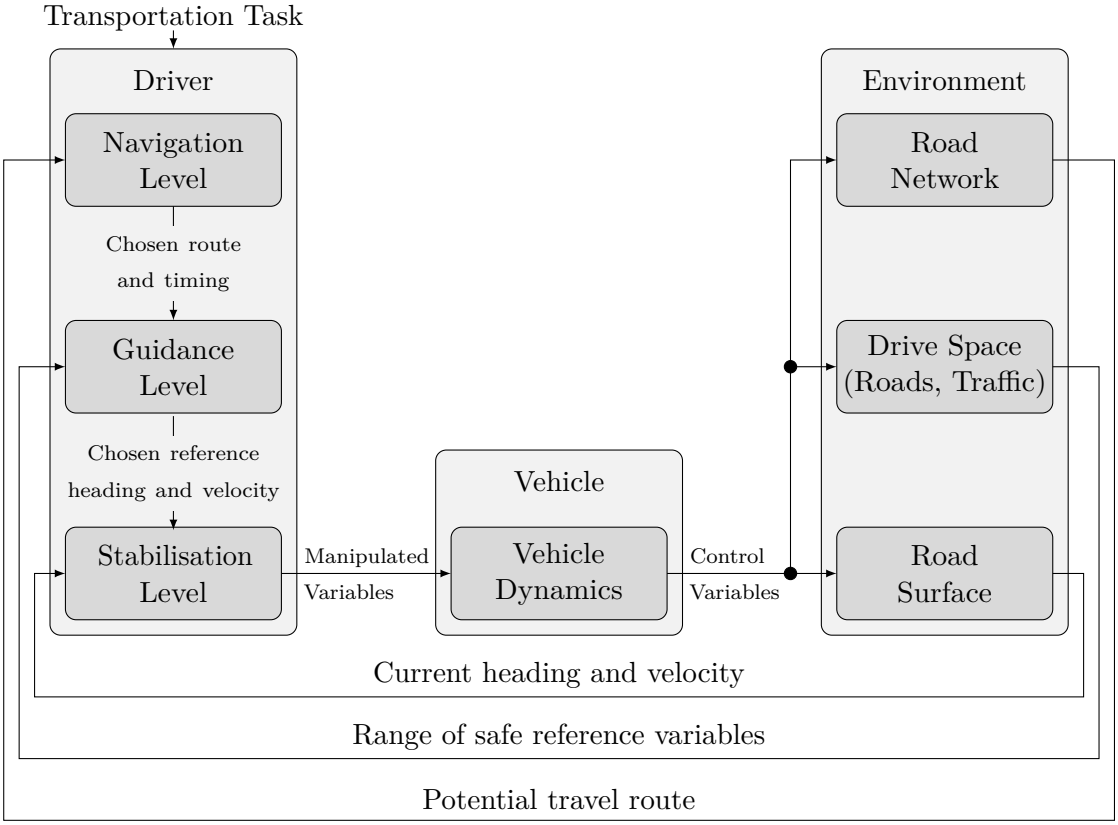

Figure 1.4.: Three-Level-Model of a driving task. [23] The illustration's translation into English is inspired by Wörle (2019). [109]

What all of the reviewed models have in common is an unconscious control behaviour at the lowest level of the driving task. In motorsport applications without the consideration of competitors, the strategic level for mission planning becomes void. The next lower manoeuvring level reveals differences in driving style of professional racing drivers. [109] However, this work focuses on the impact of MCs' on the vehicle control level which appears equally applicable to physically real and virtual environments.

1.4. Contribution and Outline

The ultimate goal of racing drivers is to minimise lap time on a given circuit by extracting a given vehicle's maximum capabilities. An essential aspect while doing so is their ability to gauge grip availability during braking, steering and accelerating. They train this task extensively to establish stabilising motor routines. [59] A DiLS provides a framework that aims to support the shift from knowledge-, over rule-, to skill-based behaviour by virtual training. [80] As a result, action patterns are obtained for the lowest level of vehicle

control which allow minimum reaction times to, for example, stabilise the vehicle at its maximum capabilities. Ideally, the same perception reaction automatisms as obtained from the virtual training can be applied for controlling the real vehicle. Hence, a demand for accurate vehicle state anticipation in the DiLS arises. In the context of car driving, vehicle state anticipation is a "high-level cognitive competence which is important for the perception and interpretation of familiar cues" [96].

At this point, there is a lack of understanding of how vehicle state anticipation is affected by sensory conflicts in the multisensory integration task [68]. However, studies are confirming that MCs have an effect in this regard [56, 61]. This work aims towards robust findings on which MCs support accurate vehicle state anticipation of professional racing drivers in nonlinear vehicle dynamics despite inevitably conflicting sensory information. Furthermore, the findings' applicability to nonprofessional drivers is of particular interest.

To that end, the following research questions (RQs) are formulated:

- RQ_1: How do varying surge, sway and yaw MCs affect professional racing drivers' vehicle state anticipation?
- RQ_2: How significant is the effect compared to the impact of varying physical fidelity?
- RQ_3: Which yaw MCs are most relevant for vehicle state anticipation in a four DoF DiLS?
- RQ_4: Are drivers' preferences of yaw motion feedback depending on their experience and driving skills?
- RQ_5: Are subjective preferences supported by enhanced driving performance?

To answer these research questions, the thesis provides the following contributions:

1. Two novel performance indicators suitable for the evaluation of near-limit vehicle handling:
    - Development of a methodology to capture driver's performance on the vehicle control level of driving tasks. Improved accuracy of vehicle state anticipation is assumed to increase performance in that sense. The optimisation-based method makes use of the DiL simulator's underlying models to formulate a distance concept between a particular vehicle state and maximum vehicle capabilities.
    - Introduction of a second evaluation method aiming at validity quantification. Driver actions to control the vehicle are described by a set of metrics that are equally applicable to DiL simulation and track operation. Initially retrieved metrics from literature are selected using correlation analyses to holistically describe the signals while reducing redundancies and complexity. A measure of similarity between track and DiL based results is proposed using kernel density estimation and the Hellinger distance metric.

2. Development of an MCA specifically suitable for the four DoF BMW M Motorsport driving simulator. The approach is based on scaling and filtering with a model-based yaw motion reference generation.
3. Two experimental, explorative studies to obtain empirical insights into drivers' vehicle state anticipation by applying contributions 1 and 2:
    - Experimental study relying on two different DiL simulators and track reference data. One DiLS is based on a full six DoF motion platform and one is the BMW M Motorsport four DoF system. Thereby, different levels of motion fidelity and physical fidelity are contrasted.
    - Experimental investigation on yaw motion cueing preferences between professional racing drivers and road vehicle drivers. At the BMW M Motorsport DiLS, 33 participants identify their personal preference which is compared to objective metrics of task completion performance and mental workload.

The thesis is structured according to Figure 1.5. This introduction is followed by three parts of the main body which separately cover:

- Evaluation Methods
- Motion Cueing Algorithms
- Experimental Studies

Those three parts are largely self-contained and both state of the art and methods are explained separately. Chapter 4, covering experimental studies, relies on evaluation methods and MCAs from chapter 2 and chapter 3 which are linked accordingly. Subsequently, in chapter 5, all methods are combined to depict overall results which are evaluated and discussed in chapter 6 and finally summarised in the concluding chapter 7.

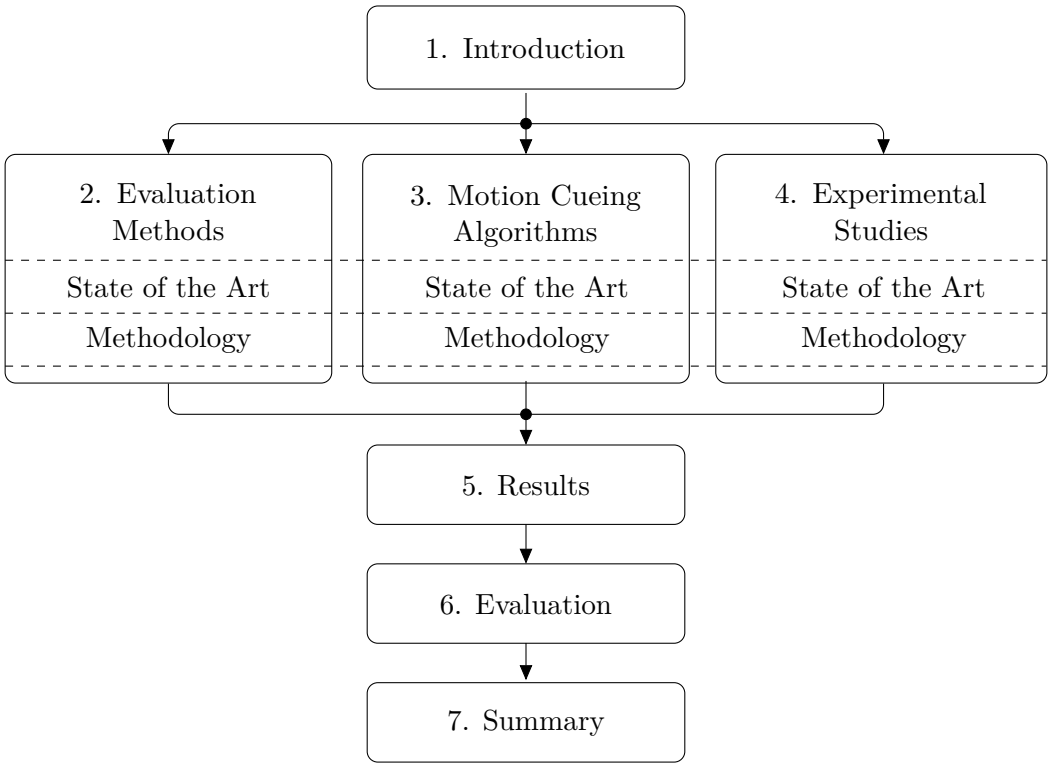

Figure 1.5.: Structure of this thesis.
The parallel main body comprises evaluation methods, motion cueing algorithms and experimental studies. Results, evaluation and conclusion are conducted on an overall scope.

2. Evaluation Methods

This chapter reviews existing performance indicators that directly or indirectly aim to evaluate DiL simulators and MCAs. Subsequently, two evaluation methodologies based on novel performance indicators are introduced.

2.1. State of the Art

An evaluation exercise in the context of DiL simulation demands answers to the following two general questions in consecutive order:

1. **What** is the evaluation aiming at?
2. **How** to capture relevant effects?

The first question implies a reduction of all study design and measurement aspects to the essence of individual factors. Answering the second question yields primary measures in the form of key performance indicators (KPIs) and puts requirements on the study design.

This review section is organised following the two high-level questions. At first, methods aiming at different evaluation targets are reviewed and categorised. Subsequently, relevant KPIs which could serve to answer the second question are presented and clustered according to their underlying observation method and temporal resolution.

2.1.1. Objectives of Driving Simulation Evaluation

The first question from above can lead to several sub-questions which should refine what effect the evaluation method aims to capture. Two important and frequently addressed evaluation targets relate to the terms validity and fidelity. Casas-Yrurzum et al. (2021) [15] define validity in this context as a measure of how closely results from simulation and real-world scenarios match whereas fidelity measures to what extent a certain experience can be replicated in a DiLS. This section covers, inter alia, validity and fidelity related aspects applicable to experimental DiLS studies.

2.1.1.1. Validity of Driving Simulation Results

There are three terms that are often used within DiLS studies that relate to validity: absolute validity, relative validity and behavioural validity. The distinction of absolute and relative validity of DiLS study results is introduced by Blaauw (1982) [5]. Absolute validity is achieved if KPIs obtained from driving simulation and real-world driving are matching in absolute terms [111]. It is therefore required to have a direct comparison between both environments as conducted in the study of Mayhew et al. (2011) [62]. They investigate the validity of a DiLS for driver skill and performance evaluation. For that purpose, an urban test route is re-constructed in the virtual environment and 60 participants complete the test route in the real and the virtual environment. During this task, driving errors such as an illegal crossing of a solid line on the road are identified and cumulated over the entire task completion. The driving errors show similar distributions between both environments. However, absolute validity is not achieved as specific driving errors show no correlation which is a mandatory requirement. In contrast, relative validity in the context of driving simulation requires the specific driving errors of the previous example to show similar sensitivities on certain independent variables [5]. Therefore, the absolute error value or distribution at a certain level of an independent variable is neglected for the concept of relative validity. In the second part of the study conducted by Mayhew et al. (2011) [62], the driving performance of three groups with varying experience in on-road driving is evaluated at a DiLS only. Out of 90 participants in total, 32 are experienced, 28 are novice drivers and 30 participants have no driving experience at all. Significant differences in driving performance are found among the groups. The relative direction between groups is in line with the level of real-world driving experience. Therefore the experimental study results claim relative validity.

Although there are no guidelines to adhere to for such validation studies, speed and speed variation are two measures that are used most frequently to demonstrate absolute validity [111]. It is worth noting that both measures are taken at OP3 of Figure 1.2. Likewise, Branzi et al. (2017) [7] compare drivers' speed behaviour in simulated and real-world urban roads. Within their study, absolute validity in the sense of speed behaviour is achieved where physical constraints of a specific driving scenario affect the driving speed. An example of such a physical constraint is the driving path curvature of a roundabout. However, the overall results of the experiment do not meet the requirements of absolute validity. Similar to the previous example, relative validity is achieved. The authors narrow down their evaluation target to the validity of drivers' behaviour which they ultimately evaluate and rate by speed and speed variation. Other recent publications refer to the validity of drivers' behaviour in a DiLS study as behavioural validity [95, 60].

The approach of behavioural validity in the context of flight simulation was introduced and investigated by Mudd (1968) [66]. In 1982, Blaauw [5] transferred the terminology to driving simulation to analyse driver behaviour and driving performance separately. According to Gemou (2013) [36], behavioural validity of DiLS results is of higher importance than physical fidelity of the DiL system when investigating performance deviations between different tasks as it directly describes the correlation between results from the

virtual and real-world environment. Another justification is based on findings where the amount of physical fidelity of a DiLS above a certain level has no significant impact on how drivers behave under varying conditions [105]. In particular, this is tested for the assessment of different in-vehicle informational interfaces. Another study on behavioural validity examines the impact of DiLS and real-world environment on HMI tasks [95]. The study compares real-world driving against two DiLS systems, one of which is a static base simulator and the other one is based on a hexapod motion platform. The results rely on behavioural benchmarks which correspond to three aspects:

- task-related measure: task completion time
- driver performance measures: mean speed, speed variability and steering wheel reversal rates
- glance behaviour: frequency of off-road glances, mean off-road glance duration and total off-road glance duration

In terms of longitudinal vehicle control, it is found that none of the DiL simulators achieves absolute behavioural validity, although the hexapod motion system significantly improves validity of the speed variability KPI.

Concluding the evaluation target of validity it is worth noting that behavioural validity is considered a sub-area of general validity and that there is no universally valid selection of measures that should be used as a best practice [111]. Behavioural validity is subject to the differentiation between absolute and relative validity [5].

2.1.1.2. Fidelity of Driving Simulators

The term fidelity in the context of driving simulation comprises various aspects such as physical fidelity, perceptual fidelity, task fidelity or motion fidelity. Wynne et al. (2019) [111] consider three primary classes of fidelity which are physical fidelity (vehicle controls, ergonomics), visual fidelity (field of view, frame rate, resolution, level of detail) and motion fidelity (kinaesthetic feedback). Physical fidelity is referred to as physical validity by some authors [34, 95]. However, according to [111], fidelity relates to research tools or independent variables whereas validity always relates to research outcomes. The present work adheres to this justification and, as introduced in the previous section, sticks to the term of physical fidelity. Another aspect of fidelity is related to the simulation's underlying track, vehicle and tire models. Apart from motion fidelity evaluation, there is no universal consensus between researchers to classify a simulator's fidelity [111]. For that reason and because the present work is focused on MCAs, related work on motion fidelity is discussed in this section.

Unlike validity evaluations of the previous section, which measure at the observation points OP1 to OP3 of Figure 1.2, motion fidelity is mainly analysed using the input-output characteristics of the motion system. Therefore, the vehicle model outputs (OP3) serve as a reference to examine the fidelity of motion system outputs (OP4).

Three objective indicators to quantify motion fidelity are proposed by Casas et al. (2015) [13]. In their research, the authors aim to characterise the human response to different MCAs by comparing the objective indicators to participants' subjective fidelity evaluation for each MCA setting. The subjective feedback is based on a post-task questionnaire asking participants to grade the motion platform's fidelity compared to the motion perceived by visual cues on a 0-to-100 range. The objective indicators aim to measure the similarity between the (simulated) vehicle motion and the motion cues provided by the cueing system. In particular, accelerations (specific forces) and angular velocities are under investigation. Therefore, the input-output characteristic of all the motion platform's six DoFs is examined separately regarding three aspects:

- Absolute Difference (AD_d): calculates the mean of differences between vehicle reference g_d^v (OP3 in Figure 1.2) and motion system output signals g_d^s (OP4 in Figure 1.2) over time. Equation (2.1) describes the indicator mathematically for a single DoF (subscript d). As the AD_d indicator compares both signals at each distinct time step i, the corresponding samples of each signal are referred as $g_{\mathrm{d},k}^\mathrm{v}$ and $g_{\mathrm{d},k}^\mathrm{s}$. The total number of discrete time steps is depicted by n.
- Cross-Correlation (CC_d): describes the shape similarity between g_d^v and g_d^s although different magnitudes and potentially delays occur between the motion system inputs and outputs. The indicator is defined according to Equation (2.2) by Grottoli et al. (2019) [41] as the cross-correlation's maximum value between g_d^v and g_d^s divided by the maximum of the reference signal's (g_d^v) auto-correlation. The latter is equivalent to the cross-correlation of the reference signal with itself. The cross-correlation operator is represented by R and τ describes the time shift between both signals.
- Delay Indicator (DI_d): estimates the delay between motion system input and output signals. Therefore, DI_d equals the particular value of τ which maximises the cross-correlation $\mathrm{R}_{g_\mathrm{d}^\mathrm{v} g_\mathrm{d}^\mathrm{s}}(\tau)$.

$$AD_\mathrm{d} = 1 + \frac{1}{n} \cdot \sum_{k=1}^{n} |g_{\mathrm{d},k}^\mathrm{v} - g_{\mathrm{d},k}^\mathrm{s}| \tag{2.1}$$

$$CC_\mathrm{d} = \frac{\max\left(\mathrm{R}_{g_\mathrm{d}^\mathrm{v} g_\mathrm{d}^\mathrm{s}}(\tau)\right)}{\max\left(\mathrm{R}_{g_\mathrm{d}^\mathrm{v} g_\mathrm{d}^\mathrm{v}}(\tau)\right)} \tag{2.2}$$

The application of these objective indicators in the study of Casas et al. (2015) concludes a higher correlation of CC_d (correlation coefficient 0.511) and DI_d (correlation coefficient 0.357) to subjective fidelity evaluation of 90 participants compared to the absolute difference AD_d (correlation coefficient 0.118) indicator.

Similar methods are applied by Grottoli et al. (2019) [41] and further analysed with regard to applicability for MCA evaluation by Kolff et al. (2020) [54].In both publications,

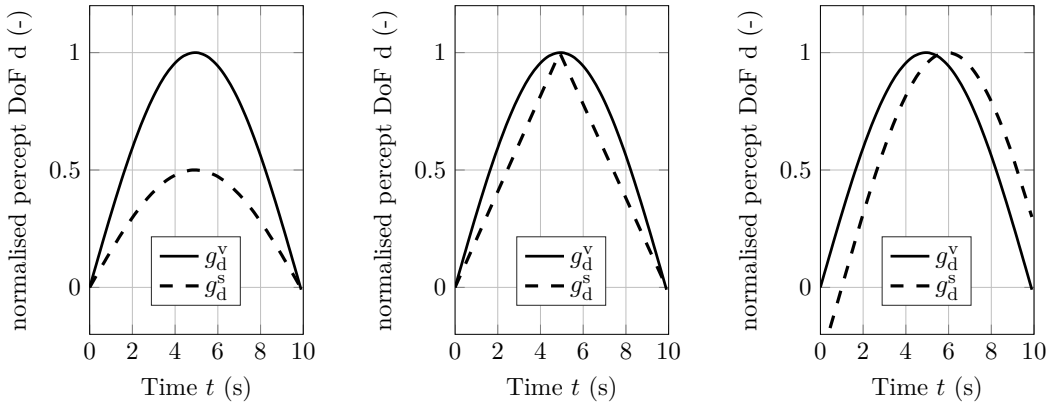

(a) $AD_{\mathrm{d}} \neq 0$, $CC_{\mathrm{d}} = 0$, $DI_{\mathrm{d}} = 0$ (b) $AD_{\mathrm{d}} \approx 0$, $CC_{\mathrm{d}} \neq 0$, $DI_{\mathrm{d}} = 0$ (c) $AD_{\mathrm{d}} \approx 0$, $CC_{\mathrm{d}} = 0$, $DI_{\mathrm{d}} \neq 0$

Figure 2.1.: Illustration of the motion fidelity KPIs.
Qualitative results of AD_{d}, CC_{d} and DI_{d} for a generic, normalised motion percept obtained from vehicle ($g_{\mathrm{d}}^{\mathrm{v}}$) and simulator ($g_{\mathrm{d}}^{\mathrm{s}}$) data.

a modified definition of the AD_{d} KPI is considered. The alternative formulation is described in Equation (2.3). It uses the ratio of the cumulated deviation between vehicle and simulator specific forces or angular velocities to the cumulated measures of vehicle reference,

$$AD_{\mathrm{d}} = \frac{\sum_{k=1}^{n} |g_{\mathrm{d},k}^{\mathrm{v}} - g_{\mathrm{d},k}^{\mathrm{s}}|}{\sum_{k=1}^{n} |g_{\mathrm{d},k}^{\mathrm{v}}|}. \tag{2.3}$$

Thereby, different prediction strategies for optimisation-based MCAs are evaluated in the work of [41]. It is found that a prediction strategy with knowledge of a vehicle's future trajectory reduces DI_{d}, increases CC_{d} and further increases workspace usage. Although each individual indicator is useful to examine particular input-output characteristics of the motion system, only a combined analysis of all three KPIs provide a suitable description of the resulting MCs as illustrated in Figures 2.1(a)-2.1(c). An absolute difference of $AD_{\mathrm{d}} = 0$ relates to identical signals. If $AD_{\mathrm{d}} \neq 0$ holds, the residual two KPIs CC_{d} and DI_{d} allow to characterise the signals' deviation. Figure 2.1(a) shows an example where $g^{\mathrm{s}} = 0.5 \cdot g^{\mathrm{v}}$ and therefore only AD_{d} is unequal to zero. Figure 2.1(b) illustrates an example where the correlation coefficient CC_{d} between g^{s} and g^{v} is unequal to zero but $DI_{\mathrm{d}} = 0$ shows the temporal alignment of both signals with $AD_{\mathrm{d}} \approx 0$. Finally, Figure 2.1(c) depicts a phase delay of $DI_{\mathrm{d}} = 1\,\mathrm{s}$ while the shape of both signals is identical and therefore CC_{d} equals zero.

2.1.1.3. Task Completion Performance

Another evaluation target, particularly interesting for motorsport applications, is related to task completion performance. The most obvious indicator for circuit racing is based on the lap times and lap time variability achieved by a driver. Lap time in this context is equivalent to the mean speed KPI used for validity analyses by Spyridakos et al. (2020) [95] and lap time variability can be treated similar to mean speed variability of non-circuit racing applications. However, there is a multitude of indicators to describe driver performance on a more detailed level. The particular measures are depending on the individual driving task. Table 2.1 summarises the most relevant types of indicators and provides some references to studies where they are applied. According to section 2.1.1.1, some of the KPIs listed here are equally applicable for validity analysis. However, there is no demand for real-world driving references if the evaluation target is purely related to task completion performance in a DiLS.

2.1.1.4. Emotional State and Workload

Many experimental studies aim to evaluate participants' emotional state (i.e., their preference of a certain MCA parametrisation over another), physical comfort (i.e., motion sickness) or their workload while accomplishing certain tasks. Frequently, these aims are defined alongside other evaluation targets such as validity or fidelity to obtain a more detailed understanding of the primary results. [34] Either as a primary task or for secondary analyses, there is a multitude of methods that measure participants' emotional state and workload. This section covers a selection of relevant techniques including application examples of related work.

A widely spread and repeatedly validated questionnaire that captures emotional states is named positive and negative affects schedule (PANAS). It was first introduced by Watson et al. (1988) [107] in the area of personality and social psychology. De Paoli et al. (2000) [22] further validated the PANAS and it is used in the context of flight simulation by [53]. The PANAS allows separate evaluation of a positive and a negative subscale which both are shown to be internally consistent and largely uncorrelated. [107] Despite its repeated validation and frequent application in the context of psychology and medicine, it is rarely used for experimental DiLS studies.

Another aspect of driving simulation is its impact on drivers' workload. In order to quantify perceived workload for any task, a NASA task load index (NASA-TLX) developed by the U.S. based National Aeronautics and Space Administration was developed in 1986 and initially published in 1988. It comprises six subscales which cover mental demand, physical demand, temporal demand, performance, effort and frustration. [42] The multi-dimensional evaluation examines the magnitude and source of different workload-related factors and combines them to a reliable estimate of workload. Quantifying spare mental capacity is the aim of the Bedford Scale which was published in 1984 by Roscoe (1984) [84]. The scale is uni-dimensional and it firstly examines whether it was or was not

Table 2.1.: Comparison of methods which aim to evaluate task completion performance.

Scope of Task Completion	**KPI Description**	**Symbol**	**Temporal Resolution**	**Remarks, References**
Time	Lap time	t_{Lap}	discrete	[48]
	Sector times	t_{Sec}	discrete	analysed per sector or manoeuvre [48]
Speed	Mean speed	$\overline{v_x}$	discrete	[111]
	Speed variability	$\sigma(v_x)$	discrete	[111]
Power	Specific longitudinal power	$\mathrm{P}_x = \mathrm{a}_x \cdot \mathrm{v}_x$	continuous	[30]
	Specific lateral power	$\mathrm{P}_y = \mathrm{a}_y \cdot \mathrm{v}_y$	continuous	[30]
Lane position	Lateral deviation from ideal (prescribed) trajectory	Δs_{y}	continuous	[58]
	Positional variability	$\sigma(\Delta s_{\mathrm{y}})$, $\sigma^2(\Delta s_{\mathrm{y}})$	discrete	[58, 40]
Lane heading	Deviation from ideal (prescribed) trajectory	$\Delta\phi_{\mathrm{z}}$	continuous	[58]
	Heading error variance	$\sigma^2(\Delta\phi_{\mathrm{z}})$	discrete	[58]
Steering wheel control	Steering wheel reversal rate	r_{swr}	discrete	adjustable threshold for reversal detection, [2]
	High frequency area	A_{HF}	discrete	captures high frequency corrections [2]
Reaction time measures	Braking response time	t_{BrkResp}	discrete	[113, 40]
Accidents, failures	Accident probability	P_{fail}	discrete	crash or spin in motorsport applications

possible to complete a certain task. In case the task was completed the questionnaire asks if the induced workload was tolerable or if it was satisfactory without reduction [84]. It is initially developed to evaluate pilots' spare mental capacity during flight tasks.

Besides the questionnaires reviewed above, there are methods based on physiological measurements which provide insights into subdomains of the overall workload. One such physiological measurement is based on an electrocardiogram (ECG) which allows capturing of heart rate (HR) and heart rate variability (HRV). The latter is a reliable indicator for stress whereas the mean HR during an experiment allows drawing conclusions about the physical demands. [53] HR and HRV are linked to participants' physical condition. It is therefore required to capture baseline measurements in a state of rest and standardise the physiological data obtained during task completion. Thereby, between-subject variability in normal condition is reduced and significant effects are more likely to be captured.

The last method covered in this review is an established questionnaire that aims to capture symptoms of simulator sickness. This simulator sickness questionnaire (SSQ) was initially proposed by Kennedy et al. in 1993 [52]. Despite its frequent application, there are disadvantages of the SSQ such as its demand for pausing the driving task. Sickness symptoms may partially attenuate until a participant fills out the form which in turn would reduce its accuracy as hypothesised by [44].

2.1.2. Observation Method

The reviewed observation methods are classified in subjective and objective methodologies. Within these two types of observations, there are multiple sub-categories such as verbal and non-verbal subjective feedback or KPIs obtained from psychophysiological measurements and those obtained from human-machine interaction. A further subdivision of both subjective and objective observation methods is made according to the temporal resolution of the results. The following two subsections review relevant examples.

2.1.2.1. Subjective Observation

Subjective feedback and evaluation provide insights into participants' personal preferences, emotional state or workload. Measurements are taken at OP1 of Figure 1.2 and can address any of the evaluation targets described in the previous section. The following items of section 2.1.1.4 can be classified as offline (pre- or post-task), non-verbal methods:

- NASA TLX
- Bedford Scale
- Positive And Negative Affects Schedule (PANAS)
- Simulator Sickness Questionnaire (SSQ)

This classification is due to the demand for pausing or completing the experimental task before the evaluation results can be obtained.

Opposite to these examples, Cleij et al. (2015) [18] introduce a continuous subjective evaluation method named continuous rating (CR). Their study aims to detect how MCA quality variation is perceived over time and how the overall quality judgement is thereby affected. The method is based on a rotary knob which is continuously controlled by the participant. The experiment relies on what is called an open-loop manoeuvre which means that participants are passengers within the driving simulation and do not actively control the vehicle motion. A detailed description of open- and closed-loop experiments is part of section 4.1.1. By turning the rotary knob, participants control a rating bar with 15 coloured indicators which are displayed on a separate screen. Within the study, different MCAs and manoeuvres are continuously rated by 16 participants. Compared to the post-task evaluation, also referred to as offline rating, the results provide additional information on the temporal evolution of perceived motion incoherence. On

the same methodical basis, Cleij et al. (2019) [17] compare filter- and optimisation-based MCAs in a study with 19 participants. Amongst others, the CR allowed identifying that participants' preference of the optimisation-based MCA over a filter-based MCA is valid for all investigated types of manoeuvres such as rural curve driving, overtaking and driving through a roundabout.

2.1.2.2. Objective Observation

Compared to subjective evaluation methods, objective measures facilitate the elimination of a potential bias and participants' assessment accuracy. While subjective evaluation methods interfere with the driver directly, objective results can be based on measurements at OP1 to OP4 of Figure 1.2. All of the task completion performance KPIs presented in Table 2.1 are related to objective observation methods. The table further distinguishes between a discrete-time and a continuous temporal resolution which are two subcategories of each observation method. Although signals are discretised at a certain sampling frequency, data obtained at a rate above double of the respective system's eigenfrequency is considered continuous within this work. KPIs such as AD_{d} or CC_{d} (see Equations (2.1) and (2.2), [13]) are based on signals captured continuously but the derived KPIs relate one scalar result to one trial. Due to the continuous recording, separate investigations on particular manoeuvres within one driving task are possible. Hence, continuous results are discretised for certain temporal or spatial sections of a task. This allows considering more data simultaneously as required for repeated measures. Therefore, the two mentioned motion fidelity evaluations have a continuous-time basis but classify as discrete-time objective methods. The same applies to HR and HRV as well as mean value, standard deviation or variance of continuously recorded data. In contrast, lap time, braking response time or accident probability relate to a discrete temporal resolution by nature.

There are methods that use time-series data directly for evaluation purposes. One such method aims to evaluate driver performance in circuit racing using specific longitudinal and lateral power [30] (see Table 2.1). Lateral deviation from an ideal or prescribed trajectory such as the road centreline or a reference vehicle is another frequently used signal to analyse task completion performance. [58, 40] However, most of these signals are compiled to single KPIs for improved clarity of the results.

2.1.3. Discussion of the State of the Art

A detailed overview of techniques including their properties of evaluation target and observation method is provided in Table 2.2. It reveals that the same KPI can be applied although the evaluation targets differ. For instance, task completion time (i.e., lap time) is used to evaluate driving performance [48] but other studies [5, 40] compare the same KPI to data obtained from an instrumented road car as they aim to evaluate behavioural validity. Mostly there is not one single but a combination of observation methods selected to benefit from individual strengths. Subjective and objective measures are frequently

combined to conduct correlation-based analyses between both results. These findings are further used to parametrise analytical driver [60] or rating models [25]. As summarised in the review of Casas-Yrurzum (2021) [15] on objective MCA evaluation techniques, there is no universal solution available with the same being true for validation purposes. [111] Therefore, it is advisable to "give some pause for thought about what a researcher's intention might be when attempting to validate a simulation" [40].

2.2. Contribution

The thesis' objectives introduced in chapter 1 create a demand for reliable MCA fidelity and behavioural validity evaluation techniques particularly suitable for motorsport applications. This chapter proposes two novel objective evaluation methods. One aims to quantify to what extent drivers can extract maximum vehicle capabilities and how different MCAs influence drivers' performance in this regard. Lap time, sector time or specific power-based analyses aim towards the same evaluation target. [48, 30] However, limitations are making them partially unsuitable for this research. Analyses based on task completion time do not provide continuous results which allow separating results for individual manoeuvres, corners or, even more detailed, for fractions of a corner. Therefore, it is not feasible to align certain motion cues with the resulting driver performance. What is more, the driving trajectory is linked to the aforementioned performance indicators which impedes the evaluation of drivers' performance on the vehicle control level of a driving task. [23] The proposed method makes use of the driving simulation's underlying two-track vehicle model in order to estimate the margin between the current vehicle state and its maximum capabilities at a sampling frequency of 100 Hz. Thereby, deviations in driving trajectories are decoupled from the results and the temporal resolution facilitates the analyses on manoeuvre specific effects. As the method makes use of maximum tire potential exploitation while respecting vehicle and trajectory constraints, it is referred to as tire potential exploitation rating (TPER).

The second evaluation method introduced in this chapter aims to quantify behavioural validity and is therefore referred to as validity quantification (VQ). In the context of near-limit vehicle operation, it is desirable that drivers interact with the simulated vehicle as similar as possible to their interaction with the physical instance of the race car. As revealed by Table 2.2 and found by Wynne et al. (2019) [111], mostly speed-related KPIs are used for DiLS validity analyses. Given the fact that racing drivers apply full throttle whenever possible to maximise the vehicles velocity on a desired path, it becomes evident that the vehicle model has a decisive impact on behavioural validity. Although there are no objections to this statement, an elimination of behavioural aspects, related to sections where drivers are limited by the vehicle's power, is required. Considering the driving task models, one could argue that methods used in relevant DiLS validation studies cover the strategic and manoeuvring level, whereas this work introduces a methodology suitable for validity analysis on the vehicle control level. It is based on driver-vehicle-interaction signals captured at OP2 of Figure 1.2. Thereby, and with the elimination of power limited sections, a reliable comparison of DiLS and track operation is obtained.

Table 2.2.: Comparison of KPIs with regard to the classification of evaluation target, observation method and temporal resolution.

Reference	**Evaluation Target**		**Observation Method**		**Temporal Resolution**		**OP**
Work	Category	Description	Category	Description	Category	Description	
Blaauw (1982) [5]	validity	system performance, driver behaviour	objective	steering wheel angle, lateral position, yaw rate, throttle pedal position, velocity	continuous	traces recorded at 4 Hz	OP3
	fidelity	compare simulator and instrumented vehicle	subjective	individual questionnaire	discrete	feedback after each task	OP3
Markkula et al. (2018) [60]	validity	driver behaviour	objective	Desired Path Yaw Rate Error Model, Modified Gordon and Magnuski Model	continuous	model deviation trace	OP2
	fidelity	perceived realism	subjective	individual questionnaire	discrete	feedback after each task	OP1
Spyridakos et al. (2020) [95]	validity	HMI evaluation	objective	task completion time, mean speed, speed variability, steering wheel reversal rates	discrete	one result per task	OP3
	validity	HMI evaluation	objective	frequency of off-road glances, Total off-road glances duration, mean off-road glange duration	discrete	one result per task	OP1
Groeger and Murphy (2020) [40]	validity	driver performance	objective	mean speed, speed stability, mean braking likelihood, mean correct lane changes, mean positional variability, mean road position	discrete	one result per task	OP3
Kolff et al. (2020) [54]	fidelity	motion fidelity, motion cueing quality	objective	absolute difference, cross-correlation, time delay, workspace management, energy consumption	discrete	one result per task per MCA	OP3, OP4
Cleij et al. [18]	fidelity	motion cueing quality	subjective	rating knob	continuous	participant continuously rates via knob	OP1, OP4
Pham and Nguyen (2021) [74]	fidelity	false cue influence on relative motion cueing quality	objective	performance indicator [76], good criterion [33]	discrete	one result per task per MCA	OP3
	fidelity	relative motion cueing quality	subjective	rate satisfaction	discrete	one result per DiLS	OP1

2.3. Tire Potential Exploitation Rating Method

Performance in the motorsport environment is a result of driver-vehicle interaction and usually quantified by lap time (t_{lap}). At a given trajectory, t_{lap} is a result of the average velocity while completing a single lap. The ability to maximise average velocity is affected in two distinct ways for a given vehicle: the vehicle's maximum capabilities, mainly characterised by power and mechanical grip, and the driver's ability of extracting the vehicle's full potential. The latter is what the TPER method aims to capture. This section is predominantly based on the publications [89] and [103]. The author's contributions are summarised on page 96.

The method is based on the quantification of an acceleration margin between maximum vehicle capabilities and a quasi-stationary treatment of vehicle states achieved by a driver in the DiLS. The latter are recorded in every run of DiLS operation and the data is saved to a logfile. To obtain an estimate of maximum capabilities, each time step of the data is treated as an independent optimisation problem. Figure 2.2 illustrates two exemplary vehicle states at time step k and time step $k+n$. The horizontal acceleration achieved by the driver is denoted $a_{\mathrm{h}}^{\mathrm{in}}$ and serves as a starting point for the estimation of the maximum attainable horizontal acceleration $a_{\mathrm{h}}^{\mathrm{oc}}$.

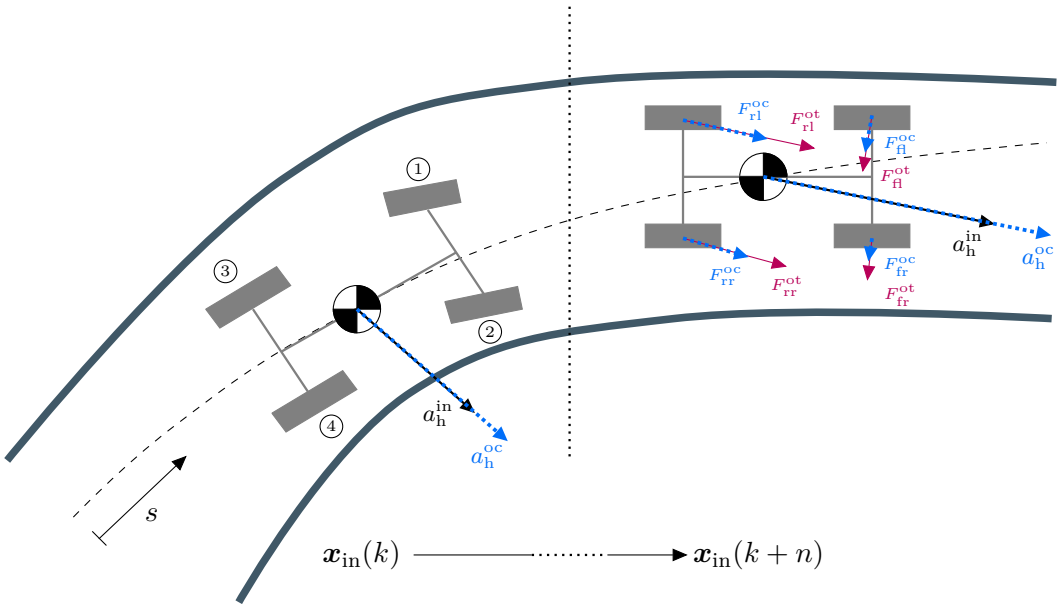

Figure 2.2.: Two track model on a path s visualised at two distinct time steps [103]. The absolute value of the initial horizontal acceleration is denoted by the vector $a_{\mathrm{h}}^{\mathrm{in}}$ whereas the theoretical maximum obtained from the TPER method is denoted $a_{\mathrm{h}}^{\mathrm{oc}}$. At time step $k+n$ the tire forces F_i^{oc} corresponding to the optimisation result are illustrated and compared to each tire's maximum force in the same direction F_i^{ot}.

In the following sections, the superscript 'in' relates to initial values obtained from logging data and superscript 'oc' relates to results obtained from the CoG acceleration optimisation procedure. The margin between the two serves as an indicator to what extent the driver extracts the full vehicle potential at the respective time step. In a second stage of the method, the tire forces which yield $a_{\mathrm{h}}^{\mathrm{oc}}$ are taken as a basis to quantify each tire's remaining margin towards its individual maximum norm of longitudinal and lateral force. Hence, this second stage of the TPER methodology neglects the kinematic relations between the tires.

As a part of the preprocessing algorithm, all samples are skipped for the evaluation where full throttle is applied which equals a request for maximum engine torque. The sections of a racetrack where this condition holds is referred to as power limited. Residual sections, where vehicle performance is limited by mechanical grip, are referred to as grip limited. To obtain the results of theoretical maximum accelerations in each time step, the optimisation problem is formulated and detailed in the following section.

2.3.1. Optimisation Problem Formulation

The method of TPER is model- and optimisation-based and follows the block diagram's structure of Figure 2.3. For every time step k of a DiLS logfile, a steering angle δ, body side slip angle β and longitudinal tire slip ratios κ_i are sought such that the horizontal acceleration of a vehicle model is maximised while retaining the trajectory given by the driver.

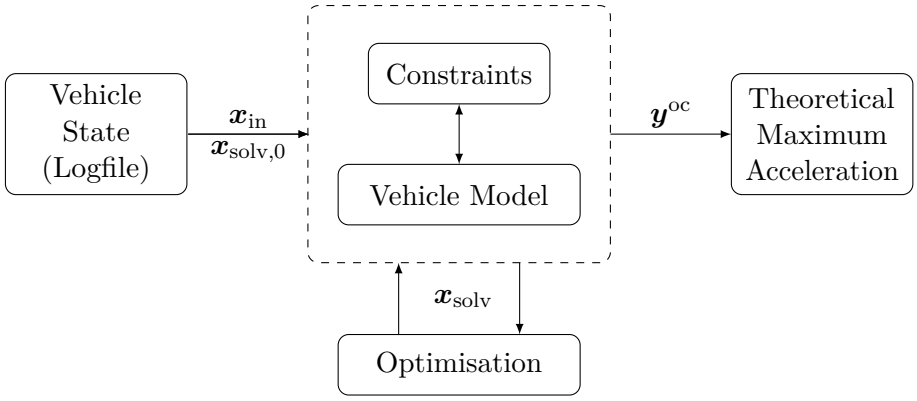

Figure 2.3.: Scheme of the optimisation process for maximum vehicle potential estimation. The input vector $\boldsymbol{x}_{\mathrm{in}}$ includes quasi-static vehicle state information, the initial values of the optimisation's decision variables are contained in the vector $\boldsymbol{x}_{\mathrm{solv},0}$ and the vector $\boldsymbol{x}_{\mathrm{solv}}$ includes the variables which are manipulated during the optimisation process. The output vector $\boldsymbol{y}^{\mathrm{oc}}$ comprises resulting longitudinal and lateral accelerations as well as tire forces.

To solve this problem statement, three prerequisites are:

- **Vehicle State Logfile:** A logfile defining the vehicle states of a certain run. This data is used to parametrise the vehicle model and the constraints for the optimisation problem of the respective time step. For example, the vertical tire loads $F_{z,i}$ are passed to the vehicle model and remain constant during the optimisation.
- **Vehicle Model:** A vehicle model, including tire model, describing longitudinal and lateral vehicle dynamics. It is aimed for minimum deviations between this model and the one used for the logfile's underlying driving simulation.
- **Constraints:** One category of constraints is introduced to retain the trajectory of the driver. This trajectory is updated in every time step of the logfile. The same applies to the second category of constraints which ensure physically feasible results by, for example, limiting the maximum driving torque at the tires according to the selected gear and the engine's capabilities.

In the further course, the general form of the optimisation problem is introduced, followed by a detailed derivation of the vehicle model and the constraints. All symbols used for the mathematical description are summarised in Table 2.3.

As the main part of the TPER methodology, a constrained nonlinear optimisation problem is solved in the form of

$$\begin{aligned}
\underset{\boldsymbol{x}_{\mathrm{solv}}}{\text{minimize}} \quad & J(\boldsymbol{x}_{\mathrm{solv}}, \boldsymbol{x}_{\mathrm{in}}, \boldsymbol{p}) && && \text{(2.4a)}\\
\text{subject to} \quad & \boldsymbol{x}_{\mathrm{solv},0} = [\delta_0, \beta_0, \kappa_{i,0}]^{\mathrm{T}} && \text{(initial state)}, && \text{(2.4b)}\\
& 0 = \boldsymbol{f}(\boldsymbol{x}_{\mathrm{solv}}, \boldsymbol{x}_{\mathrm{in}}, \boldsymbol{p}) && \text{(equality constraints)}, && \text{(2.4c)}\\
& 0 \geq \boldsymbol{h}(\boldsymbol{x}_{\mathrm{solv}}, \boldsymbol{x}_{\mathrm{in}}, \boldsymbol{p}) && \text{(inequality constraints)}. && \text{(2.4d)}
\end{aligned}$$

Its objective is to maximise the vehicle's norm of longitudinal and lateral accelerations (a_x and a_y). Transferring this objective into a minimisation problem, the cost function of Equation (2.4a) is written as

$$J\left(\boldsymbol{x}_{\mathrm{solv}}, \boldsymbol{x}_{\mathrm{in}}, \boldsymbol{p}\right) \;=\; -\sqrt{a_x^2\left(\boldsymbol{x}_{\mathrm{solv}}, \boldsymbol{x}_{\mathrm{in}}, \boldsymbol{p}\right) + a_y^2\left(\boldsymbol{x}_{\mathrm{solv}}, \boldsymbol{x}_{\mathrm{in}}, \boldsymbol{p}\right)}\,, \tag{2.5}$$

with the parameters $\boldsymbol{p} = [m, l_{\mathrm{f}}, l_{\mathrm{r}}, J_{\mathrm{zz}}]^{\mathrm{T}}$ set according to the DiL simulator's underlying model parameters and the decision variables

$$\boldsymbol{x}_{\mathrm{solv}} = [\delta\ \beta\ \kappa_i]^{\mathrm{T}}\,. \tag{2.6}$$

The initial values of the decision variables in $\boldsymbol{x}_{\mathrm{solv},0}$ are obtained from the logfile as illustrated in Figure 2.3. Similarly, the initial vehicle state vector $\boldsymbol{x}_{\mathrm{in}}$ is passed to the

algorithm and its entries are kept constant during the optimisation of one logging sample. The initial vehicle state (subscript or superscript 'in') is composed according to Equation (2.7), which reads

$$\boldsymbol{x}_{\text{in}} = [\omega_z \; v \; F_{z,i} \; \alpha_{i,n-1} \; \mu_i \; b_i \; F_{x,\text{D}} \; F_{y,\text{D}} \; \gamma_i \; r_i \; n_{\text{Engine}} \; i_{\text{Tot}}]^{\text{T}} \; . \tag{2.7}$$

The vehicle model is integrated into the optimisation algorithm in the form of equality constraints, see Equation (2.4c). It is represented by a reduced two track vehicle model for planar motion which is described on pages $565 - 661$ in [49] by Jazar (2017). The tire forces ${}_tF_{x,i}$ and ${}_tF_{y,i}$, resulting from the tire model in a local tire coordinate system, are used to obtain the differential equations of motion (2.8-2.10). All variables without any prefix subscripts relate to the vehicle fixed coordinate system according to ISO 8855 [47]. The derivation and a description of the considered coordinate systems is detailed in appendix A.1.

$$\begin{aligned} m \cdot (\dot{v}_x - \omega_z v_y) \; = \; & {}_tF_{x,\text{rl}} \cdot \cos\delta_{\text{rl}} + {}_tF_{x,\text{rr}} \cdot \cos\delta_{\text{rr}} - {}_tF_{y,\text{rl}} \cdot \sin\delta_{\text{rl}} - {}_tF_{y,\text{rr}} \cdot \sin\delta_{\text{rr}} + \\ & {}_tF_{x,\text{fl}} \cdot \cos\delta_{\text{fl}} + {}_tF_{x,\text{fr}} \cdot \cos\delta_{\text{fr}} - {}_tF_{y,\text{fl}} \cdot \sin\delta_{\text{fl}} - {}_tF_{y,\text{fr}} \cdot \sin\delta_{\text{fr}} + \\ & F_{x,\text{ext}} \end{aligned} \tag{2.8}$$

$$\begin{aligned} m \cdot (\dot{v}_y + \omega_z v_x) \; = \; & {}_tF_{x,\text{rl}} \cdot \sin\delta_{\text{rl}} + {}_tF_{x,\text{rr}} \cdot \sin\delta_{\text{rr}} + {}_tF_{y,\text{rl}} \cdot \cos\delta_{\text{rl}} + {}_tF_{y,\text{rr}} \cdot \cos\delta_{\text{rr}} + \\ & {}_tF_{x,\text{fl}} \cdot \sin\delta_{\text{fl}} + {}_tF_{x,\text{fr}} \cdot \sin\delta_{\text{fr}} + {}_tF_{y,\text{fl}} \cdot \cos\delta_{\text{fl}} + {}_tF_{y,\text{fr}} \cdot \cos\delta_{\text{fr}} + \\ & F_{y,\text{ext}} \end{aligned} \tag{2.9}$$

$$\begin{aligned} J_{zz} \cdot \dot{\omega}_z \; = \; & l_{\text{f}} \cdot ({}_tF_{x,\text{fl}} \cdot \sin\delta_{\text{fl}} + {}_tF_{x,\text{fr}} \cdot \sin\delta_{\text{fr}} + {}_tF_{y,\text{fl}} \cdot \cos\delta_{\text{fl}} + {}_tF_{y,\text{fr}} \cdot \cos\delta_{\text{fr}}) - \\ & l_{\text{r}} \cdot ({}_tF_{x,\text{rl}} \cdot \sin\delta_{\text{rl}} + {}_tF_{x,\text{rr}} \cdot \sin\delta_{\text{rr}} + {}_tF_{y,\text{rl}} \cdot \cos\delta_{\text{rl}} + {}_tF_{y,\text{rr}} \cdot \cos\delta_{\text{rr}}) + \\ & b_{\text{fr}} \cdot ({}_tF_{x,\text{fr}} \cdot \cos\delta_{\text{fr}} - {}_tF_{y,\text{fr}} \cdot \sin\delta_{\text{fr}}) + \\ & b_{\text{fl}} \cdot (-{}_tF_{x,\text{fl}} \cdot \cos\delta_{\text{fl}} + {}_tF_{y,\text{fl}} \cdot \sin\delta_{\text{fl}}) + \\ & b_{\text{rr}} \cdot ({}_tF_{x,\text{rr}} \cdot \cos\delta_{\text{rr}} - {}_tF_{y,\text{rr}} \cdot \sin\delta_{\text{rr}}) + \\ & b_{\text{rl}} \cdot (-{}_tF_{x,\text{rl}} \cdot \cos\delta_{\text{rl}} + {}_tF_{y,\text{rl}} \cdot \sin\delta_{\text{rl}}) + \\ & M_{z,\text{fl}} + M_{z,\text{fr}} + M_{z,\text{rl}} + M_{z,\text{rr}} \end{aligned} \tag{2.10}$$

The calculation of longitudinal and lateral tire forces (${}_tF_{x,i}$, ${}_tF_{y,i}$) in the respective wheel fixed coordinate system is based on a Pacejka Magic Formula tire model [72] which captures the tires' nonlinear characteristics in proximity to peak traction. The same model is used for the vehicle dynamics simulation of the considered DiL simulators within this work.

Table 2.3.: Description of the variables and parameters which are used for the TPER's optimisation problem formulation.

Symbol	Description
a_x, a_y	longitudinal and lateral vehicle acceleration
$\alpha_{i,n-1}$	tire slip angles of the previous sample
b_i	half track widths
β	vehicle side slip angle
β_0	initial vehicle side slip angle
γ_i	camber angles
δ	steering angle
δ_0	initial steering angle
δ_i	wheel steer angles (including toe)
$F_{x,\mathrm{D}}$, $F_{y,\mathrm{D}}$	longitudinal, lateral aerodynamic drag force
$F_{x,\mathrm{ext}}$	external longitudinal force
${}_tF_{x,i}$	longitudinal tire forces (wheel-fixed coordinate system)
$F_{y,\mathrm{ext}}$	external lateral force
${}_tF_{y,i}$	lateral tire forces (wheel-fixed coordinate system)
$F_{z,i}$	vertical tire loads
i_g	engaged gear
i_Tot	overall gear ratio from the engine to the tires
J_{zz}	moment of inertia around the vehicle's vertical axis
κ_i	tires' longitudinal slip ratios
$\kappa_{i,0}$	initial tires' longitudinal slip ratios
l_f	CoG distance to front axle
l_r	CoG distance to rear axle
m	vehicle mass
$M_{z,i}$	self-aligning torques
μ_i	dynamic toe angles
n_Engine	rotational speed of the engine
r_i	tire radii
T_i	braking and driving torques
v	resultant velocity of the vehicle
ω_z	angular velocity around the vehicle's vertical axis
$\dot{\omega}_z$	angular acceleration around the vehicle's vertical axis
in	superscript, variable associated to initial vehicle state
oc	superscript, variable associated to vehicle state optimised at CoG
ot	superscript, variable associated to optimisation results of tire forces

The external forces $F_{x,\text{ext}}$ and $F_{y,\text{ext}}$ acting on the planar vehicle model's CoG in longitudinal and lateral direction respectively are described by

$$\begin{aligned} F_{x,\text{ext}} &= -F_{x,\text{D}}, \\ F_{y,\text{ext}} &= F_{y,\text{D}}, \end{aligned} \tag{2.11}$$

with the longitudinal and lateral aerodynamic drag forces $F_{x,\text{D}}$ and $F_{y,\text{D}}$.

As a next step of the problem formulation, constraints limiting the vehicle states to a feasible subset are introduced. The entries of $\boldsymbol{x}_{\text{solv}}$ are directly or indirectly controlled by the driver while interacting with the vehicle. Instead of using the throttle input as a decision variable, which requires additional modelling, the slip ratios are manipulated directly. However, this creates a demand for constraints which ensure certain drive train characteristics by limiting the space of feasible solutions for the solver. Likewise, physically valid results are obtained.

In this regard, constraints affecting tire slip ratios κ_i and tire side slip angles α_i are introduced. The inequality constraints are formulated according to Equations (2.12) and (2.13) and limit the tires' side slip angles to $\alpha_{\max} = \pm 25°$ and the longitudinal slip ratios to $\kappa_{\max} = \pm 30\%$. The constraint described by Equation (2.14) specifies a maximum driving torque at the rear axle T_{r} according to the engine capabilities $T_{\text{Engine,max}}$ and the gear ratio i_{Tot}. In addition, Equation (2.15) retains the initial distribution of braking and driving torque T_i between left and right tire on the front and rear axle. Thereby, a mechanically infeasible, although optimal, torque distribution for the optimisation result is prevented. The braking torque distribution of front and rear axle is not adjustable for a driver during braking manoeuvres. Therefore the distribution is considered to remain at the same value as provided by the initial vehicle state vector. To still allow the solver the manipulation of braking and driving torques, a braking distribution (br_{dist}) constraint is introduced according to Equation (2.16). The first factor of br_{dist}, namely br_{drv}, is the constant braking distribution selected by the driver. The second factor ensures continuous differentiability for the transition between non-zero braking torque and the driving torque limitation $T_{\text{f}} \leq 0$ at the front axle as rear wheel driven cars are considered exclusively. The transition as a smooth saturation is characterised by a smoothness parameter $\epsilon_1 = 10^4$ and an offset parameter $\epsilon_2 = 0$ which are both selected empirically.

$$\left(\frac{\alpha_i}{\alpha_{\max}}\right)^2 - 1 \leq 0 \tag{2.12}$$

$$\left(\frac{\kappa_i}{\kappa_{\max}}\right)^2 - 1 \leq 0 \tag{2.13}$$

$$\begin{aligned} T_\mathrm{r} - T_\mathrm{Engine,max} \cdot i_\mathrm{Tot} \;&\leq\; 0, \text{with} \\ i_\mathrm{Tot} &= f(i_\mathrm{g}) \end{aligned} \tag{2.14}$$

$$\begin{aligned} T_\mathrm{fl}^\mathrm{oc} - T_\mathrm{fr}^\mathrm{oc} - (T_\mathrm{fl}^\mathrm{in} - T_\mathrm{fr}^\mathrm{in}) \;&=\; 0 \\ T_\mathrm{rl}^\mathrm{oc} - T_\mathrm{rr}^\mathrm{oc} - (T_\mathrm{rl}^\mathrm{in} - T_\mathrm{rr}^\mathrm{in}) \;&=\; 0 \end{aligned} \tag{2.15}$$

$$\begin{aligned} &T_\mathrm{f} - (T_\mathrm{f} + T_\mathrm{r}) \cdot br_\mathrm{dist} \;=\; 0, \text{ with} \\ &T_\mathrm{f} = T_\mathrm{fl} + T_\mathrm{fr}, \\ &T_\mathrm{r} = T_\mathrm{rl} + T_\mathrm{rr}, \\ &br_\mathrm{dist} \;\approx\; br_\mathrm{drv} \cdot \left[\frac{\arctan\Big(-\epsilon_1 \cdot (T_\mathrm{f} - \epsilon_2) \Big)}{\pi} + \frac{1}{2} \right] \end{aligned} \tag{2.16}$$

In addition to the constraints covering physical limitations, there is a second category of constraints, which serves the purpose of driving trajectory retention. The resulting trajectory of the optimisation process should match the trajectory obtained from the initial vehicle state vector. This requirement is met by retaining the initial angular acceleration $\dot{\omega}_z^\mathrm{in}$ and the direction of the horizontal acceleration. The resulting constraints are described in Equations (2.17) and (2.18).

$$\frac{a_x^\mathrm{oc}}{a_y^\mathrm{oc}} - \frac{a_x^\mathrm{in}}{a_y^\mathrm{in}} \;=\; 0 \tag{2.17}$$

$$\dot{\omega}_z^\mathrm{oc} - \dot{\omega}_z^\mathrm{in} \;=\; 0 \tag{2.18}$$

To sum up, the equations describing equality constraints (2.8-2.10) and (2.15-2.18), inequality constraints (2.12-2.14) and objective function (2.5) complete the introduced problem formulation of Equations (2.4a - 2.4d). The introduction of the optimisation output vector $\boldsymbol{y}^\mathrm{oc}$ in Equation (2.19) concludes the first stage of the TPER methodology. It contains the obtained longitudinal and lateral accelerations (a_x^oc and a_y^oc) as well as the resulting horizontal tire forces ${}_tF_{x,i}^\mathrm{oc}$ and ${}_tF_{y,i}^\mathrm{oc}$.

$$\boldsymbol{y}^\mathrm{oc} \;=\; [a_x^\mathrm{oc}, a_y^\mathrm{oc}, {}_tF_{x,i}^\mathrm{oc}, {}_tF_{y,i}^\mathrm{oc}]^\mathrm{T} \;. \tag{2.19}$$

As a second stage of the methodology, the maximum horizontal tire force is calculated using an additional optimisation problem formulation. It aims to quantify the balance of

the tire potential exploitation from the first stage's output y^{oc}. In order to obtain the maximum horizontal tire force comprising ${}_tF_{x,i}^{\mathrm{ot}}$ and ${}_tF_{y,i}^{\mathrm{ot}}$, the objective function

$$L\left(\alpha_i, \kappa_i\right) \;=\; -\sqrt{{}_tF_{x,i}^2\left(\alpha_i, \kappa_i\right) + {}_tF_{y,i}^2\left(\alpha_i, \kappa_i\right)} \tag{2.20}$$

is formulated. As the tire forces result from a Pacejka Magic Formula tire model, combined longitudinal and lateral slip effects are considered. It is worth noting, that the vertical tire load $F_{z,i}$ and camber angle γ_i are both passed to the tire model according to the value in the initial vehicle state vector $\boldsymbol{x}_{\mathrm{in}}$. The constraint which ensures that the optimised tire force vector (superscript 'ot') maintains the direction resulting from ${}_tF_{x,i}^{\mathrm{oc}}$ and ${}_tF_{y,i}^{\mathrm{oc}}$ is described by Equation (2.21) and the output vector $\boldsymbol{y}^{\mathrm{ot}}$ consists of the maximum forces at each tire ${}_tF_{x,i}^{\mathrm{ot}}$ and ${}_tF_{y,i}^{\mathrm{ot}}$ according to Equation (2.22).

$$\frac{{}_tF_{x,i}^{\mathrm{ot}}}{{}_tF_{y,i}^{\mathrm{ot}}} - \frac{{}_tF_{x,i}^{\mathrm{oc}}}{{}_tF_{y,i}^{\mathrm{oc}}} \;=\; 0 \tag{2.21}$$

$$\boldsymbol{y}^{\mathrm{ot}} \;=\; \left[{}_tF_{x,i}^{\mathrm{ot}}, {}_tF_{y,i}^{\mathrm{ot}}\right]^{\mathrm{T}} \tag{2.22}$$

The entries of this second optimisation's result vector are illustrated in Figure 2.2. Due to the independent consideration of each tire, the results do not produce feasible vehicle states. However, the deviation of horizontal tire forces between first and second stage allow incorporating vehicle setup and trajectory related aspects into the analysis. This procedure is covered in section 2.3.2.

With both optimisation problems being constrained and nonlinear, the list of potentially suitable solvers from the *MathWorks® MATLAB optimisation toolbox* reduces to *fseminf*, *fmincon* and *fminbnd*. [97] The latter supports only one-dimensional problems and is therefore dropped, whereas the *fmincon* solver fulfils all requirements. The same applies to *fseminf* which additionally allows adding an infinite number of constraints to the problem formulation by transforming the problem in a way that it can be addressed by *fmincon*. As this feature is not required to solve the described optimisation problems of the TPER methodology, the *fmincon* solver is selected. It is configured for sequential quadratic programming which iteratively transforms the nonlinear optimisation problem into quadratic programming subproblems and thereby provides stable convergence and efficient handling of nonlinear constraints. The values included in $\boldsymbol{x}_{\mathrm{solv},0}$ are passed to the solver as initial values. Within this work, two criteria are considered to accept an optimisation result as valid. The optimisation is terminated successfully if either the first order optimality condition is met or the step size drops below a tolerance of $f_{\mathrm{tol}} = 0.0001$.

2.3.2. Postprocessing

This section covers how the results of $\boldsymbol{y}^{\mathrm{oc}}$ and $\boldsymbol{y}^{\mathrm{ot}}$ are processed towards a tire potential exploitation-based evaluation. The optimisation output vector $\boldsymbol{y}^{\mathrm{oc}}$ includes maximum longitudinal and lateral accelerations ($a_{x,k}^{\mathrm{oc}}$ and $a_{y,k}^{\mathrm{oc}}$) for each sample k of the considered logfile. The maximum horizontal acceleration at each time step is derived by the vectors' euclidean norm $a_{h,k}^{\mathrm{oc}}$ according to Equation (2.23). The respective horizontal acceleration achieved by the driver $a_{h,k}^{\mathrm{in}}$ is calculated by Equation (2.24) in the same way. Subsequently, the relative tire potential margin (TPM) of time step k is calculated by Equation (2.25).

$$a_{h,k}^{\mathrm{oc}} = \sqrt{(a_{x,k}^{\mathrm{oc}})^2 + (a_{y,k}^{\mathrm{oc}})^2} \tag{2.23}$$

$$a_{h,k}^{\mathrm{in}} = \sqrt{(a_{x,k}^{\mathrm{in}})^2 + (a_{y,k}^{\mathrm{in}})^2} \tag{2.24}$$

$$TPM_k = [1 - \frac{a_{h,k}^{\mathrm{in}}}{a_{h,k}^{\mathrm{oc}}}] \cdot 100\% \tag{2.25}$$

An exemplary result of the TPM while cornering is depicted in the lower row of Figure 2.4. The upper row displays the steering angle δ, throttle pedal position r_{Thr} and brake pressure p_{Brk}, all of which are normalised by their respective maximum absolute value of the displayed manoeuvre. During the initial braking phase between 0.5 s and 1 s, the TPM linearly decreases from the maximum tire potential margin ($TPM = 100\%$) and approaches almost 0% at the point of maximum brake pressure B_{max}. The initially high TPM is mainly caused by the finite gradient of brake pressure build-up. In the area of maximum brake pressure at $t = 1\,\mathrm{s}$, the TPM increases to 15%. In this particular case, it is caused by minor wheel locking, which is characterised by the longitudinal braking slip ratio exceeding its optimum value with regard to the resulting friction coefficient. Starting from the point of maximum brake pressure B_{max}, the entry phase is defined which ends with the off-brake point B_{off}. During that phase, the TPM remains within 10% and 0%. The same applies to the mid-corner phase which commences at the end of the entry phase and ends at the on-throttle point T_{on} where the driver picks up the throttle. At the initial throttle application ($t = 4\,\mathrm{s}$), the driver keeps the highest acceleration margin within this corner and therefore the value increases to $TPM = 28\%$. There is no critical vehicle state in terms of vehicle stability (i.e., oversteer) present which is why the driver is assumed to retain a certain stability margin at this point. The spike at $t = 5.2\,\mathrm{s}$ is almost the same severity but it results from an on-power oversteer as indicated by the driver's reaction (i.e., clearly reduced steering angle although no counter steer, drop in throttle pedal position) to stabilise the vehicle. The TPM calculation is suspended as soon as full throttle is applied which also marks the end of a corner's exit phase. To conclude,

the TPM is an indicator for the overall acceleration margin under consideration of the drivers' chosen trajectory. It should therefore serve as a KPI to evaluate the vehicle control or handling performance of a driver.

In addition to that, a vehicle trajectory related KPI is obtained using the optimisation results of individual tire forces $\boldsymbol{y}^{\mathrm{ot}}$ from Equation (2.22). For that purpose, the absolute horizontal forces are calculated per tire by the following two equations:

$$F_{\mathrm{h},i}^{\mathrm{oc}} = \sqrt{({}_tF_{\mathrm{x},i}^{\mathrm{oc}})^2 + ({}_tF_{\mathrm{y},i}^{\mathrm{oc}})^2}, \tag{2.26}$$

$$F_{\mathrm{h},i}^{\mathrm{ot}} = \sqrt{({}_tF_{\mathrm{x},i}^{\mathrm{ot}})^2 + ({}_tF_{\mathrm{y},i}^{\mathrm{ot}})^2}. \tag{2.27}$$

The results are cumulated within the respective optimisation results according to Equation (2.28) and (2.29).

$$F_{\mathrm{h}}^{\mathrm{oc}} = F_{\mathrm{h,fl}}^{\mathrm{oc}} + F_{\mathrm{h,fr}}^{\mathrm{oc}} + F_{\mathrm{h,rl}}^{\mathrm{oc}} + F_{\mathrm{h,rr}}^{\mathrm{oc}} \tag{2.28}$$

$$F_{\mathrm{h}}^{\mathrm{ot}} = F_{\mathrm{h,fl}}^{\mathrm{ot}} + F_{\mathrm{h,fr}}^{\mathrm{ot}} + F_{\mathrm{h,rl}}^{\mathrm{ot}} + F_{\mathrm{h,rr}}^{\mathrm{ot}} \tag{2.29}$$

The maximum tire forces $F_{\mathrm{h},i}^{\mathrm{oc}}$ which are feasible at the given trajectory are compared to the maximum tire forces attainable without trajectory and vehicle kinematics related constraints ($F_{\mathrm{h},i}^{\mathrm{ot}}$). This comparison yields a second KPI which describes how balanced the TPM is across the four tires. It is therefore referred to as the balance of tire potential margin TPB and described by Equation (2.30).

$$TPB_k = [1 - \frac{F_{\mathrm{h},k}^{\mathrm{oc}}}{F_{\mathrm{h},k}^{\mathrm{ot}}}] \cdot 100\% \tag{2.30}$$

Although the vehicle states obtained from the tire force optimisation are not feasible to be reached, the results are useful to investigate how well-suited the driver's chosen trajectory is for the given vehicle setup. If both, the vehicle and its setup, remain identical, the TPB reveals relative effects related to the vehicle's balance on the given driving trajectory. The analysis of time-based TPM or TPB results provides insights into a driver's performance, for example in a particular corner of the race track. However, as the quantity of data increases for analyses of multiple laps, race tracks or drivers, scalar KPIs reveal effects more intuitively. For that purpose, mean TPM and TPB results are calculated for the entire cornering phase as well as for the entry-, mid- and exit-phase individually. Equations (2.31) and (2.32) summarise the calculation basis with

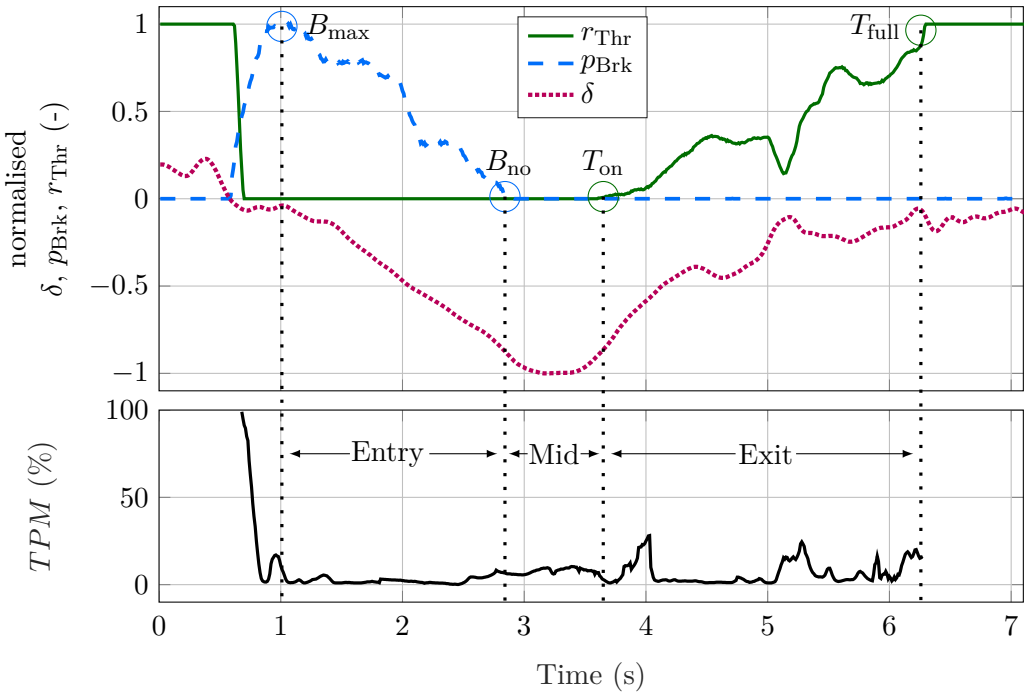

Figure 2.4.: Exemplary TPM result and detection of characteristic cornering points in throttle position r_{Thr} and brake pressure p_{Brk} used to define corner entry-, mid- and exit-phase.
In chronological sequence, there are max-brake (B_{max}) and no-brake (B_{no}) points, followed by on-throttle (T_{on}) and full-throttle (T_{full}) points.

$\mathrm{p} \in \{\mathrm{All}, \mathrm{Entry}, \mathrm{Mid}, \mathrm{Exit}\}$, $k_{\mathrm{p},1}$ representing the section's first sample index and $k_{\mathrm{p,end}}$ representing the section's last sample index. In the case of $\mathrm{p} = \mathrm{All}$, $k_{\mathrm{p},1}$ equals the first index of the entry phase and $k_{\mathrm{s,end}}$ is set to the last index of the exit phase.

$$TPM_{\mathrm{p}} = \frac{1}{k_{\mathrm{p,end}} - k_{\mathrm{p},1}} \cdot \sum_{k=k_{\mathrm{p},1}}^{k_{\mathrm{p,end}}} TPM_i \tag{2.31}$$

$$TPB_{\mathrm{p}} = \frac{1}{k_{\mathrm{p,end}} - k_{\mathrm{p},1}} \cdot \sum_{k=k_{\mathrm{p},1}}^{k_{\mathrm{p,end}}} TPB_i \tag{2.32}$$

2.3.3. Model Validation

The optimisation results' validity is reviewed for the particular use case of near-limit vehicle operation. The validation is based on a comparison of the underlying models of DiLS and TPER. To obtain comparable results, $\boldsymbol{x}_{\text{in}}$ is passed to the TPER vehicle model but the optimisation process is disabled. Likewise, the resulting output vector should match the accelerations of the corresponding logfile's time step. The described validation method is applied to selected runs of the studies of chapter 4 and results are summarised in Table 2.4. Absolute and relative errors of lateral, longitudinal and combined horizontal accelerations are represented by their maximum and mean values as well as their standard deviation and 95% quantile. The results show a mean relative error of 1% for the combined horizontal acceleration error e_h^{rel}. This particular error is most relevant for the TPER methodology as it directly propagates to the TPM results and characterises the related accuracy. Furthermore, it can be stated that the model is accurate within 3% with a confidence of 95%. Since the related KPIs are applied to identify relative effects rather than analyse the absolute tire potential exploitation, the low relative error confirms acceptable model validity.

2.3.4. Limitations

Although the approach proved to provide detailed insights into time-varying driver performance in a preliminary study [89] and in Figure 2.4, it comes with a few known limitations. The approach assumes tire loads to remain constant during the optimisation process. However, due to the deviation between initial and maximum horizontal acceleration, a change in tire loads is induced which in turn affects the maximum acceleration attainable. This leads to the acceleration margin being overestimated by the TPER. A dynamic load transfer due to high accelerations would reduce maximum vehicle capabilities and

Table 2.4.: Validation of the underlying modelling approach of the Tire Potential Exploitation Rating.
Errors between DiLS vehicle model accelerations and the accelerations returned by the TPER vehicle model without optimisation. The results are listed separately for longitudinal, lateral and combined horizontal errors as well as in absolute and relative terms.

Error	**Maximum**	**Mean**	**Standard Deviation**	95% **quantile**
e_x^{abs}: absolute longitudinal	$3.2\,\text{m}\,\text{s}^{-2}$	$0.1\,\text{m}\,\text{s}^{-2}$	$0.1\,\text{m}\,\text{s}^{-2}$	$0.2\,\text{m}\,\text{s}^{-2}$
e_y^{abs}: absolute lateral	$5.1\,\text{m}\,\text{s}^{-2}$	$0.4\,\text{m}\,\text{s}^{-2}$	$0.3\,\text{m}\,\text{s}^{-2}$	$0.5\,\text{m}\,\text{s}^{-2}$
e_h^{abs}: absolute combined horizontal	$4.9\,\text{m}\,\text{s}^{-2}$	$0.3\,\text{m}\,\text{s}^{-2}$	$0.3\,\text{m}\,\text{s}^{-2}$	$0.5\,\text{m}\,\text{s}^{-2}$
e_x^{rel}: relative longitudinal	1.3	0.02	0.03	0.02
e_y^{rel}: relative lateral	0.4	0.02	0.02	0.04
e_h^{rel}: relative combined horizontal	0.4	0.01	0.02	0.03

therefore reduce the margin between initial and maximum horizontal acceleration. However, the smaller the margin, the smaller the effect of this particular limitation. Another limitation concerns model validity. Due to the tire model's lack of continuous differentiability, minor modifications are applied for the optimisation-based approach. These modifications mainly concern approximations for sign functions. Another simplification is related to the steering system. Tire steering angles are calculated employing a linear relation from the steering wheel angle and an offset equal to the actual tire toe angles. Caused by this model inaccuracy, an error propagates through the vehicle model to the tire model. However, as suggested by Kutluay et al. (2014) [57], "[a] model's validity is only defined within the limits of [...] the intended application" which is what is claimed at this stage.

2.4. Validity Quantification Method

Driving a vehicle, particularly in the area of near-limit handling, is a multisensory integration task for human drivers. [9] In driving simulation, the sensory information are provided by the cueing systems introduced in chapter 1 and Figure 1.2. The sum of perceptions is processed by the driver who establishes stabilising motor routines [59] which are also referred to as perception reaction automatisms [23]. The proposed method aims to capture the reaction part of these automatisms, which in this context are inseparable from feed-forward actions of the driver, by analysing the driver-vehicle interaction at OP2 of Figure 1.2. Parts of the following sections, including the fundamental idea of the methodology and a preliminary analysis is published in [91]. The author's contribution is listed on page 96. However, significant improvements are developed and applied within this work.

The minimum interaction channels required to operate a considerable race car are throttle, brake and steering wheel actuation. Thus, all three of them are considered to quantify behavioural validity. In order to obtain a scalar KPI, multiple metrics are selected first which describe a driver's braking, steering and throttle actuation characteristics separately and holistically. A fourth dimension is added to describe their temporal interrelations. The separate consideration allows to evaluate each of the four subscales individually. Another benefit is based on the assumption of orthogonality between the subscales due to the physically separated actuation of the throttle pedal, brake pedal and steering wheel. Orthogonality in this context is required to combine the subscales to a scalar validity indicator using an euclidean distance concept. The selection of descriptive metrics as well as the derivation of a combined validity indicator are introduced in the following sections.

2.4.1. Metrics Selection

Manifold metrics aiming to describe driving behaviour at different levels of a driving task are published by Wörle (2019) [109] and on pages 155 – 184 of Trzesniowski (2017) [99]. Possible applications of these metrics are related to driver characterisation, partially in combination with machine learning approaches. [104, 110, 108] The metric selection process of this section comprises two phases. First, a list of metrics aiming to capture the characteristics of each subscale holistically is picked from [109]. Table 2.5 lists the initial selection of metrics. It includes detailed descriptions which in combination with the definition of characteristic cornering points according to Figure 2.5 confer each metric an illustrative meaning. Selected features of the temporal interrelation subscale are marked in the upper row of Figure 2.5 which provides an overlay of normalised throttle pedal position r_{Thr}, brake pressure p_{Brk} and steering wheel angle δ.

In a second step, the metric space dimensionality and therewith complexity is reduced while obtaining a meaningful measure of proximity is facilitated. [1] The objective of this step is to remove redundant descriptions of a certain characteristic. As an example, the number of local maxima in the throttle pedal position signal r_{Thr} ($NThrPeaks$, see Table 2.5) and the number of zero-crossing of the throttle pedal position's derivative $\dot{r}_{\mathrm{Thr}}$ ($NdThrZero$, see Table 2.5) are considered. For the detection of a local maximum in the signal r_{Thr} a zero crossing of $\dot{r}_{\mathrm{Thr}}$ is a necessary but not sufficient condition. Therefore, the metric $NdThrZero$ captures the same (and more) characteristics as $NThrPeaks$. In order to not assign a higher weighting on this particular characteristic implicitly, it should be captured by one metric only which is why $NThrPeaks$ is neglected. The following paragraph describes the methodology for metric selection or, in other words, dimensionality reduction.

The process is based on correlation analyses within each subscale using the Pearson correlation coefficient r. Its results between all metrics of the throttle subscale are listed in Table 2.6. As the method aims to describe each signal's characteristics without redundancies, a correlation threshold is introduced and set to $r_{\mathrm{Thrshld}} = 0.6$, above which a descriptive metric is dropped. The exact value is obtained empirically as a trade-off between redundancy minimisation and a holistic description of the subscale characteristics. Taking $NdThrZero$ as an example, the metric shows a correlation above the threshold to $NThrPeaks$ and $rd2ThrRmse$. The decision of which metric is dropped is based on a pairwise ranking of their mean correlation coefficients within the subscale. The mean values are listed in the bottom row of Table 2.6. In this particular case, $NdThrZero$ is kept for further analyses with a mean correlation coefficient within the subscale of $r = 0.34$ while $NThrPeaks$ ($r = 0.37$) and $rd2ThrRmse$ ($r = 0.45$) are dropped. The same procedure is applied to the entire list of Table 2.5. Finally, the selection is reduced to 23 items which are highlighted in the same Table by the rightmost column.

Table 2.5.: Selected metrics for the description of race drivers' behaviour from ([109]). They characterise driver-vehicle interaction at the vehicle control level of a driving task. Metric IDs are unique within each subscale. The rightmost column indicates which metrics are considered for the proposed VQ method after dimensionality reduction.

Subscale	ID	Metric Name	Description	VQ
Throttle (Thr)	T.1	$drThrOff$	Gradient of r_{Thr} between T_{off} and T_{no}	X
	T.2	$drThrOn$	Gradient of r_{Thr} between T_{on} and T_{full}	X
	T.3	$rThrRmseLin$	RMSE of r_{Thr} respective to a linear approximation between T_{on} and T_{full}	X
	T.4	$rThrGradInit$	Gradient of r_{Thr} in proximity of T_{on}	X
	T.5	$rThrGradEnd$	Gradient of r_{Thr} in proximity of T_{full}	X
	T.6	$rdThrRmse$	RMSE of $\dot{r}_{\text{Thr}}$ to zero	
	T.7	$rd2ThrRmse$	RMSE of $\ddot{r}_{\text{Thr}}$ to zero	
	T.8	$rdThrVar$	Variance of $\dot{r}_{\text{Thr}}$	
	T.9	$rd2ThrVar$	Variance of $\ddot{r}_{\text{Thr}}$	X
	T.10	$NThrPeaks$	No. local maxima in r_{Thr} between T_{on} and T_{full}	
	T.11	$NdThrZero$	No. zero crossings in $\dot{r}_{\text{Thr}}$ between T_{on} and T_{full}	X
Brake (Brk)	B.1	$dpBrkOff$	Gradient of p_{Brk} between B_{max} and B_{no}	
	B.2	$dpBrkOffNorm$	Normalised gradient of p_{Brk} between B_{max} and B_{no}	X
	B.3	$dpBrkOn$	Gradient of p_{Brk} between B_{on} and B_{max}	
	B.4	$dpBrkOnNorm$	Normalised gradient of p_{Brk} between B_{on} and B_{max}	X
	B.5	$pBrkRmseLin$	RMSE of p_{Brk} respective to a linear approximation between B_{max} and B_{no}	X
	B.6	$pBrkMax$	Maximum value of p_{Brk}	X
	B.7	$pBrkMaxWidth$	Width of plateau in proximity to B_{max}	X
	B.8	$pBrkInitGrad$	Gradient of p_{Brk} in proximity to B_{on}	X
	B.9	$rdBrkRmse$	RMSE of $\dot{p}_{\text{Brk}}$ to zero	
	B.10	$rd2BrkRmse$	RMSE of $\ddot{p}_{\text{Brk}}$ to zero	
	B.11	$rd2BrkVar$	Variance of $\ddot{p}_{\text{Brk}}$	
	B.12	$NBrkPeaks$	No. local maxima in p_{Brk}	
	B.13	$NdBrkZero$	No. zero crossings in $\dot{p}_{\text{Brk}}$	X
Steering (Str)	S.1	$aStrMax$	Maximum value of δ_{Str}	X
	S.2	$aStrRange$	Value range of δ_{Str}	X
	S.3	$dStrRange$	Value range of $\dot{\delta}_{\text{Str}}$	X
	S.4	$rdStrVar$	Variance of $\dot{\delta}_{\text{Str}}$	X
	S.5	$rd2StrVar$	Variance of $\ddot{\delta}_{\text{Str}}$	
	S.6	$rdStrRmse$	RMSE of $\dot{\delta}_{\text{Str}}$ to zero	X
	S.7	$rd2StrRmse$	RMSE of $\ddot{\delta}_{\text{Str}}$ to zero	
	S.8	$NStrPeaks$	No. local maxima in RMSE of δ_{Str}	
	S.9	$NdStrZero$	No. zero crossing in $\dot{\delta}_{\text{Str}}$	X
Temporal Inter-relation (Rlt)	R.1	$tBrkDly$	Absolute time between T_{off} and B_{on}	X
	R.2	$tRollAbs$	Absolute time between B_{no} and T_{on}	
	R.3	$tRollRel$	Time between B_{no} and T_{on} relative to $T_{\text{full}} - T_{\text{off}}$	X
	R.4	$tTrailRel$	Time between S_{in} and B_{no} relative to $T_{\text{full}} - T_{\text{off}}$	X
	R.5	$sTrailRel$	Distance covered between S_{in} and B_{no} relative to distance covered in $T_{\text{full}} - T_{\text{off}}$	

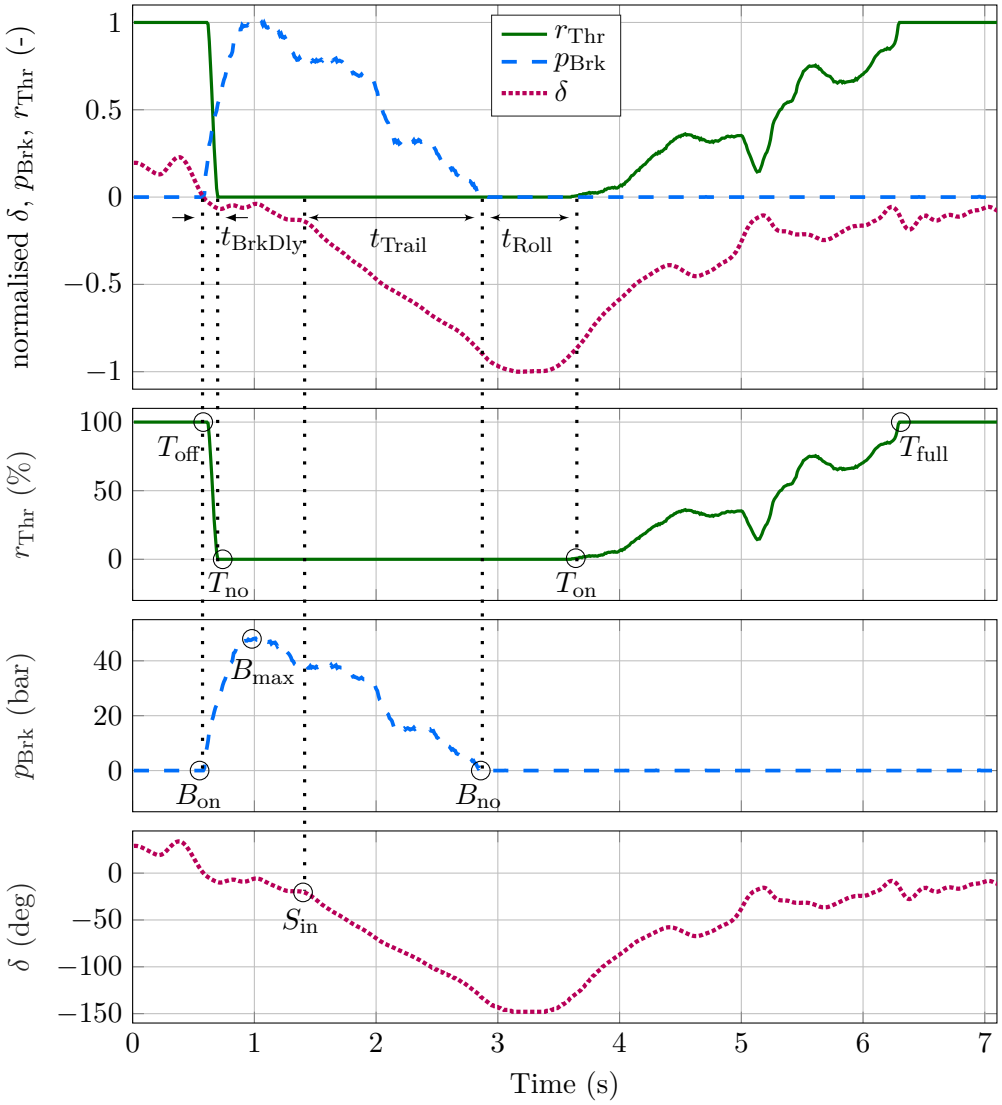

Figure 2.5.: Detection of characteristic cornering points in throttle position r_{Thr}, brake pressure p_{Brk} and steering angle δ signals.
In chronological sequence, there are off-throttle (T_{off}), no-throttle (T_{no}), on-throttle (T_{on}) and full-throttle (T_{full}) point, on-brake (B_{on}), max-brake (B_{max}) and no-brake (B_{no}) point as well as the steering turn-in point (S_{in}).

2.4.2. Distance Concept

A suitable distance concept should measure the proximity of racing drivers' behaviour between DiLS and real-world operation. The previously described metrics to characterise driver-vehicle interaction form the basis of the proposed concept. The following requirements are defined for the concept to meet:

- Universal applicability to selected metrics: The metrics' results are considered random variables which show diverse probability distributions. The distance concept must be able to cope with this property.
- Avoidance of over-idealisation: Even if median or mean values of a random variable are identical, their actual distributions may differ substantially which must be captured.
- Normalised distance range: Distances within each metric space are supposed to be aggregated to obtain a scalar validity indicator. Therefore, distances are required to be normalised.

The last requirement is motivated by the resulting metric data being highly heterogeneous. Not only do the results differ in magnitude, but units, distributions and number of metrics per subscale are manifold. There are two methods which are frequently used to obtain meaningful measures of proximity of high dimensional and heterogeneous data. One is based on aggregation after component-wise proximity evaluation which may include standardisation and the other concept demands for a transformation of heterogeneous data into homogeneous data. [79] The first approach is used for the validity quantification method.

Table 2.6.: Correlation matrix of initially selected metrics in the Throttle subscale. Pearson correlation coefficients $r \geq 0.6$ are highlighted and the affected metrics are dropped according to their mean correlation coefficient within the subscale.

ID	T.1	T.2	T.3	T.4	T.5	T.6	T.7	T.8	T.9	T.10	T.11
T.1		-0.34	-0.12	-0.04	-0.25	0.055	0.42	0.12	0.107	0.59	0.51
T.2	-0.34		0.00	0.27	0.58	0.37	-0.034	0.50	0.59	-0.44	-0.55
T.3	-0.12	0.00		0.13	0.20	0.52	0.31	0.39	0.10	0.08	0.15
T.4	-0.04	0.27	0.13		-0.16	0.06	-0.13	0.06	0.01	-0.21	-0.24
T.5	-0.25	0.58	0.20	-0.16		0.43	0.22	0.52	0.51	-0.13	-0.20
T.6	0.05	0.37	0.52	0.06	0.43		0.83	0.81	0.63	0.41	0.28
T.7	0.42	-0.03	0.31	-0.13	0.22	0.83		0.68	0.57	0.73	0.62
T.8	0.12	0.50	0.39	0.06	0.52	0.81	0.68		0.82	0.17	0.03
T.9	0.11	0.59	0.10	0.01	0.51	0.63	0.57	0.82		0.12	-0.01
T.10	0.59	-0.44	0.08	-0.21	-0.13	0.41	0.73	0.17	0.12		0.82
T.11	0.51	-0.55	0.15	-0.24	-0.20	0.28	0.62	0.03	-0.01	0.82	
mean	0.26	0.37	0.20	0.13	0.32	0.44	0.45	0.41	0.35	0.37	0.34

As the metrics are applied repeatedly for all grip limited sections in multiple laps, a probability distribution can be obtained. Therefore, measuring proximity in this context is to be considered a statistical rather than determinate task. [92] An exemplary histogram of the *rThrRmseLin* metric's distribution for track operation is depicted in Figure 2.6. The metric describes the root mean square error of the throttle pedal position r_{Thr} respective to a linear approximation between the points T_{on} and T_{full} which are illustrated in Figure 2.5. Taking into account the entire set of metrics, most but not all resulting random variables follow the characteristics of a gaussian or alpha-stable distribution. For that reason and to avoid over-idealisation of, for example, multimodal distributions, a kernel density estimation is used. The kernel density estimator $\hat{f}_b(x)$ is constructed according to Equation (2.33) and estimates the probability density function (pdf) of a random variable x. Distinct observations of the random variable are represented by x_k, n denotes the total number of observations and b is the bandwidth. The latter is a free parameter affecting the pdf's smoothness. The term $\frac{1}{n \cdot b}$ ensures that Equation (2.34) is satisfied. Within this work, a gaussian kernel function $k(u)$ according to Equation (2.35) is applied, with $u = \frac{x_k - x}{b}$.

$$\hat{f}_b(x) = \frac{1}{n \cdot b} \cdot \sum_{k=1}^{n} k(\frac{x_k - x}{b}) \tag{2.33}$$

$$\int \hat{f}_b(x) \mathrm{d}x = 1 \tag{2.34}$$

$$k(u) = \frac{1}{\sqrt{2\pi}} e^{-\frac{u^2}{2}} \tag{2.35}$$

The pdf corresponding to *rThrRmseLin* for track operation obtained by a kernel density estimation is denoted f_{TRK} and displayed in Figure 2.6. The same kernel density estimation method is used to calculate the pdfs of two exemplary DiLS settings described by f_{SIM_1} and f_{SIM_2}. As an illustrative example one could imagine subscript SIM_1 relating to a DiLS in normal condition and SIM_2 relating to the same DiLS but with disable motion system. It appears that all three distributions of *rThrRmseLin* share approximately the same mean values which would, if this measure is used for proximity quantification, correspond to minimum distance between both DiL and track operation. What is more, a distance concept based on mean, median or mode requires additional normalisation. The same holds for the Bhattacharyya similarity. [3]

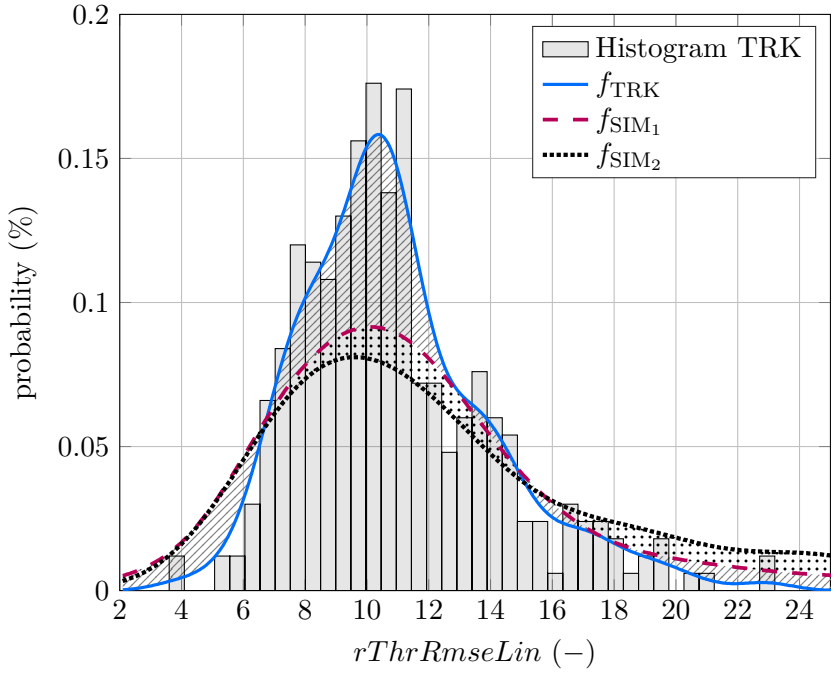

Figure 2.6.: Exemplary fitted probability distributions of the RMSE of r_{Thr}.
The metric captures the RMSE respective to a linear approximation between T_{on} and T_{full} (rThrRmseLin) obtained from three different scenarios: track operation (TRK), simulator operation with setup 1 (SIM_1) and simulator operation with setup 2 (SIM_2). The histogram illustrates the metric's distribution used for kernel density estimation resulting in f_{TRK}.

By contrast, the Hellinger distance takes values from 0 to 1 and is defined according to the Equation

$$H(f_{\mathrm{TRK}}, f_{\mathrm{SIM}}) = \frac{1}{\sqrt{2}} \sqrt{\sum_{k=1}^{end} \left(\sqrt{f_{\mathrm{TRK},k}} - \sqrt{f_{\mathrm{SIM},k}} \right)^2} . \tag{2.36}$$

A result of $H = 1$ corresponds to maximum distance, which is characterised by no overlapping of the considered pdfs and illustrated in Figure 2.7(a). It is worth noting that $H = 1$ holds for both DiLS distributions in this example. By contrast, Figure 2.7(b) shows one example of $H \approx 0$ which characterises minimum distance. While both of the previous examples are constructed for demonstration, Figure 2.6 relates to the true results of $rThrRmseLin$. The Hellinger distance is calculated between both DiL setup pdfs f_{SIM_1}, f_{SIM_2} and the track operation pdf f_{TRK}. The result can be interpreted as the area enclosed by the pdfs of DiLS operation with track operation. In this case, $H(f_{\mathrm{TRK}}, f_{\mathrm{SIM}_1}) < H(f_{\mathrm{TRK}}, f_{\mathrm{SIM}_2})$ is identified.

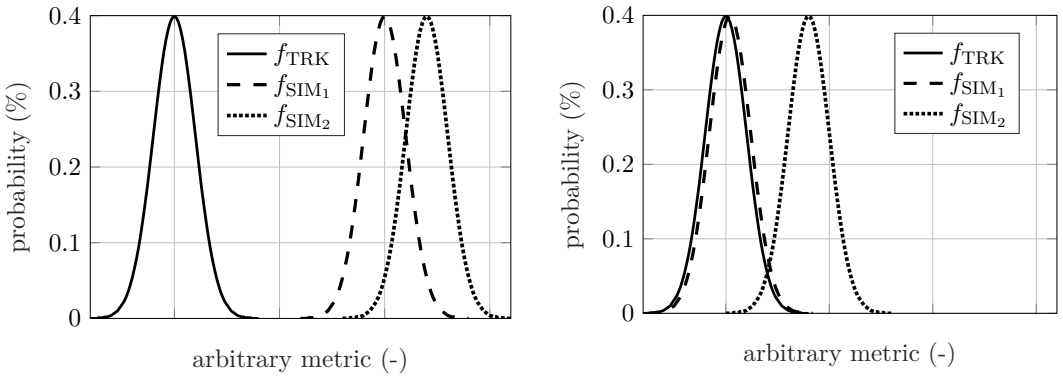

(a) $H(f_{\mathrm{TRK}}, f_{\mathrm{SIM}_1}) = H(f_{\mathrm{TRK}}, f_{\mathrm{SIM}_2}) = 1$

(b) $H(f_{\mathrm{TRK}}, f_{\mathrm{SIM}_1}) \approx 0,\ 0 < H(f_{\mathrm{TRK}}, f_{\mathrm{SIM}_2}) < 1$

Figure 2.7.: Illustration of maximum and minimum Hellinger distance characterised by $H = 1$ and $H = 0$ respectively.
The left figure shows that there is an infinite set of distributions corresponding to $H = 1$. Therefore, the method can not distinguish between them. If the pdfs are overlapping with the respective reference pdf (f_{TRK}) a comparison of distances becomes feasible as depicted in the right figure.

Given this approach, all of the requirements defined at the beginning of this section are met. The kernel density estimation ensures that the workflow is equally applicable for diverse probability distributions of the metrics introduced in the previous section. The pdf estimation prevents an over-idealisation of the actual distributions. Finally, all distances are normalised and retain within a range of $[0, 1]$ which is due to the attributes of the Hellinger distance.

As a final step, the validity scores are defined for each of the four subscales individually and on an overall validity scale. Within each subscale, the scores are based on the mean of the Hellinger distances. On the basis of the Equation

$$VI_{\mathrm{sub}} = \left[\frac{1}{n_{\mathrm{sub}}} \cdot \sum_{ID=1}^{n_{\mathrm{sub}}} H(f_{\mathrm{ID,TRK}}, f_{\mathrm{ID,SIM}})\right] \cdot 100\% \ , \tag{2.37}$$

the subscale validity indicators VI_{sub} are given. The index sub describes the particular subscale and therefore follows $\mathrm{sub} \in \{\mathrm{Thr}, \mathrm{Brk}, \mathrm{Str}, \mathrm{Rlt}\}$. The metric identifier is ID and n_{sub} denotes the number of metrics in the respective subscale. The maximum VI_{sub} score of 100% is obtained if all corresponding pdfs $f_{ID,\mathrm{TRK}}$ and $f_{ID,\mathrm{SIM}}$ are identical as depicted in Figure 2.7(b) for $H(f_{\mathrm{TRK}}, f_{\mathrm{SIM}_1})$.

The overall validity indicator VI is based on the euclidean distance d_{scales} between the cumulated results of each subscale which is expressed as

$$d_{\text{scales}} = \Bigg[\Bigg(\sum_{ID=1}^{n_{\text{Thr}}} H(f_{ID,\text{TRK}}, f_{ID,\text{SIM}}) \Bigg)^2 + \Bigg(\sum_{ID=1}^{n_{\text{Brk}}} H(f_{ID,\text{TRK}}, f_{ID,\text{SIM}}) \Bigg)^2 + \Bigg(\sum_{ID=1}^{n_{\text{Str}}} H(f_{ID,\text{TRK}}, f_{\text{ID,SIM}}) \Bigg)^2 + \Bigg(\sum_{ID=1}^{n_{\text{Rlt}}} H(f_{ID,\text{TRK}}, f_{ID,\text{SIM}}) \Bigg)^2 \Bigg]^{\frac{1}{2}} . \tag{2.38}$$

The index ID denotes the metric ID within the respective subscale. For the assessment of validity, the distance indicator d_{scales} is rewritten to

$$VI = (1 - \frac{d_{\text{scales}}}{\sqrt{4}}) \cdot 100\% \ , \tag{2.39}$$

such that it provides results in the range of $[0\%, 100\%]$.

2.4.3. Limitations

This section is devoted to addressing a few known limitations of the proposed VQ methodology. As indicated in the previous section there are multiple approaches to obtain measures of proximity. In particular for heterogeneous data, there is no universally valid method and hence the same data may lead to different views of proximity [79]. This implies that $VI = 100\%$ refers to absolute behavioural validity only in the sense of the proposed VQ. Within the proposed methodology, the evaluation of absolute and relative effects remain unaffected.

Although it is claimed in section 2.4.2 that over-idealisation is avoided by the kernel density estimation, the association of a single indicator to the proximity of pdfs is referred to as such by some researchers [92]. A hypothetical, illustrative example is created by three pdfs, whereof one represents the reference pdf. In case both of the residual pdfs do not overlap with the reference pdf (see Figure 2.7(a)), both their Hellinger distances are $H = 1$. In this particular case, the VQ methodology can not identify any effects, no matter what the effect size may be.

Finally, it should be noted that the proposed method is considered most suitable for the vehicle control task where professional racing drivers operate a vehicle close to its maximum capabilities. It is assumed that the method is not limited to motorsport scenarios as near-limit vehicle handling is found in road car related use cases, i.e. avoidance manoeuvres. However, the author does not claim universal applicability to validate the strategic or manoeuvring levels of a driving task.

3. Motion Cueing

This chapter is devoted to Motion Cues (MCs) and the algorithms required to translate a virtual vehicle's motion into MCs. The so-called Motion Cueing Algorithm (MCA) has been introduced in flight simulation around 1970 [87] and was applied in driving simulation subsequently. Since their first application in this area, MCAs have been studied and developed in manifold ways. The first part of this chapter covers the theory and working principles of state of the art MCAs. The second part introduces an MCA which is particularly suitable for the scope of identifying relevant motion cues for near-limit vehicle operation within the framework of a four DoF motion simulator.

3.1. State of the Art

Selected MCA approaches are described in this section including the presentation of results from relevant publications. Mainly two distinct categories of MCAs are discussed: Those based on mathematical optimisation on the one hand and filter- or scaling-based MCAs on the other hand. The latter are introduced in the following subsection.

3.1.1. Filter- and Scaling-based Motion Cueing

Despite the effort being put into MCA research, filter- and scaling-based approaches still represent the most frequently used method in practice. [10] For that reason, this type of MCA is also referred to as the classical filter approach. It enables fast implementation and robust execution. Its structure is following the illustration of Figure 3.1. The inputs $\boldsymbol{a}_\mathrm{v}$ and $\boldsymbol{\omega}_\mathrm{v}$ denote translational accelerations and rotational rates of a virtual vehicle. The MCA's outputs are simulator motion demands (i.e., translational acceleration $\boldsymbol{a}_\mathrm{s}$ and rotational rates $\boldsymbol{\omega}_\mathrm{s}$) for the motion system, with $\dim(\mathrm{s}) \leq \dim(\mathrm{v})$ assuming nun-redundant DoF actuation. Depending on the motion platform's architecture, a certain transformation of coordinate systems is required to obtain feasible motion demands. For simplicity reasons, these transformations are not integrated into Figure 3.1. The following paragraphs describe the individual components responsible for the MCA's input-output transfer characteristics in more detail.

The first operation on input signals is scaling. These blocks partially address the limited workspace of a DiLS and require adaptation to each motion system's capabilities. An overall motion scaling of $K = 0.5$ to $K = 0.7$ is found to be rated subjectively higher by the participants than a scaling of 1 in several experimental studies. [2, 33]. Lower values

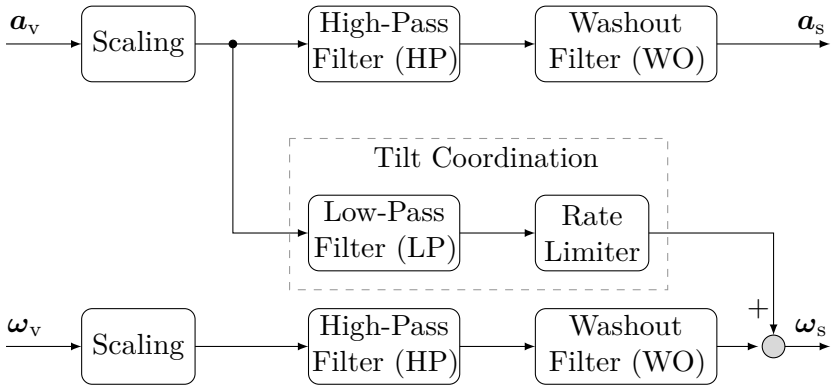

Figure 3.1.: Structure of a filter-based MCA.
The input vector $\boldsymbol{a}_\mathrm{v}$ denotes translational accelerations of the virtual vehicle and $\boldsymbol{\omega}_\mathrm{v}$ its rotational rates. The index s on the output side denotes respective demands for accelerations and rotational rates in the motion system's coordinate system.

decrease subjective evaluation results and driving performance. It is worth noting that the scaling factors can be tuned individually for each DoF.

The scaling blocks' output vectors are passed to High-Pass Filters (HP) which aim to extract relevant characteristics of driving dynamics. In this regard, Figure 3.2 shows a peaking power spectrum of an exemplary vehicle's vertical CoG acceleration at 4 Hz. The position of this peak is vehicle and vehicle setup dependent. Particularly in motorsport applications, where the vehicle setup is adjusted frequently, it is essential to provide this information to the driver. Thus, signal components in the right half-plane (non-shaded area) should remain unaffected from the HP filtering by selecting a break frequency that corresponds to the left half-plane (shaded area). A first-order HP transfer function follows

$$G_\mathrm{HP}(s) = K_\mathrm{HP}\frac{s}{s+\omega_\mathrm{HP}}, \tag{3.1}$$

where K_HP denotes the filter gain and ω_HP is the break frequency. In general, the filter order and parametrisation of $G_\mathrm{HP}(s)$ is use case dependent whereas the washout filters' (WO) parametrisation is motion platform dependent. Thereby, an allocation of parametrisation objectives is obtained: The HP extracts relevant cues describing driving dynamics and the WO together with overall scaling prevents exceeding a given motion envelope. It is worth noting that the WO parametrisation also depends on the HP parametrisation. Filter parametrisation guidelines are proposed by [39] which may act as a baseline for further tuning to match the requirements of a certain use case.

WO filter-based approaches are characterised by a continuous pull towards a neutral platform position. To achieve this, the minimum WO filter order is defined for specific forces and rotational rates. According to the limit theorem of Laplace transforms a third-order HP filter is required as a washout filter $G_\mathrm{WO}^{3\mathrm{rd}}(s)$ to compensate for the double integration

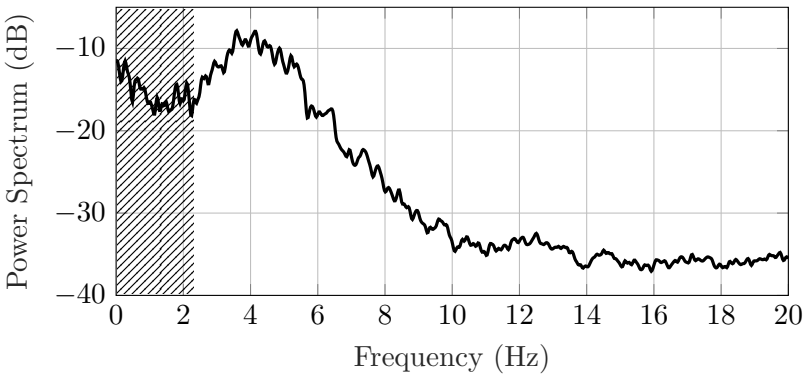

Figure 3.2.: Power spectrum of the simulated vehicle's vertical acceleration at the CoG. The shaded area indicates low frequency signal components. The increasing signal power from 2 Hz towards 0 Hz corresponds to the race track's elevation profile.

between translational accelerations and platform position. The effect is illustrated in Figure 3.3 for translational motion. The first-order WO filter's acceleration step response settles at zero acceleration and constant velocity. Therefore, the corresponding position in the lower row of Figure 3.3 exceeds the y-axis limitation of the graph. A second-order WO filter settles at zero velocity and therefore constant position. However, only WO filters of third or higher order settle at the neutral position after an acceleration step input excitation. For an excitation characterised by a rotational rate or velocity step input, a second-order WO filter $G_{\mathrm{WO}}^{2\mathrm{nd}}(s)$ is suitable. Both are described by the following Equations:

$$G_{\mathrm{WO}}^{2\mathrm{nd}}(s) = K_{\mathrm{HP}} \cdot \frac{s^2}{s^2 + 2D\omega_{\mathrm{WO}}s + \omega_{\mathrm{WO}}^2} \tag{3.2}$$

$$G_{\mathrm{WO}}^{3\mathrm{rd}}(s) = K_{\mathrm{HP}} \cdot \frac{s^3}{s^3 + 3\omega_{\mathrm{WO}}s^2 + 3\omega_{\mathrm{WO}}^2 s + \omega_{\mathrm{WO}}^3} \tag{3.3}$$

The WO filter's break frequency is described by ω_{WO} and the parameter D denotes the damping coefficient.

Low frequency excitations as they appear in motorsport applications with high amplitudes (i.e., sustained high lateral acceleration during high speed cornering) yield large motion platform deflections which may result in infeasible motion demands. Use cases such as urban driving scenarios allow applying a technique named tilt coordination. Thereby, a frequency divider by means of HP and LP filtering is integrated into the translational motion signals. High frequency signal components are reproduced by motion system translation whereas low frequency components are emulated by tilting the motion platform.

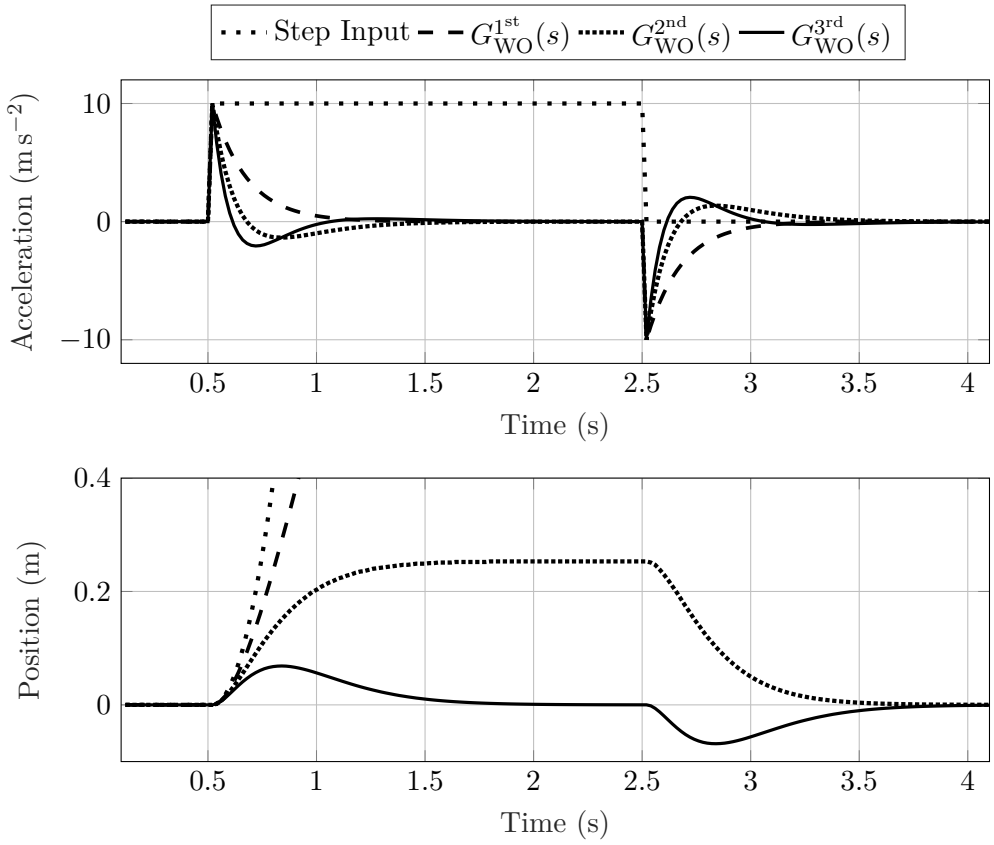

Figure 3.3.: Acceleration step response of first- to third-order washout filters.
Only $G^{3rd}_{WO}(s)$ returns the platform to neutral (Position = 0 m) position. At time $t = 2.5$ s the false cue caused by the filters' backlash characteristic is depicted.

Hence, the technique makes use of humans' sensory inability to distinguish between gravitational and translational accelerations. [6] To obtain a certain tilt angle, the motion platform rotates in a way that is not aligned with rotational input rates of $\boldsymbol{\omega}_v$. Therefore, a rate limitation block is inserted in Figure 3.1 which limits the intensity of false cues caused by tilt coordination below human perception thresholds. [20] As indicated above, this technique is, amongst others, mostly applied in urban driving scenarios. In circuit racing applications, by contrast, the characteristics of sustained accelerations are conflicting with the rate limitation of tilt coordination [20], because fast transitions between consecutive turns in opposite directions require a change of sign of the tilt angle. Therefore, the technique is considered unsuitable for the scope of this work.

Another modification of the classical filter approach is proposed by Garrett et al. (2012) [35] who introduce a new motion reference for cueing yaw motion in a DiLS. Particular emphasis is on information of the vehicle state relative to its own inertial frame. Physical

yaw motion is supposed to be provided via the visualisation system, whereas the yaw platform provides information on lateral stability. [35] At this stage, it is anticipated that the approach is most suitable for driving in the area of nonlinear vehicle dynamics and will be discussed again briefly in section 3.1.2.3.

Significant disadvantages of filter-based MCAs are suboptimal workspace handling, false cues due to filter backlash and phase errors induced by the filters. The latter is supported by Jonik et al. (2011) [50] who identify a phase-error detection threshold of 22°. For applications where phase errors may affect the validity of study outcomes, such as for the assessment of lateral vehicle dynamics in a DiLS, MCAs based on pure scaling are occasionally preferred by researchers. [8].

Additional features have been investigated to overcome some of the limitations. In this regard, prepositioning allows to virtually increase the motion envelope by making use of human perception thresholds. [8] Such algorithms require preliminary information on future vehicle motion or driver actions. However, if this information is available, the WO can be parametrised with a lower break frequency ω_{WO} as the prepositioning is supposed to cover the workspace handling. Another feature is related to the backlash behaviour identified in Figure 3.3 at time $t = 2.5\,\mathrm{s}$. Salisbury et al. (2016) [85] propose a 'Miscue-Reshaping Module' which uses a variable definition of the neutral position towards which the WO is pulling the platform. An alternative method relies on adaptive filter gains which decrease the cued acceleration magnitude during false cueing. [81]

Concluding this section it should be noted that the tuning process of the classical approach is classified to be straightforward by some authors [25], whereas other researchers hold in-depth control system knowledge and an expert driver for valuable feedback accountable for the opposite. [102] The tuning process is compared to other MCA approaches such as optimisation-based ones. Presumably, the complexity of MCA tuning is more a subjective feeling depending on researchers' or engineers' field of expertise.

3.1.2. Optimisation-based Motion Cueing

The forms of optimisation-based MCAs are manifold but their intrinsic motivation is similar. Following Bruschetta et al. (2018) [11], the effectiveness of a dynamic driving simulator relies on its ability to provide a reliable driving sensation to the driver, while maintaining the motion platform within its limitations of operational space. This section details the most relevant optimisation-based MCAs and further provides examples for extensions to the basic structure.

3.1.2.1. Offline Optimal Control

The motivation introduced above yields an optimisation problem with the objective of minimising the incongruence between virtual vehicle and motion platform regarding their acceleration and rotational rate signals. It is therefore referred to as an optimal

control (OC) problem. Adding a model of the vestibular system yields a perception-based MCA, where the perception error introduced in chapter 1 is penalised and therefore minimised numerically. [63] Offline MCAs are using pre-recorded data and calculate the corresponding motion platform trajectory before the actual task in a DiLS is conducted. Further details on offline MCAs in DiL studies are covered in chapter 4. One key characteristic of offline MCAs is that the vehicle trajectory of an entire driving task such as one lap at a race track is available to the algorithm. To obtain an optimal motion platform trajectory, an optimisation problem as described by Equations (3.4a)-(3.4f) is formulated.

$$\begin{aligned}
&\underset{\boldsymbol{x},\boldsymbol{z},\boldsymbol{u}}{\text{minimize}} && J(\boldsymbol{x},\boldsymbol{z},\boldsymbol{u},\boldsymbol{p}) && && \text{(3.4a)}\\
&\text{subject to} && \boldsymbol{x}_0 = \widetilde{\boldsymbol{x}}(t_0) && \text{(initial state)}, && \text{(3.4b)}\\
& && 0 = f(\boldsymbol{x},\boldsymbol{z},\boldsymbol{u}) && \text{(equalities)}, && \text{(3.4c)}\\
& && \underline{\boldsymbol{x}} \leq \boldsymbol{x} \leq \overline{\boldsymbol{x}} && \text{(differential state bounds)}, && \text{(3.4d)}\\
& && \underline{\boldsymbol{z}} \leq \boldsymbol{z} \leq \overline{\boldsymbol{z}} && \text{(algebraic state bounds)}, && \text{(3.4e)}\\
& && \underline{\boldsymbol{u}} \leq \boldsymbol{u} \leq \overline{\boldsymbol{u}} && \text{(input bounds)} && \text{(3.4f)}
\end{aligned}$$

The vectors $\boldsymbol{x}$ and $\boldsymbol{z}$ comprise differential and algebraic states of the modelled system. The system dynamics are described by the equality constraints of Equation (3.4c) which additionally depends on the constant parameter vector $\boldsymbol{p}$. The system inputs $\boldsymbol{u}$, differential states and algebraic states are bounded by Equations (3.4d)-(3.4f). For the particular case that the system of differential algebraic equations (DAEs) described by $f(\boldsymbol{x},\boldsymbol{z},\boldsymbol{u},\boldsymbol{p})$ comprises motion platform dynamics only, all constraints result from the motion system's capabilities. In consideration of the introduced constraints, different cost functions $J(\boldsymbol{x},\boldsymbol{z},\boldsymbol{u},\boldsymbol{p})$ can be formulated depending on what measure should be minimised for the particular use case. A frequently used cost function relies on three distinct terms

$$J(\boldsymbol{x},\boldsymbol{z},\boldsymbol{u},\boldsymbol{p}) = [\hat{\boldsymbol{y}}_\mathrm{r} - \hat{\boldsymbol{y}}_\mathrm{s}]^T \boldsymbol{P} [\hat{\boldsymbol{y}}_\mathrm{r} - \hat{\boldsymbol{y}}_\mathrm{s}] + \boldsymbol{u}^T \boldsymbol{Q} \boldsymbol{u} + \boldsymbol{x}_\mathrm{pos}^T \boldsymbol{R} \boldsymbol{x}_\mathrm{pos}, \tag{3.5}$$

where the first term $[\hat{\boldsymbol{y}}_\mathrm{r} - \hat{\boldsymbol{y}}_\mathrm{s}]^T \boldsymbol{P} [\hat{\boldsymbol{y}}_\mathrm{r} - \hat{\boldsymbol{y}}_\mathrm{s}]$ penalises motion incongruence errors, the second term $\boldsymbol{u}^T \boldsymbol{Q} \boldsymbol{u}$ is related to simulator control effort and the third term $\boldsymbol{x}_\mathrm{pos}^T \boldsymbol{R} \boldsymbol{x}_\mathrm{pos}$ penalises position ($\boldsymbol{x}_\mathrm{pos}$) deviation from a neutral position. The matrices $\boldsymbol{P}$, $\boldsymbol{Q}$ and $\boldsymbol{R}$ are weighting parameters that serve for MCA tuning. The incongruence error is defined as a deviation between the estimated perceived motion from a vehicle reference $\hat{\boldsymbol{y}}_\mathrm{r}$ and the actual simulator motion perception $\hat{\boldsymbol{y}}_\mathrm{s}$. Both vectors consist of six entries, each of which represents one degree of freedom of vestibular motion perception (i.e. longitudinal, lateral, vertical acceleration and rotational rates around the corresponding three axes). Similar to this generic problem formulation, a multitude of approaches are developed and used frequently. [102, 17, 25, 51, 63]

As such MCAs are optimal in some explicit sense, they can be used as a reference for real-time executable MCAs [85]. Furthermore, a simulation-based assessment of kinematic properties to be put on a new motion system is feasible [70]. Koyuncu et al. (2020) [55] use the results of an optimal control-based MCA to train the transfer characteristics using a Neural Network to reproduce its behaviour. Although this is an interesting step towards real-time applicability, which is required for circuit racing use cases, robustness is a critical concern. This chapter is considered a comprehensible intermediate step towards online optimisation-based MCAs which are detailed in the following section.

3.1.2.2. Model Predictive Control

A demand for real-time applicability of optimisation-based MCAs implies additional challenges concerning computational effort [12], estimation of future vehicle motion caused by driver activities [41] and robustness [28, 29]. The formulation of an OC problem as it was described in the previous section for a limited time horizon is referred to as model predictive control (MPC)-based MCAs. Apart from the limited prediction horizon T, the problem formulation remains similar with regard to its structure, objective and constraints. The corresponding problem formulation for a generic MPC-based MCA is described by Equations (3.6a-3.6g).

$$\underset{\boldsymbol{x},\boldsymbol{z},\boldsymbol{u}}{\text{minimize}} \quad \int_{t_0}^{t_0+T} J(\boldsymbol{u}(t),\boldsymbol{x}(t),\boldsymbol{z}(t),\hat{\boldsymbol{y}}_\mathrm{r}(t),\hat{\boldsymbol{y}}_\mathrm{s}(t))\mathrm{d}t \tag{3.6a}$$

$$\text{subject to} \quad \boldsymbol{x}(t_0) = \widetilde{\boldsymbol{x}}(t_0) \quad \text{(initial state)}, \tag{3.6b}$$

$$\boldsymbol{x}(t_0+T) \in \mathbb{X} \quad \text{(terminal set)}, \tag{3.6c}$$

$$0 = f(\boldsymbol{x}(t),\boldsymbol{z}(t),\boldsymbol{u}(t)) \quad \text{(equalities)}, \tag{3.6d}$$

$$\underline{\boldsymbol{x}} \leq \boldsymbol{x}(t) \leq \overline{\boldsymbol{x}} \quad \text{(differential state bounds)}, \tag{3.6e}$$

$$\underline{\boldsymbol{z}} \leq \boldsymbol{z}(t) \leq \overline{\boldsymbol{z}} \quad \text{(algebraic state bounds)}, \tag{3.6f}$$

$$\underline{\boldsymbol{u}} \leq \boldsymbol{u}(t) \leq \overline{\boldsymbol{u}} \quad \text{(input bounds)} \tag{3.6g}$$

The objective of Equation (3.6a) is a function of time t as the optimisation is solved separately at each point in time. The terminal state $\boldsymbol{x}(t_0+T)$ must remain within some terminal set $\mathbb{X}$ to ensure the continuous operation of the MPC controller. [51] In terms of computational effort, increasing availability of computational power and efficient implementations as proposed by Katliar (2020) [51] allow target control frequencies of up to 200 Hz. [12] However, absolute numbers are highly dependent on the prediction horizon length T, process model $f(\boldsymbol{x}(t),\boldsymbol{z}(t),\boldsymbol{u}(t))$ complexity as well as the realisation of (nonlinear) constraints. [67] Besides the integration of vestibular models as proposed by [21, 12, 65, 25], proprioceptive perception is considered in the process model of Duc-An et al. (2019) [73]. Similar to other control systems, a multi-stage or cascaded MPC is proposed by Bruschetta et al. (2017) [12]. The high-level controller comprises a process model of the human perceptual system whereas the low-level controller covers

a dynamic motion platform model and its constraints. Thereby, system dynamics (i.e., time constants) are addressed individually which allows an appropriate choice of control frequency and hence computational cost further reduce at similar performance.

An essential aspect of the MPC-based MCAs relates to the reference signal prediction within the prediction horizon. For an objective function in the form of Equation (3.5), a reference prediction for the six DoFs included in $\hat{\boldsymbol{y}}_{\mathbf{r}}$ is required. Although reasonable cueing quality can be achieved using a constant reference, delays are reduced and correlation to the actual reference signal is increased using an ideal motion prediction. [41] Recently published approaches tackle this problem using fuzzy neural networks [16], time-series neural networks [78] or model-based approaches [4].

3.1.2.3. Optimal Motion Cueing Filters

Besides OC- and MPC-based MCAs, there are approaches combining both optimisation and filtering. This class is referred to as optimal (washout) filter MCAs. One of the first publications in this context is provided by Elloumi et al. (2004) [26]. They formulate an optimisation problem that minimises the perception error during a pre-recorded manoeuvre by manipulating a washout filter's parameters. A more detailed and particularly relevant study in this regard is conducted by Salisbury et al. (2017) [86]. They formulate an optimisation problem to design optimal lateral and yaw cueing filters. As an objective, the perception error in the respective motion channels is minimised together with the platform displacement, velocity and acceleration. The last three aspects yield an effect similar to a WO. Each of the cost function's four terms presented in [86] is weighted individually. Instead of constant gains, they use weighting functions to increase flexibility during the tuning process. Following this approach, one optimal yaw cueing filter and three different, optimal lateral cueing filters are proposed. Each lateral cueing filter is optimal in the sense of the particular weighting of the four terms in the cost function used for the optimisation. In order to evaluate their performance, the simulated vehicle's stability and response characteristics in proximity to steady-state operating points are examined. Eigenvalue analyses are conducted to determine cornering stability at different speeds. Thereby, operating points are identified where eigenvalues approach a positive real part which is accompanied by changing response characteristics (i.e., system instability). Particular vehicle responses are analysed using step steer inputs at relevant speeds as identified in the previous analysis. The results are used to tune and ultimately select one out of three options of optimal filters for lateral acceleration cueing. The resulting transfer functions of the lateral and yaw cueing filters are

$$G_{\mathrm{lat}}(s) = \frac{83s^3 + 17s^2 + 0.0033s - 1.7e^{-7}}{s^4 + 546s^3 + 25136s^2 + 6255s + 250} \,, \tag{3.7}$$

$$G_{\mathrm{yaw}}(s) = \frac{8.47s^6 + 635s^5 + 12012s^4 + 117627s^3 + 404881s^2 + 696129s + 70}{s^7 + 70s^6 + 2421s^5 + 49718s^4 + 590875s^3 + 2910807s^2 + 7942101s + 9214671} \,. \tag{3.8}$$

In comparison to the classical approach from section 3.1.1, HP and WO parts are no longer distinct. This complicates parameter adjustments for tuning purposes past the optimal filter design. What is more, the resulting yaw motion characteristic using F_{yaw} is similar to the vehicle's side slip gradient. A comparison of both signals according to section 2.1.1.2 reveals an absolute difference of $AD = 0.81$, cross-correlation of $CC = 0.63$ and delay indicator of $DI = 0.02\,\text{s}$.

3.2. Contribution

The thesis' objective to identify MCs that support accurate vehicle state anticipation creates a demand for different MCs to be tested in DiL studies. As a first step towards such findings, the general statement is narrowed down to vehicle state anticipation related to lateral vehicle dynamics. The previously presented approaches of Garrett et al. (2012) [35] and Salisbury et al. (2017) [86] indicate that alternative objectives besides the minimisation of perception errors should be considered. As the link from MC perception to anticipation and action remains largely unknown, there is no mathematical representation of such alternative objectives. One could state that it remains unclear what the perceptual basis for driver's vehicle state anticipation during near-limit vehicle operation is. However, if this perceptual basis is identified, the perception error can be redefined and hence the methods introduced for online optimisation-based approaches become feasible and valuable.

Based on this overarching objective, the MCA presented in the following section is designed. It aims to replicate distinct signal components of the simulated vehicle's yaw rate which are extracted using a single track model-based approach. Although a separation of signal components is possible using LTI filters, those can not distinguish between distinct driving dynamics whose effects are reflected in an overlapping frequency range. Due to the four DoF motion system, surge and sway MCs can not be transmitted to the driver which limits the overall replication of lateral vehicle dynamics on the one hand but reduces the problem dimensionality on the other hand. However, the proposed method takes a_y into account for the extraction of distinct yaw rate signal components. Thereby, investigations on the vehicle dynamics related basis of relevant MCs become feasible.

3.3. Model-based 4 DoF Motion Cueing

Parts of this section are published [89] with the author's contribution according to page 96. An overview of the MCAs scheme is provided in Figure 3.4. Its structure is inspired by and similar to that of the classical filter approach (see Figure 3.1). The vehicle's roll, pitch and yaw rate are summarised by $\boldsymbol{\omega}_{\text{v}} = [\omega_{x,\text{v}}, \omega_{y,\text{v}}, \omega_{z,\text{v}}]^T$ and the reduced translational accelerations respectively by $\boldsymbol{a}_{\text{v}} = [a_{\text{y,v}}, a_{\text{z,v}}]^T$. Vertical vehicle dynamics

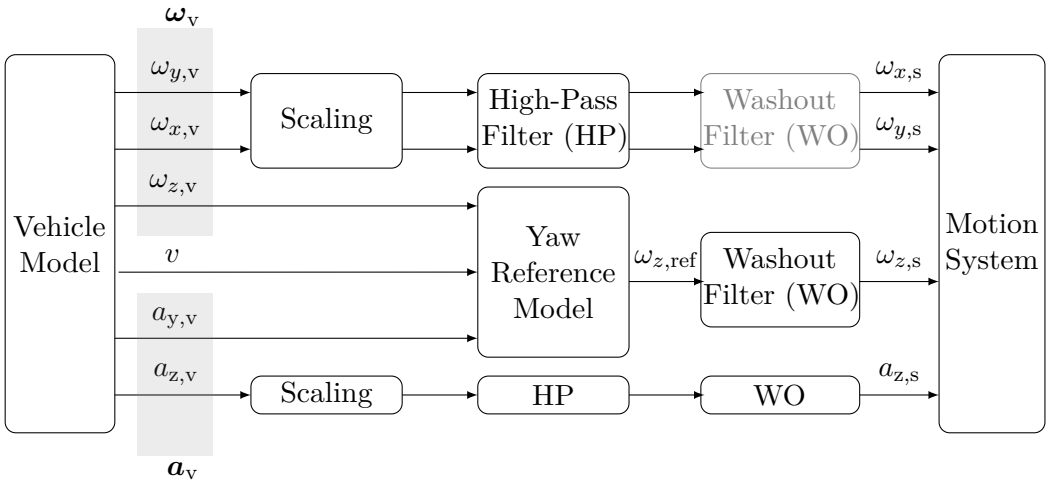

Figure 3.4.: Scheme of the proposed MCA.

are related to $\omega_{x,\mathrm{v}}$, $\omega_{y,\mathrm{v}}$ and $a_{z,\mathrm{v}}$ which are processed according to the classical approach by scaling, HP filtering and a WO. In contrast, the yaw motion demand $\omega_{z,\mathrm{s}}$ is obtained from a yaw reference model. The following subsections chronologically describe the parametrisation of the classical approach devoted to vertical vehicle dynamics and the yaw reference model including the WO filter design.

3.3.1. Vertical Vehicle Dynamics

The scaling $K_\mathrm{d} = 0.5$ of the three DoFs mainly related to vertical vehicle dynamics, ω_x, ω_y and a_z, is derived empirically under consideration of racing drivers' subjective preferences. An identical scaling factor for the three DoFs is motivated by minimum scaling incongruence between distinct motion percepts. Subsequently, the signals propagate through the HP filters with a general form of

$$G_\mathrm{d}(s) = \frac{s^2}{s^2 + 2D_\mathrm{d}\omega_{\mathrm{HP,d}}s + \omega_{\mathrm{HP,d}}^2}. \tag{3.9}$$

The HP filters are parametrised individually for each DoF denoted by the subscript d. The parametrisation firstly aims to capture signal components close to the vehicle body's eigenfrequencies and above. In addition, low frequency signal components which have their origin in track elevation or banking (incline) are eliminated. Table 3.1 contains a list of chosen parameters for each DoF. As detailed in section 3.1.1, a third-order HP is required to continuously pull the motion platform to a neutral position for the vertical acceleration a_z. For this purpose, an additional first-order HP filter is applied with a break frequency of $\omega_{\mathrm{WO,z}} = 0.01\,\mathrm{rad\,s^{-1}}$. Its transfer behaviour does not produce a perceptible impact on the signal's characteristics which are determined by the previous second-order

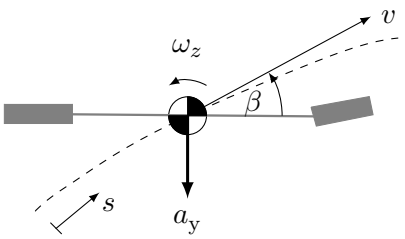

Figure 3.5.: Reduced single track model on a circular path.
The reduced model is limited for a circular path s with yaw rate ω_z, lateral acceleration a_y, side slip angle β and constant path velocity v.

HP filtering. No such WO is applied to the rotational DoFs, as the vehicle's roll and pitch angles naturally remain within the simulator's motion capabilities. Therefore, the WO block is depicted transparently in Figure 3.4.

3.3.2. Lateral Vehicle Dynamics

The behaviour related to lateral vehicle dynamics can be simplified and described by a single track model. [27] The model which is illustrated in Figure 3.5 generally has three DoFs: longitudinal (x) and lateral (y) translation as well as the heading angle ψ. However, on a circular path s during steady-state cornering, the system reduces to two DoFs which are denoted by the yaw rate $\omega_z = \dot{\psi}$ and the side slip angle β. The relation of lateral acceleration, yaw rate, path velocity v and gradient of the side slip angle $\dot{\beta}$ is described by

$$\omega_z = \frac{a_y}{v} + \dot{\beta}. \tag{3.10}$$

Following this model, the vehicle yaw rate comprises two distinct terms, one of which is the gradient of the side slip angle. The other term is a function of lateral acceleration and path velocity. As the four DoF DiLS can not provide MCs related to horizontal accelerations, it is questionable if or to what extent drivers benefit from yaw MCs correlating to the term $\frac{a_y}{v}$. To investigate the relative importance of yaw motion signal

Table 3.1.: Parameters of the HP filters used for the classical filter approach which is applied to vertical vehicle dynamics.

DoF (d)	K_d	$\omega_{\mathrm{HP,d}}$	D_d
ω_x	0.5	$4.7\,\mathrm{rad\,s^{-1}}$	1.4
ω_y	0.5	$4.7\,\mathrm{rad\,s^{-1}}$	1.4
a_z	0.5	$9.4\,\mathrm{rad\,s^{-1}}$	1.4

components, a yaw reference model is sought, which allows a relative weighting between both terms. This is achieved by rearranging Equation 3.10 to $\dot{\beta} = \omega_z - \frac{a_y}{v}$, introducing a relative weight k_2 and replacing the side slip gradient with the reference model's output $\omega_{z,\mathrm{ref}}$ such that $\omega_{z,\mathrm{ref}} = \omega_z - k_2 \cdot \frac{a_y}{v}$. In order to provide additional tunability with regard to yaw motion amplitudes, the final yaw rate reference model of Figure 3.4 is proposed according to

$$\omega_{z,\mathrm{ref}} = k_1 \cdot c(k_2) \cdot \underbrace{[\omega_z - k_2 \cdot \frac{a_y}{v}]}_{=\dot{\beta},\ \text{if}\ k_2=1}, \tag{3.11}$$

where $k_1 \in [0, 1]$ denotes the overall gain and $k_2 \in [0, 1]$ the relative weight on $\dot{\beta}$. The structure of Equation (3.11) allows to independently tune yaw motion characteristic using k_2 and yaw motion intensity through k_1. For the scope of this work, three different intensities are considered and manipulated by k_1. To achieve this decoupled control, the overall gain is multiplied by $c(k_2)$, which is a linear function to compensates for the approximated linear increase of intensity of the term in brackets with decreasing k_2. Intensity is considered as the root mean square (RMS) of $\omega_{z,\mathrm{s}}$. The starting point is at $k_1 = 0.5$ as proposed by literature. The other two options increase ($\mathrm{MCA_{X,high}}$) or decrease ($\mathrm{MCA_{X,low}}$) the gain k_1 by 25% respectively. Apart from different intensities, three sets of parameters are defined and listed in Table 3.2 which relate to signal characteristics. $\mathrm{MCA_A}$ is identical to the approach of Garrett et al. (2012) [35] where the vehicle's side slip gradient is used as $\omega_{z,\mathrm{ref}}$. $\mathrm{MCA_B}$ and $\mathrm{MCA_C}$ gradually introduce a dependency on the calculated steady-state yaw rate by decreasing k_2.

The consideration of sustained yaw rate signal components yields the demand for a WO filter. It aims to operate below the vestibular perception threshold which is assumed at $3\,^\circ\,\mathrm{s}^{-1} = 0.052\,\mathrm{rad\,s}^{-1}$ within this work. [43] More precisely, the absolute value of false cues which occur between $\omega_{z,\mathrm{ref}}$ and $\omega_{z,\mathrm{s}}$ to pull the platform back to the neutral position must be lower than the defined threshold. At this point, advantage is taken from professional racing drivers for the WO filter parametrisation. Data obtained from racing drivers can be considered as a worst-case scenario. At a given race track, the yaw rate amplitudes and the resulting heading angles are constrained if driving anomalies are neglected. Although the heading angle trace over distance remains similar for different speed traces, the yaw rate amplitudes differ. Therefore, the WO procedure is tuned for professional racing drivers where the highest yaw rate amplitudes occur. Furthermore, a margin of 5° towards the maximum excursion of the yaw motion system is kept to handle driving anomalies. The WO filter parameters are listed in Table 3.2 in the two rightmost columns and its qualitative transfer characteristics are displayed in Figure 3.6. The perception threshold at $0.052\,\mathrm{rad\,s}^{-1}$ is illustrated by the dashed lines for both positive and negative yaw rates. After passing a right-hand turn between $t = 2\,\mathrm{s}$ and $t = 7\,\mathrm{s}$, the reference yaw rate $\omega_{z,\mathrm{ref}}$, obtained from the yaw reference model, settles close to $\omega_{z,\mathrm{ref}} = 0\,\mathrm{rad\,s}^{-1}$ whereas the simulator yaw rate motion demand $\omega_{z,\mathrm{s}}$ shows

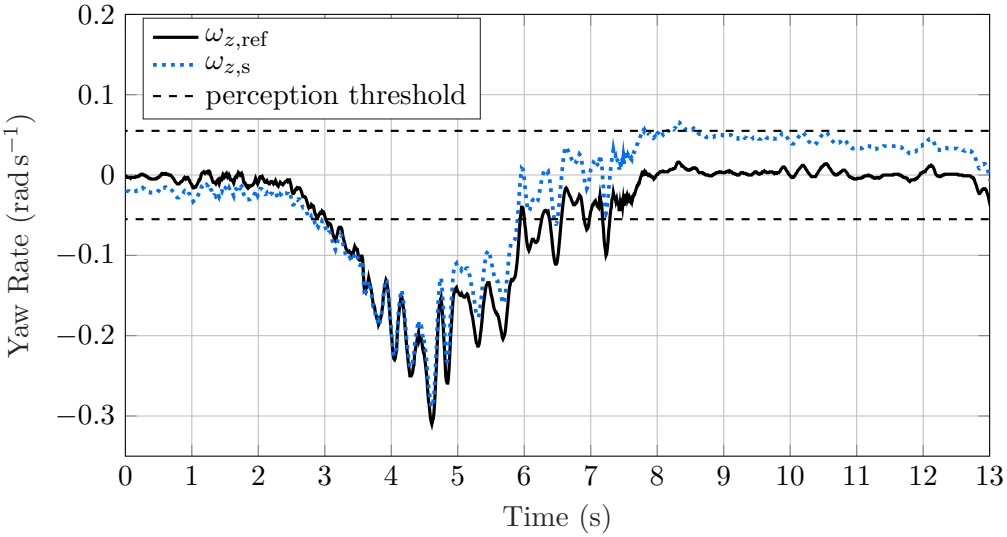

Figure 3.6.: Illustration of a worst-case scenario of the washout procedure.

negative values which relate to the WO process. The depicted scenario is generated by the application of $\mathrm{MCA}_{\mathrm{C,high}}$ to 20 pre-recorded laps of professional racing drivers. As $\mathrm{MCA}_{\mathrm{C,high}}$ results in the highest workspace exploitation compared to the alternative options of Table 3.2, it is considered as a worst-case scenario in terms of WO requirements. The proposed WO is tuned such that it operates below the vestibular perception threshold which is indicated between $t = 8\,\mathrm{s}$ and $t = 13\,\mathrm{s}$ in Figure 3.6.

3.4. Analysis

The three parametrisation options described in the previous section result in significantly different transfer characteristics between vehicle and simulator yaw rate. An exemplary manoeuvre is displayed in Figure 3.7 where the qualitative differences between all three

Table 3.2.: Three sets of parameters of the yaw reference model and WO filters that are used to obtain yaw motion cues.

MCA name	k_1	k_2	w_{WO,ω_z}	D_{ω_z}
$\mathrm{MCA}_{\mathrm{A}}$	0.5	1	$0.09\,\mathrm{rad\,s^{-1}}$	0.71
$\mathrm{MCA}_{\mathrm{B}}$	0.5	0.8	$0.09\,\mathrm{rad\,s^{-1}}$	0.71
$\mathrm{MCA}_{\mathrm{C}}$	0.5	0.6	$0.09\,\mathrm{rad\,s^{-1}}$	0.71
$\mathrm{MCA}_{\mathrm{X,high}}$	$0.5 \cdot 1.25$	k_2	$0.09\,\mathrm{rad\,s^{-1}}$	0.71
$\mathrm{MCA}_{\mathrm{X,low}}$	$0.5 \cdot 0.75$	k_2	$0.09\,\mathrm{rad\,s^{-1}}$	0.71

parametrisations become readily apparent. While $\mathrm{MCA_A}$ operates mostly below the vestibular perception threshold, $\mathrm{MCA_B}$ and $\mathrm{MCA_C}$ increasingly follow the trace of the vehicle's reference yaw rate $\omega_{z,\mathrm{v}}$. The qualitative observations of Figure 3.7 are also reflected by the objective MCA evaluation methods CC_{ω_z}, DI_{ω_z} and AD_{ω_z} in Table 3.3. For quantitative MCA comparisons, these methods use the observation points OP3 and OP4 as described in Figure 1.2 and the table summarises the results of all MCAs and indicators which are applied to the yaw rate ω_z and yaw acceleration $\dot{\omega}_z$. While mainly angular velocity is sensed by the vestibular system, rotational accelerations yield cues perceptible by the somatosensory system. Therefore, both signals are considered for the analysis. According to the results, the consideration of the calculated steady-state yaw rate yields an increased cross-correlation at identical signal delays and decreased absolute difference. The same trends apply to yaw acceleration related results. However, the differences are smaller in absolute terms. Between $\mathrm{MCA_A}$ and $\mathrm{MCA_C}$, CC_{ω_z} increases from 0.17 to 0.84 whereas $CC_{\omega_{\dot{z}}}$ increases from 0.57 to 0.74. To conclude this section, $\mathrm{MCA_C}$ shows the most promising characteristics with respect to established MCA quality indicators. The following chapter introduces an experimental study design that aims to identify how this preliminary analysis correlates to results obtained from closed-loop driving tasks.

Table 3.3.: Results of the three MCA parametrisations with respect to CC_{ω_z}, DI_{ω_z} and AD_{ω_z}.
The DI takes discrete values with a step size of 0.01 s which is explained by the data logging frequency.

	CC_d			DI_d			AD_d		
	$\mathrm{MCA_A}$	$\mathrm{MCA_B}$	$\mathrm{MCA_C}$	$\mathrm{MCA_A}$	$\mathrm{MCA_B}$	$\mathrm{MCA_C}$	$\mathrm{MCA_A}$	$\mathrm{MCA_B}$	$\mathrm{MCA_C}$
ω_z	0.17	0.7	0.84	0.01 s	0.01 s	0.01 s	0.99	0.94	0.91
$\dot{\omega}_z$	0.57	0.65	0.74	0.01 s	0.01 s	0.01 s	0.79	0.77	0.77

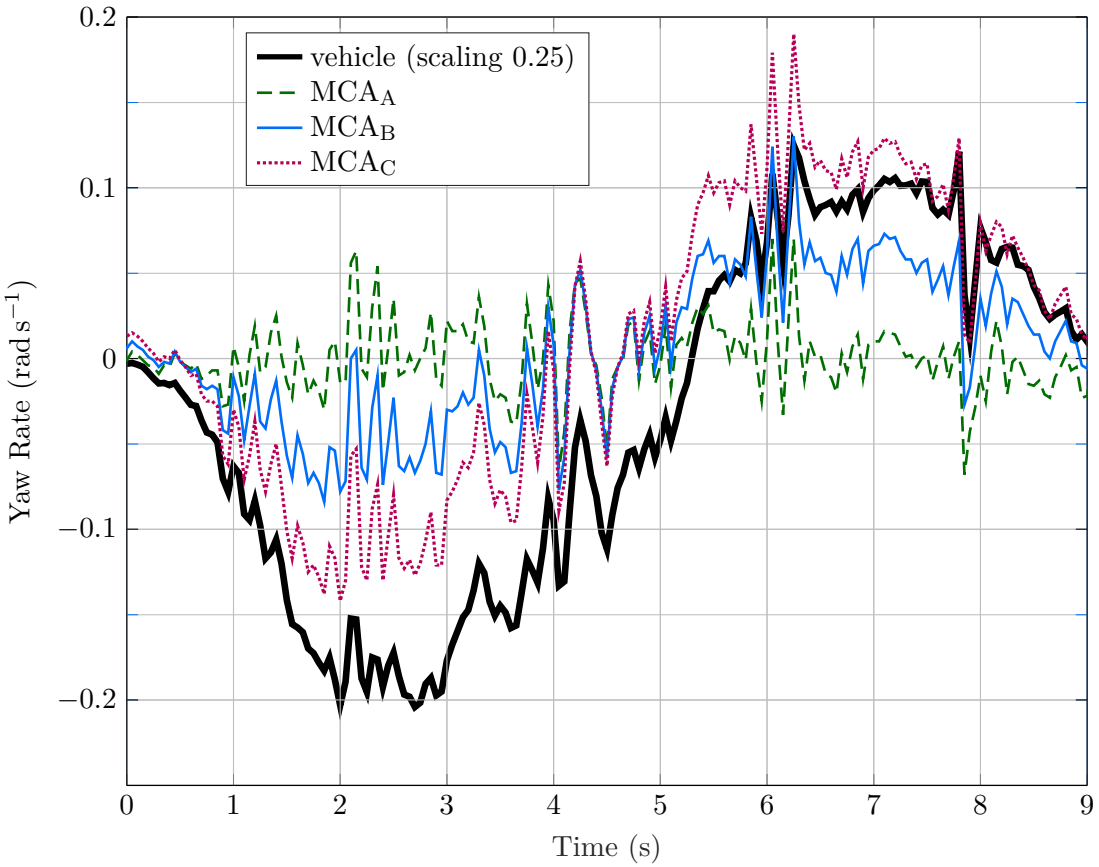

Figure 3.7.: Exemplary motion demands $\omega_{z,\mathrm{s}}$ obtained from MCA$_\mathrm{A}$, MCA$_\mathrm{B}$ and MCA$_\mathrm{C}$. The vehicle reference is scaled down to 25% of its original amplitude for improved readability of the figure.

4. Studies

The third part of the thesis' body is devoted to experimental studies in the field of driving simulation. Similar to the previous chapters, the first section reviews related work, followed by this work's particular contribution. Two experimental study designs complete the chapter.

4.1. State of the Art

In the review of Wynne et al. (2019) [111] on driving simulator validation studies, little uniformity in the experimental designs is found. To still obtain a structured overview, publications related to this work are reviewed and categorised with respect to manoeuvre types, independent variables and dependent variables. As stated by [24] on page 192, an experiment is a procedure where one or multiple independent variables are manipulated to observe, analyse and evaluate the effect on one or multiple dependent variables. The differentiation of manoeuvre types is motivated by studies which rely on open-loop, closed-loop or both scenarios. Some of the most relevant studies are discussed in the following subsection.

4.1.1. Open- and Closed-Loop Methods

A differentiation between open- and closed-loop manoeuvres for experiments in the field of driving simulation is related to the driver's activity during the experiment. An active driving task, where participants have control over a vehicle's trajectory, is referred to as a closed-loop experiment. This type of experiment is conducted by Berthoz et al. (2013) [2] where a total of 65 participants complete slalom manoeuvres with varying scaling factors on lateral MCs. The study aims to examine the effects of motion scaling on motion perception and driving performance. The dependent variables rely on subjective and objective measurement data. The subjective results are based on preference evaluations between scaling configurations. On top of that, an objective evaluation based on steering wheel reversal rate r_{swr} and high frequency area A_{HF} is conducted, see Table 2.1. It is essential to run a closed-loop experiment to obtain meaningful results of such objective KPIs. The same applies to the study of Lakerveld et al. (2016) [58] where the effects of yaw and sway motion cues on path tracking performance are examined. The final example of this category relates to the study of Markkula et al. (2018) [60] who aim to quantify behavioural validity using a driver-model-based evaluation approach.

In contrast, there are applications where participants take a passenger's role. In that case, the link between driver and vehicle model in Figure 1.2 is disconnected. Such a scenario is referred to as open-loop. It is applicable if purely subjective methods or objective methods based on physiological measurements are applied. In other words, if the perception reaction automatisms while car driving ([23]) are not part of the investigation. A study where this requirement holds is conducted by van Leeuwen et al. (2019) [101]. Their work aims to identify the impact of lateral specific force scaling conditions on participants' perceived visual-vestibular incongruence. Time-varying effects are of particular interest which is why corner entry, sustained part and corner exit phase are investigated separately. This is achieved utilising the CR method described in section 2.1.2.1. The independent variable of the experiment is represented by the lateral specific force scaling conditions. In contrast to a closed-loop experiment, no attention of participants is drawn to driving activities which allows higher evaluation accuracies and eliminates the interference between driving activities and subjective evaluation results. [102, 19] Another research area where open-loop experiments are frequently applied is dedicated to investigations on non-realtime executable MCAs (see section 3.1.2.1) or MCs obtained from pre-recorded data of on-road measurements. [69]

4.1.2. Independent Variables

Each experiment comprises a multitude of parameters. The particular subset of parameters that is under investigation includes the independent variables (or factors). It is mandatory that independent variables can be set precisely and repeatably. The distinct settings of an independent variable are referred to as levels. An overview of the fundamental terms for the design of an experiment is provided in [94] on pages $2-9$. In the field of driving simulation studies, the selection of independent variables depends on the individual study's aim. Independent variables frequently used in relevant studies are described in this subsection.

Environment

Choosing the driving environment as an independent variable relates either to a comparison of separate DiL simulators or between on-road and simulator originated results. The latter is particularly relevant for studies which aim to quantify simulator validity. Therefore, Markkula et al. (2019) [60] and Romano et al. (2019) [83] use an instrumented vehicle on a test track to gather on-road data which is used as a reference for the second part of the experiment conducted in a DiLS. To investigate the applicability of findings for a wider range of applications and simulator systems, some studies take multiple driving simulators into account. In this manner the impact of different motion scaling factors between 0.4 and 0.75 is investigated in three different DiL simulators which are the DESDEMONA simulator at TNO in the Netherlands, the ULTIMATE simulator from Renault located in France and the CyberMotion Simulator of the Max Planck Institute in Germany. [2]

DiLS configuration

Different simulator configurations allow to investigate the effects of a simulator's distinct features such as steering force feedback, auditory cues, MCs for separate perception channels as well as visual cues. The effects of sway and yaw motion cues are examined by Lakerveld et al. (2016) [58]. In their experiment, participants are asked to follow the centre-line of a winding road while wind is acting as a disturbance on the simulated vehicle. The same procedure is conducted without motion, with yaw motion only, with sway motion only as well as with both sway and yaw motion activated. As a reference for the effect of visual cues, the procedure is further conducted with two settings of visual road preview which are set to 5 m and 100 m respectively. It is found that reduced steering control activity results from yaw motion feedback, improved performance of disturbance rejection from sway motion feedback and overall the effects of sway and yaw motion cues are much smaller than that of visual road preview. Another study where the simulator configuration is used as an independent variable was conducted by Markkula et al. (2018) [60]. They investigate the effect of the presence or absence of steering torques and MCs on the parametrisation of driver steering models. By means of different DiLS configurations, it is possible to mimic a whole different driving simulator. This is done in the work of Berthoz et al. (2013) [2] by disabling the entire motion feedback. Thus, a static driving simulator is emulated.

MCA

For the purpose of MCA development, studies are designed to compare different approaches or parametrisations. In this context, Salisbury et al. (2017) [86] test three motion cueing filters for lateral motion as well as one filter and one sideslip angle-based cueing for yaw motion. All tests are executed by a professional (PRO) racing driver on a section of the Circuit de Barcelona-Catalunya. It is found that optimisation-based cueing filters tuned to capture changes in vehicle behaviour allow the racing driver to operate the vehicle near its performance limit. For the specific case of yaw motion cues, no significant improvement compared to a sideslip angle-based approach is identified. A more universal investigation is conducted by Venrooij et al. (2015) [102] who compare an optimisation-based MCA to a classical filter-based approach. The latter receives significantly lower ratings from the ten participants. Similar results are published by Cleij et al. (2019) [17] who conduct a follow-up experimental study with 18 participants. The optimisation-based approach, which minimises a cost function similar to Equation (3.5) while respecting simulator constraints, consistently achieves higher ratings. The aforementioned studies both rely on open-loop manoeuvres.

Driving task

Different DiLS applications put different requirements on an MCA or an evaluation method. Thus, a newly developed methodology must be verified for specific use cases

individually. One strategy for the development process relies on isolated investigations in a limited amount of repeatable manoeuvres before running the final, usually more time-consuming manoeuvre. Likewise, an oval track is used in [89] to minimise the duration of power limitation per lap. Thus, more data of corner entries and exits is obtained within a feasible period of time from PRO drivers controlling a race car. In a second step, the evaluation method is validated using race track data as a reference and conducting circuit racing at the DiLS. In contrast, Cleij et al. (2015) [18] use one driving task for their investigations on a continuous subjective rating method only. However, the temporal resolution of their methodology allows to individually quantify results for different sections of the manoeuvre which, inter alia, are pure braking, braking, accelerating and running at constant velocity. In this case, different driving tasks are conducted within single runs and separated in retrospect.

Subjects

The main aspect which differs between studies with regard to participants is the absolute amount. While Salisbury et al. (2017) [86] have to rely on a single subject for their study, Lakerveld et al. (2016) [58], Markkula et al. (2018) [60] and Romano et al. (2019) [83] consider eight participants. It is worth mentioning, that the amount of applicable subjects highly depends on specific requirements such as preliminary experience in race car driving or driving simulation which possibly reduces the target group significantly. The review article of Wynne et al. (2019) [111] reveals that up to 2000 participants are considered for certain DiLS studies. Berthoz et al. (2013) [2] reports 65 participants and van Leeuwen et al. (2019) [101] consider 16 participants. In the latter study, a second aspect besides the absolute amount of subjects is relevant: Three groups of varying experience levels are compared. The levels are named novice (first time in a DiLS), intermediate (some experience in a DiLS) and expert (motion cueing researchers).

4.1.3. Dependent Variables

Dependent variables of an experimental study serve as a measure of an effect induced by different levels of an independent variable. There is no objection to considering multiple dependent variables simultaneously. The selection of dependent variables is directly linked to a study's aim and their suitability for the particular use case is a decisive factor towards conclusive results. [94] The application of evaluation methods' performance indicators, introduced in chapter 2, yields such dependent variables. An overview including references to related work is provided in Table 2.2.

4.2. Experimental Study Design: DRIVEenvironment

This study is conducted at two different DiL simulators and further takes data from physical track operation as a reference. As the environment is chosen as an independent variable, the study is named DRIVEenvironment. The following subsection details the objective of DRIVEenvironment. Subsequently, the study design is described regarding independent variables, dependent variables and procedure.

4.2.1. Objective

The objective of DRIVEenvironment is closely linked to the high-level research question of how drivers' near limit vehicle operation is affected by different types of MCs. As identified through literature research on DiLS studies, only little attention is paid to such driving scenarios. Although it is confirmed by independent studies that MCs have a significant impact on how drivers perceive and anticipate different vehicle states [2, 61], it remains unclear which cues (motion- or non-motion-related) contribute to what extent and how those cues affect behavioural validity. The motorsport environment appears highly suitable for such investigations due to three aspects:

- **Professional racing drivers** are used to both driving a race car on a real race track and in a virtual environment. Therefore, driving performance is highly consistent which is beneficial for any objective measure. However, at the same time, the highly specialised target group is a significant limitation, due to the intrinsically limited number of participants.
- **Validated tire and vehicle models** are developed over the term of a full racing season. A part of the validation process is detailed in Appendix A.2. These models are used for the study at both DiL simulators. Likewise, the errors caused by model inaccuracies are kept at a minimum.
- **Track data** is obtained as a by-product from test and race events. This data is used as a reference for the study without additional expenses related to time or cost.

Not only is the relative impact of MCs relevant, but the absolute, quantitative change in driving performance and behavioural validity as well. There are many DiL simulators that use a generic vehicle mockup. The approach of only one physical cockpit representation at the DiLS while using varying underlying vehicle and interface models is based on time and cost considerations. Thereby, the seat, seating position, field of view, steering wheel size and shape, pedal actuation and further HMIs differ compared to the physical vehicle. However, the actual impact on drivers' performance or behavioural validity is largely unknown. For that purpose, the BMW M Motorsport DiLS (DiLS_{BMW}) is used as a reference within this study to obtain a meaningful comparison between the impact of MCs and physical fidelity. As described in the driving simulation preliminaries of chapter 1, the chassis used at DiLS_{BMW} is based on an original monocoque of the respective race

car including individual racing seats for each driver. Likewise, the HMIs are close to what the drivers know from the physical instance of the race car and hence high physical fidelity is assumed.

The compilation of all those aspects leads to a four factorial design with the independent variables environment, driver, MCA and race track. All factors are within-subject factors, meaning that all participants complete the same trials. Each factor is described individually and in more detail by the following subsections. The research questions stated in the introduction are transferred to the following (alternative) hypotheses (H_a):

- H_{a1}: Surge and sway MCs increase drivers' ability to extract maximum vehicle capabilities.
- H_{a2}: Surge and sway MCs increase behavioural validity.
- H_{a3}: The level of physical fidelity affects behavioural validity.

4.2.2. Independent Variables

Driver in the Loop Simulators

In accordance with the statement of the previous contribution section, the experiment is conducted at two different DiL simulators. One of them is the BMW M Motorsport DiLS which is introduced in section 1.3. The second simulator is developed and run by a third party company. For a clear distinction between the two, they are referred to as DiLS_{BMW} and $\text{DiLS}_{\text{THRD}}$ in the course of this work. The screen dimensions are similar in both simulators whereas the used graphics engine, visualisation software and track models are identical (rFpro [82]). Clear differences relate to physical fidelity and the motion system. $\text{DiLS}_{\text{THRD}}$ uses an open chassis mockup of a grand touring (GT) type racing car without physical side doors, windscreen or roof. Instead, these elements are part of the visualisation on the curved screen. The motion system of $\text{DiLS}_{\text{THRD}}$ allows MCs in six DoFs. In addition to heave, pitch, roll and yaw motion, as it is configured at DiLS_{BMW}, the motion system allows lateral translational motion (sway) with a total range of at least 4 m and longitudinal translational motion (surge) with a range of at least 0.8 m. A comparison of response characteristics including both systems is depicted in Figure A.4 of Appendix A.3.

Motion Cueing Algorithms

Three different MCAs are used in total, one of which is introduced in section 3.3. It controls four DoFs and hence works for both motion platforms. Due to this fact, a comparison of results between DiLS_{BMW} and $\text{DiLS}_{\text{THRD}}$ becomes feasible. This MCA is referred to as MCA_{4D}. The residual two MCAs are filter-based as well. Filter tuning is done empirically based on subjective feedback of one racing driver during six preliminary runs at $\text{DiLS}_{\text{THRD}}$. The tuning procedure yields an MCA which makes use of all six DoFs. It is referred to as MCA_{6D}. The third MCA uses MCA_{6D} as a basis and superimposes the vehicle's side slip gradient on the filtered yaw rate. It is therefore referred to

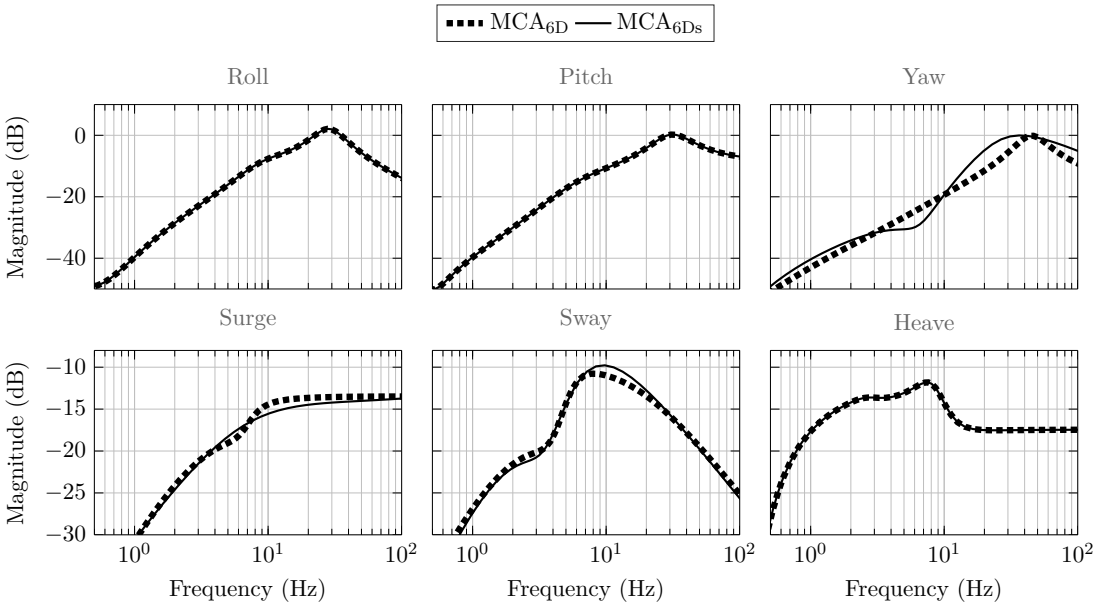

Figure 4.1.: Transfer characteristics of MCA_{6D} and MCA_{6Ds} which are identical for pitch, roll and heave and individually tuned for yaw, surge and sway motion.

as MCA_{6Ds}. Since MCA_{6D} and MCA_{6Ds} make use of six DoFs they do not apply to $DiLS_{BMW}$. The transfer characteristics between vehicle output (MCA input) and MCA output are displayed for both six DoF MCAs (MCA_{6D} and MCA_{6Ds}) in Figure 4.1. All DoFs which are controlled by the MCAs are compared separately. The main deviation relates to yaw motion where the MCA_{6Ds} is characterised by a wider peak around 20 Hz.

Participants

Two PRO drivers participate in the experiment. Both of them are familiar with the physical instance of the simulated vehicle from at least two full seasons of racing in the respective class. Furthermore, both have been driving professional driving simulators for more than 100 h. One driver is highly familiar with the BMW M Motorsport DiLS, having driven the system actively for at least 100 h in total, thereof at least 5 h in the last 30 d before the experiment. The other driver has no prior experience with the latest configuration of the BMW M Motorsport DiLS.

Race Tracks

Figure 4.2 shows maps of both race tracks considered for this study. The left track map shows the Hockenheimring in Germany whereas the right one depicts the TT Circuit Assen in the Netherlands. Corner numbering is added to the Hockenheimring track to align results to specific corners in chapter 5. The combination of both tracks allows capturing a variety of different corner characteristics. The hairpin (T3) in Hockenheim

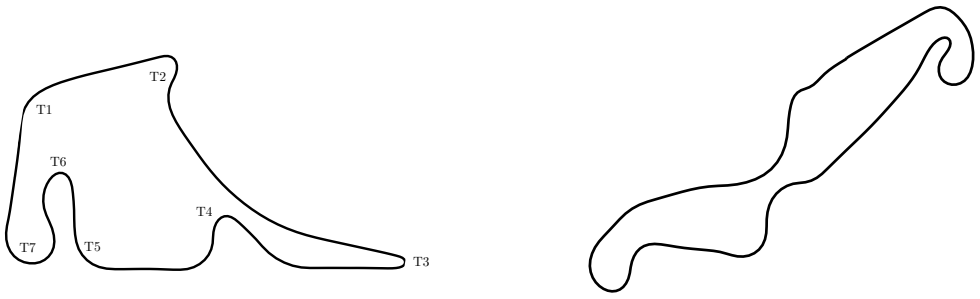

(a) Hockenheimring (Germany)

(b) TT Circuit Assen (Netherlands)

Figure 4.2.: Track map of both race tracks considered for the DRIVEenvironment study. Turn numbering is indicated by T1-T7 and, opposite to the official numbering, merged consecutive corners to match the defined entry, mid and exit phases.

as well as low-speed corners (T2, T6) are opposed to the high-speed cornering sections in Assen. Another significant characteristic is provided by the top right corner of the Assen race track. Turning almost 360° with a decreasing cornering radius represents a significant challenge for the MCAs.

4.2.3. Dependent Variables

The dependent variables are selected among the KPIs reviewed and introduced in chapter 2. The following list uses the observation points of Figure 1.2 to categorise all considered dependent variables:

- OP1: HR, HRV
- OP2: VI, VI_{Thr}, VI_{Brk}, VI_{Str}, VI_{Rlt}
- OP3: TPM_{p}, TPB_{p} t_{Lap}, r_{swr}, N_{fail}
- OP4: CC_{d}, AD_{d}, DI_{d}

A chest ECG device (Chronocord Joysys A.4) is used to capture the drivers' HR and HRV. The HRV is calculated as the root mean square of successive differences (RMSSD) which is a measure of parasympathetic activity and hence an indicator of drivers' regenerative capabilities. It further constitutes an indicator of stress. [53] Baseline corrections are performed using rest measurements of each participant to obtain comparable results between subjects. The VI, TPM, TPB, t_{Lap} and r_{swr} related dependent variables are used according to their definitions in chapter 2 whereas N_{fail} denotes the cumulated number of spins or crashes. It is closely related to P_{fail} from chapter 2 which expresses the probability of a failure within each lap. To obtain a holistic picture of the processes, the objective motion fidelity KPIs CC_{d}, AD_{d} and DI_{d} are applied to $\mathrm{MCA}_{\mathrm{6D}}$ and $\mathrm{MCA}_{\mathrm{6Ds}}$.

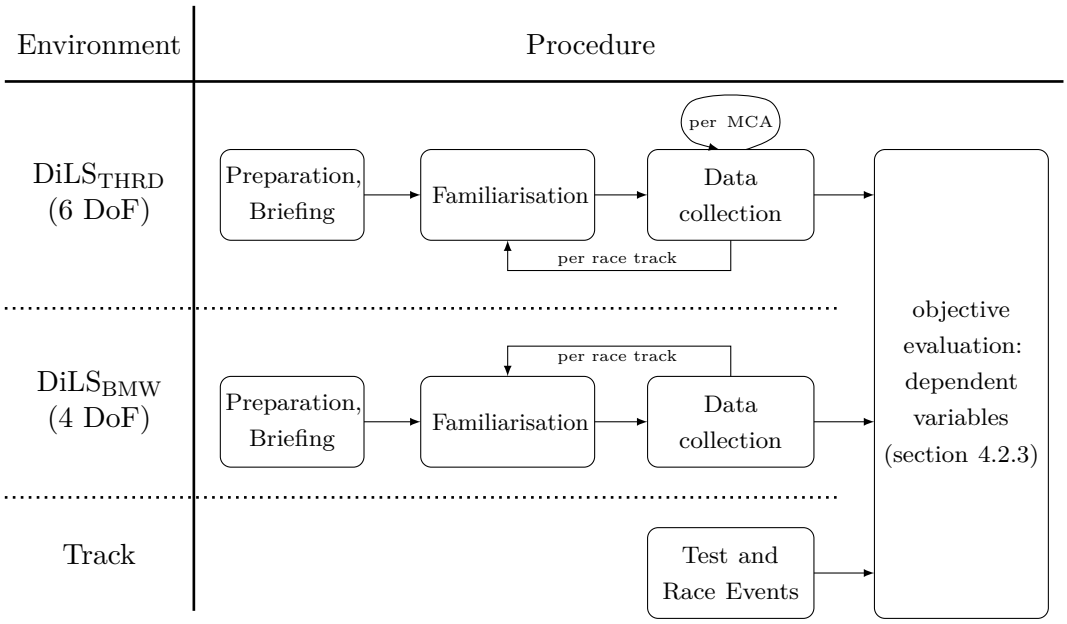

Figure 4.3.: DRIVEenvironment study procedure.

4.2.4. Procedure

An overview of the experimental procedure is provided in Figure 4.3. The track data is available from earlier races of both drivers at the respective race tracks. Regarding DiL environments, the procedure is identical besides the number of MCAs used in each environment. The preparation phase includes HR rest measurements which are used for baseline correction purposes. Afterwards, the familiarisation phase is started at a certain race track. All three MCAs are presented during the familiarisation phase for at least ten laps and until the drivers have subjectively familiarised with the respective settings and environment. The data collection block consists of 20 laps for each MCA, each track and each driver which in total yields 320 laps from simulator operation. The order in which the MCAs and tracks are presented is reversed between both participants to reduce the potential impact of learning effects. The first part of the experiment is conducted at DiLS$_{THRD}$ and it is completed at DiLS$_{BMW}$. It is worth noting that the vehicle model and its parametrisation is identical at both DiL simulators.

4.3. Experimental Study Design: DRIVEmotion

Despite the applicability of the professional motorsport environment for investigations on near-limit vehicle operation, there is a limitation that is not negligible. Due to the overall small number of professional race car drivers and even less within one racing series, there are usually between one and three participants considered in related studies.[86, 89]

However, wider applicability for human drivers is desirable. This consideration is the basis for the second experimental study design. It considers two professional and 31 nonprofessional drivers.

4.3.1. Objective

As stated in chapter 3, the MCA tuning guidelines or cost functions for road car applications vary significantly from those applicable to near-limit vehicle operation. However, road car driving tasks are conducted by road car drivers and motorsport driving tasks by professional racing drivers. It is therefore unknown whether the relevance of certain cues is use case dependent or rather depending on participants' experience. As a consequence, the question arises whether or to what extent results from studies with professional racing drivers apply to normal road car drivers, referred to as amateur (AM) drivers, and vice versa. This observation constitutes the working hypothesis of the following experimental study design. The proposed study which is referred to as DRIVEmotion aims to identify participants' subjective MCA preferences with respect to yaw motion characteristics and yaw motion intensity. Both are adjusted individually via k_1 and k_2 of Equation (3.11). The participants are asked to choose their preferences depending on which settings make it easiest to maximise their driving performance for circuit racing. Driving performance in this particular case is defined and communicated verbally to the participants as minimising t_{Lap} while avoiding to spin the car at any cost. The latter amendment clearly does not add additional information to the statement of minimising t_{Lap}. However, participants are reminded that a clean lap without spinning is the number one priority.

The aforementioned aspects lead to a three factorial design with the independent variables participant group, MCA yaw characteristic and MCA yaw intensity. The latter two are within-subject factors, meaning that all participants completed the same trials. The entire experimental study is conducted at the $\mathrm{DiLS_{BMW}}$. As a race track, the Hockenheimring is selected, see 4.2(a). Each factor is described individually and in more detail by the following section. The research questions stated in the introduction are transferred to the following (alternative) hypotheses:

- $\mathrm{H_{a4}}$: There is a common preference of yaw characteristics between subject groups.
- $\mathrm{H_{a5}}$: There is a common preference of yaw intensity between subject groups.
- $\mathrm{H_{a6}}$: The MCA which maximises drivers' vehicle control performance is not subject group dependent.

4.3.2. Independent Variables

Participants

There are 31 subjects who, in the field of race car driving, are declared AM drivers. Table 4.1 shows the results of a biographical survey form which is completed by each

participant of this AM group. In total, 26 out of 31 subjects completed the experiment, whereas four subjects aborted due to symptoms related to motion sickness and one participant is neglected due to a defect in data acquisition. All participants hold at least a driver's license for passenger cars. None of the participants is familiar with the latest configuration of the DiLS_{BMW}, although four have been driving the simulator with a different motion platform, MCA or simulated vehicle. Five participants have prior experience in some sort of SIM racing, whereas a total of seven participants have been driving in other DiL simulators before. Besides the AM drivers, two professional race car drivers (PRO) are considered. Both are familiar with the DiLS_{BMW}, the race track and the physical instance of the simulated vehicle.

Motion Cueing Algorithm Settings

The MCA used for this experiment is the one introduced in section 3.3.2. During the experiment, a total of four MCA settings are presented to each participant. Three different yaw motion characteristics are described by the first three rows of Table 3.2 and indicated by subscripts A, B and C. The fourth parametrisation is dependent on the participant's individual preference of yaw motion characteristics and her or his choice if increased or decreased intensity would further facilitate the task completion. Both options are described by the fourth and fifth row of Table 3.2. Likewise, a preference pair consisting of MCA characteristic and intensity preference is obtained for each participant.

4.3.3. Dependent Variables

Similar to the DRIVEenvironment experiment, dependent variables are selected among the KPIs of chapter 2. The following list uses the observation points of Figure 1.2 to categorise all considered dependent variables:

- OP1: HR, HRV, NASA TLX, PANAS, SSQ, Cockpit Questionnaire (CQ), Bedford Scale
- OP3: TPM_{p}, t_{Lap}, r_{swr}, $\mu(N_{\text{fail}})$

Table 4.1.: Results of the biographical survey form completed by the AM participants, comprising one female and 30 males.

	Min.	**Max.**	**Mean**	**Median**
age (y)	20	60	34.7	30
annual driving distance (5 year average)	1500	50000	16214	15000
last 90 days driving distance	0	8000	3252	3500
total DiLS experience (h)	0	150	8	0
last 90 days DiLS experience (h)	0	5	0.36	0
total Sim-racing experience (h)	0	750	45.7	0
last 90 days Sim-Racing experience (h)	0	10	0.86	0

In addition to the measurements obtained from the chest ECG device, multiple questionnaires are used to observe effects at observation point OP1. The CQ aims to identify participants' justifications for their preference selection. It includes the Bedford Scale as a measure of mental workload, followed by three questions which are rated on an interval scale between -5 and $+5$:

- How accurate were you able to feel the vehicle behaviour during cornering?
- How did the motion feedback affect your driving performance?
- How much did the motion feedback make the driving task more predictable / consistent?

The TPM, t_{Lap} and r_{swr} related dependent variables are used according to their definitions in chapter 2 whereas $\mu(N_{\mathrm{fail}})$ denotes the average number of spins per lap per participant.

4.3.4. Procedure

The chronological procedure of DRIVEmotion is summarised in Figure 4.4. Apart from a preliminary off-site briefing, the entire study is conducted at the BMW M Motorsport DiLS. The off-site briefing is part of the preparation phase in the top left corner of the procedure illustrated in Figure 4.4. It aims to familiarise participants with the most important interfaces of the DiLS. Steering wheel functionalities are explained alongside pedal actuation and the radio communication system. Another part of the initial off-site briefing is a video-based familiarisation with the Hockenheimring racetrack. A total duration of 30 min is planned for this preparation and a confirmation of its completion is verified upon arrival on site. The preparation on site continues with the installation of ECG electrodes and some safety instructions. Afterwards, the participant enters the DiL simulator's chassis and a first heart rate rest measurement is completed. Therefore, participants are asked to close their eyes and relax inside the chassis for 2 min. Lights in the room are turned off. The first rest measurement serves as a familiarisation phase with the environment and the entire situation. It is neglected for the baseline correction procedure.

Subsequently, the first block of driving is started which consists of two parts. The first one aims to generally familiarise participants with the physical and virtual environment while driving. For this purpose, there are two guided laps where participants verbally obtain standardised information regarding on-brake points, turn-in points, on-throttle points and driving line via an intercommunication system (intercom). These two laps are followed by laps of free driving without any further assistance. This part of the familiarisation is stopped as soon as 10 laps are completed or three lap times in a row have settled within a 1 s margin. Another three laps are used to familiarise participants with $\mathrm{MCA_A}$, $\mathrm{MCA_B}$ and $\mathrm{MCA_C}$ which ends the first driving block. The total duration of the familiarisation is 30 min on average whereas the exact individual duration is depending on the participant's lap times.

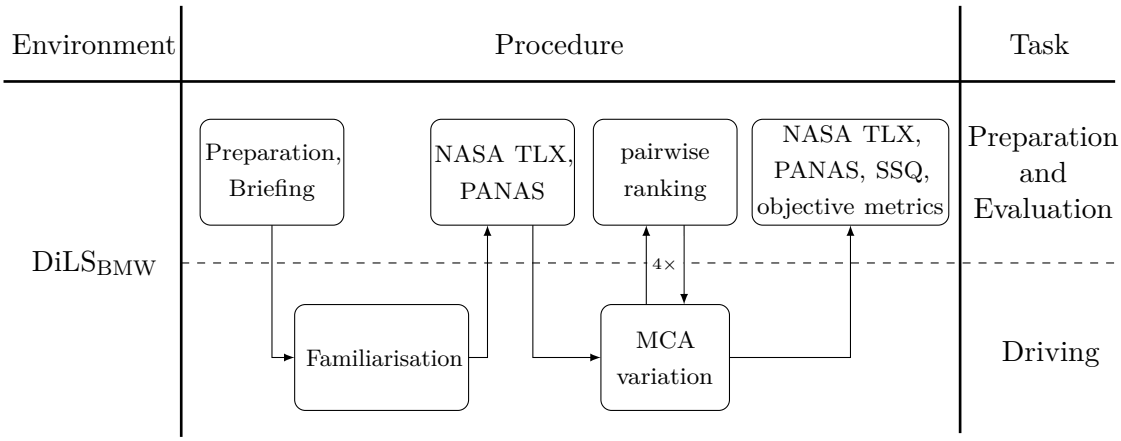

Figure 4.4.: DRIVEmotion study procedure.

The familiarisation is followed by the completion of the NASA TLX and PANAS questionnaires and a relaxation phase outside of the chassis. After approximately 45 min, the participant re-enters the chassis to complete the second HR rest measurement with the same procedure as described before.

In the second block of active driving, participants are asked to pairwise rank two MCA settings. Each setting is active for three consecutive laps. There is no dedicated break between the two runs which should be compared. Participants are asked to come to a stop after crossing the start-finish line of the third lap and the vehicle is repositioned to a pre-defined location at the end of the lap while the MCA parameters are adjusted. Within 10 seconds the comparative run is started. The pairwise ranking includes a verbal preference declaration and completion of the CQ. The same procedure is conducted for all combinations of MCA characteristics. Finally, as soon as the characteristics preference is identified, participants are asked whether increased or decreased yaw motion intensity could improve their task completion performance. Depending on their individual choice, the preferred characteristic is compared to increased (+25%) or decreased (−25%) intensity with the same pairwise ranking procedure. This concludes the second block of active DiLS operation and leads to the final completion of the NASA TLX, PANAS and SSQ questionnaires.

The order in which participants are running the MCA settings is balanced. One group starts with setting MCA_A, continues with MCA_B and ends with MCA_C whereas the second group is running the settings in reverse order. The allocation of participants to both groups is randomised.

4.3.5. Analysis

For the purpose of comprehensible data analysis and to obtain a more detailed insight into the extensive amount of questionnaire and logging data, participants are categorised according to the following aspects:

- MCA characteristic preference
- MCA intensity preference
- driving performance
- track racing experience

The latter refers to the distinction between PRO and AM drivers. A classification of driving performance in three groups - high, medium and low performing - is realised with respect to each participants' run where the best (lowest) TPM result is achieved. Figure 4.5 depicts participants and the corresponding performance group. The TPM range for each group is selected such that comparable group sizes emerge.

There are two more categories used to cluster participants, both of which refer to the participants' subjective MCA characteristics and intensity preference. According to the experimental study design, there are three groups representing the MCA characteristic (A, B, C) and another three groups representing the MCA intensity (high, medium, low) preference. To assign participants to their related group, the subjective evaluation results need to be analysed which are presented in chapter 5.

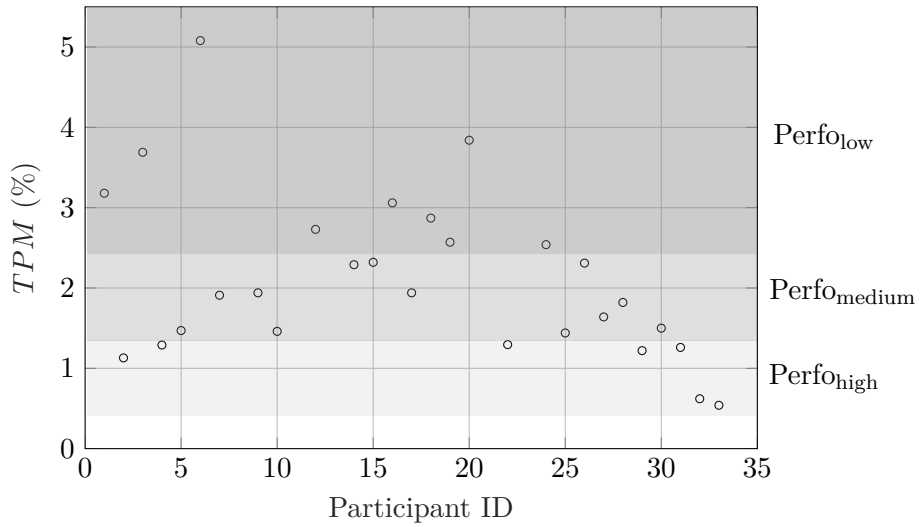

Figure 4.5.: Visualisation of participant performance classification according to their TPM results.
Perfo$_{high}$ represents the best performing participants, Perfo$_{low}$ the least performing participants and Perfo$_{medium}$ those in between.

5. Results

This chapter presents selected results of the DiLS studies introduced in the previous chapter. Quantitative results are obtained by the application of the proposed TPER and VQ methodologies next to state of the art evaluation methods. Hence, chapters 2, 3 and 4 are combined at this point. The alternative hypotheses $H_{a,1}$ - $H_{a,6}$ are accepted or rejected in the course of the following sections. For that purpose, statistical significance is examined where applicable using methods suitable for repeated measures designs. For the analyses of a factor with three levels, the repeated measures ANOVA is used if the results are normally distributed and if the sphericity assumption holds. Otherwise, the non-parametric Friedmann test is applied. For the examination of two levels, a paired t-test for normally distributed results and otherwise the Wilcoxon signed rank test is applied.

5.1. DRIVEenvironment

This section covers selected results of the DRIVEenvironment study which is conducted at two DiL simulators and at a physical race track. Firstly, the two six DoF MCAs are analysed using CC_d, AD_d and DI_d. The results are listed in Table 5.1. While the CC_d shows reasonable values for $\mathrm{d} \coloneqq a_z$, $\mathrm{d} \coloneqq \omega_x$ and $\mathrm{d} \coloneqq \omega_y$, a comparison of

Table 5.1.: Results of CC_d, AD_d and DI_d applied to all six DoFs and to combinations of percepts.
Apart from the two leftmost columns, the top row indicates which DoF d is considered. The two rightmost columns compare extracted vehicle signals to a simulator percept such as the vehicle's side slip gradient $\dot{\beta}_\mathrm{v}$ to the simulator's yaw rate $\omega_{z,\mathrm{s}}$.

KPI	**MCA**	a_x	a_y	a_z	ω_x	ω_y	ω_z	$\frac{\omega_z}{a_y}$	$\frac{\dot{\beta}_\mathrm{v}}{\omega_{z,\mathrm{s}}}$	$\frac{v_\mathrm{v} \cdot \dot{\beta}_\mathrm{v}}{a_{y,\mathrm{s}}}$
CC_d	$\mathrm{MCA_{6D}}$	0.04	0.01	0.82	0.77	0.81	0.09	0.33	0.62	0.33
	$\mathrm{MCA_{6Ds}}$	0.04	0.01	0.82	0.80	0.83	0.11	0.24	0.66	0.31
AD_d	$\mathrm{MCA_{6D}}$	1	1	0.85	0.78	0.63	1	1	1	0.98
	$\mathrm{MCA_{6Ds}}$	1	1	0.85	0.77	0.61	1	1	1	0.98
DI_d	$\mathrm{MCA_{6D}}$	0.09	0.04	0	0.01	0	0.02	0.04	0	0.03
	$\mathrm{MCA_{6Ds}}$	0.1	0.04	0	0.01	0.01	0.02	0.04	0.01	0.03

the MCAs regarding a_x, a_y and ω_z is inconclusive. Searching for an objective motion fidelity indication of MC's relevance, combinations of interrelated signals are added to the analysis. $\text{MCA}_{6\text{Ds}}$ shows a higher CC_d between the simulator's yaw rate $\omega_{z,\text{s}}$ and the vehicle's side slip gradient $\dot{\beta}_\text{v}$ which is caused by the superimposed side slip cue. A finding less apparent is the better alignment of yaw and sway motion cues $\text{d} := \frac{\omega_z}{a_y}$ which is identified for $\text{MCA}_{6\text{D}}$ at $CC_\text{d} = 0.33$ compared to $\text{MCA}_{6\text{Ds}}$ with $CC_\text{d} = 0.24$. By contrast, the AD_d and DI_d KPIs show no differences between the two MCAs. This table of KPIs objectively describes the MCA fidelity at OP4 and serves as a basis for post hoc comparisons to results obtained from TPER. In the following sections, the impact of the DiLS environment as well as the impact of the MCAs on dependent variables related to driving performance are presented. Thereafter, the impact of the same independent variables on behavioural validity is examined.

5.1.1. Driving Performance

A first overview related to driving performance is provided through a lap time comparison. Figure 5.1 compares achieved lap times of both drivers with three different MCAs and two DiLS environments. The variation of independent variables is indicated by the x-axis labels. The left part of Figure 5.1 corresponds to the results obtained at the Hockenheimring and the right part covers results from the Assen race track. Track maps of both race tracks have been introduced in section 4.2.2. Within the environment of DiLS_THRD, a decrease of lap time from $\text{MCA}_{4\text{D}}$ to $\text{MCA}_{6\text{D}}$ and $\text{MCA}_{6\text{Ds}}$ occurs. This holds for median lap times of the experiment's data collection phase with the respective settings. Similar behaviour is identified for minimum achieved lap times which are

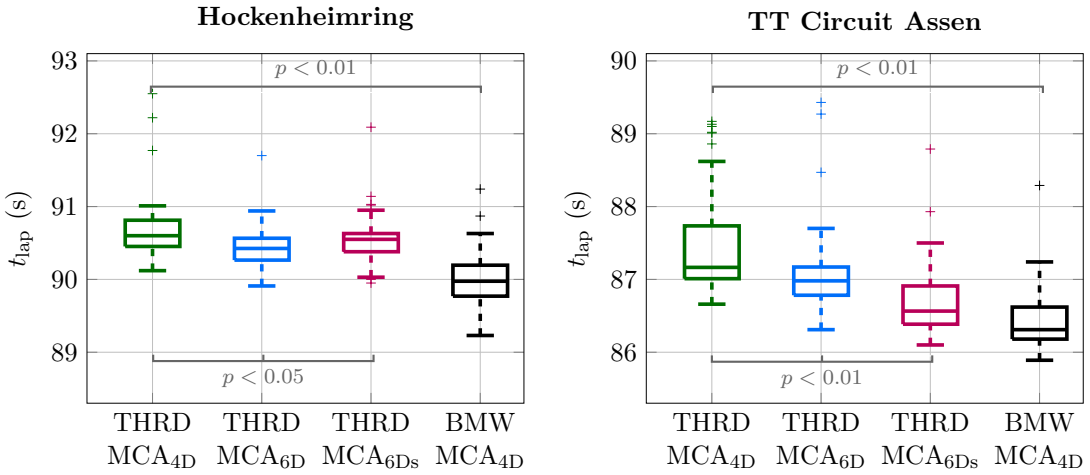

Figure 5.1.: Achieved lap times combined for both drivers.
The p values indicate the statistical significance of effects related to the independent variables MCA (three levels) and DiLS (two levels).

indicated by the lower limits or lower outliers of the boxplots. The additional slip cue of $\mathrm{MCA_{6Ds}}$ has a positive impact on lap times in Assen whereas in Hockenheim this MCA results in an increased median lap time by 0.12 s. Changing the DiLS environment with the same $\mathrm{MCA_{4D}}$ results in a decrease from $t_{\mathrm{Lap}} = 90.60\,\mathrm{s}$ at $\mathrm{DiLS_{THRD}}$ down to $t_{\mathrm{Lap}} = 89.98\,\mathrm{s}$ at $\mathrm{DiLS_{BMW}}$. The same configuration leads to the lowest median lap time of $t_{\mathrm{Lap}} = 86.31\,\mathrm{s}$ achieved in Assen.

Other than absolute lap times, the TPER results are comparable across different race tracks. Thus, results of both drivers at both tracks are depicted in Figure 5.2. The left column shows TPM results for corner entry-, mid- and exit-phase. Additionally, in the bottommost row, the results for the entire cornering phases are displayed. The right column shows corresponding TPB results. All subplots compare the results obtained from $\mathrm{MCA_{4D}}$, $\mathrm{MCA_{6D}}$ and $\mathrm{MCA_{6Ds}}$ at $\mathrm{DiLS_{THRD}}$ as well as $\mathrm{MCA_{4D}}$ at $\mathrm{DiLS_{BMW}}$. At

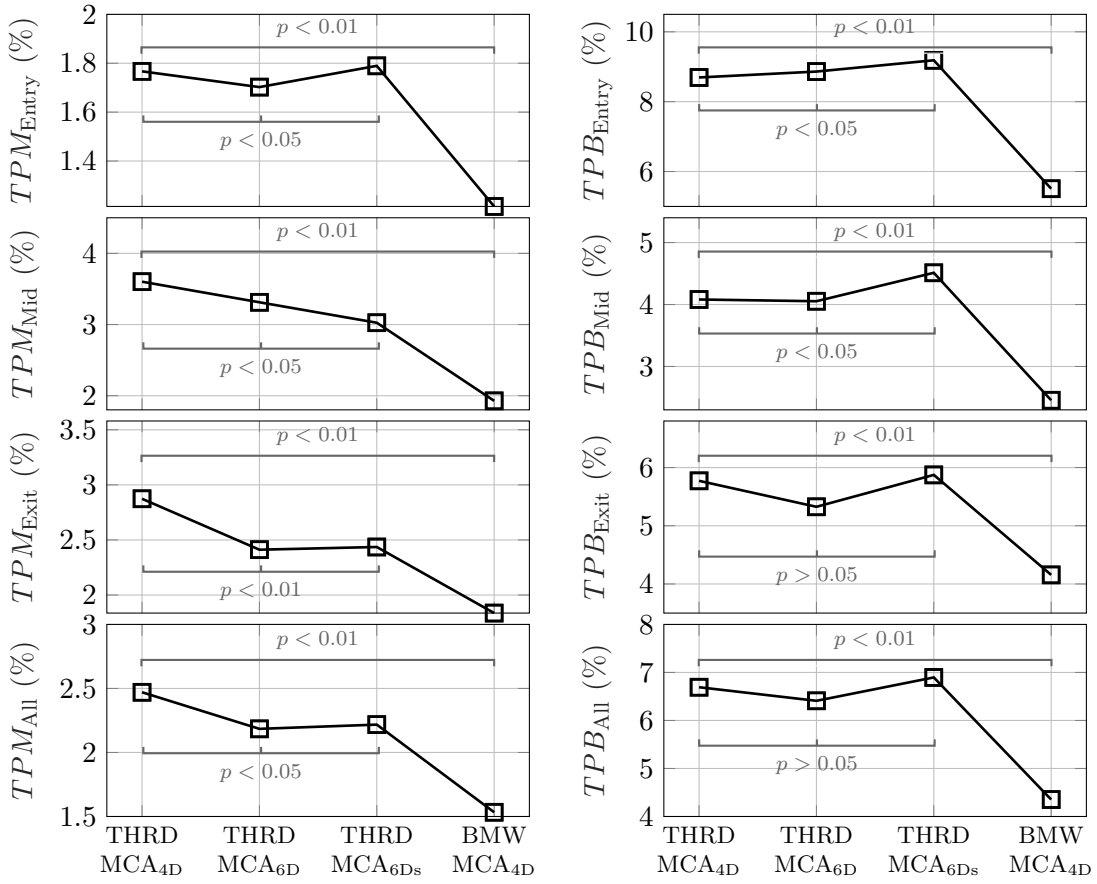

Figure 5.2.: Overall results of TPM_{s} and TPB_{s} combined for both drivers and race tracks.

The p values indicate the statistical significance of effects related to the independent variables MCA (three levels) and DiLS (two levels).

$\text{DiLS}_{\text{THRD}}$ there is an overall TPM reduction of 12% from $TPM_{\text{All}} = 2.5\%$ (MCA_{4D}) to $TPM_{\text{All}} = 2.2\%$ (MCA_{6D} and MCA_{6Ds}). The same trend appears for TPM_{Exit} with the results improving by 16%. In mid-corner phases, MCA_{6Ds} further improves the TPM_{Mid} results whereas the opposite is true in corner entry phases. Regardless of the cornering phase, the best results are obtained at DiLS_{BMW} with an overall value of $\text{TPM}_{\text{All}} = 1.5\%$. In terms of TPB_{All} a step of more than 45% between all MCAs at $\text{DiLS}_{\text{THRD}}$ and the results at DiLS_{BMW} appears. Results within $\text{DiLS}_{\text{THRD}}$ show that overall and particularly in the exit-phase, the resulting trajectory is more advantageous in terms of a balanced tire potential exploitation with MCA_{6D}. However, it should be noted that the effect is not statistically significant considering a significance level of 5%. For the entry- and mid-corner phase, a significant degradation of tire potential exploitation balance is identified for MCA_{6Ds} which is characterised by higher TPB results.

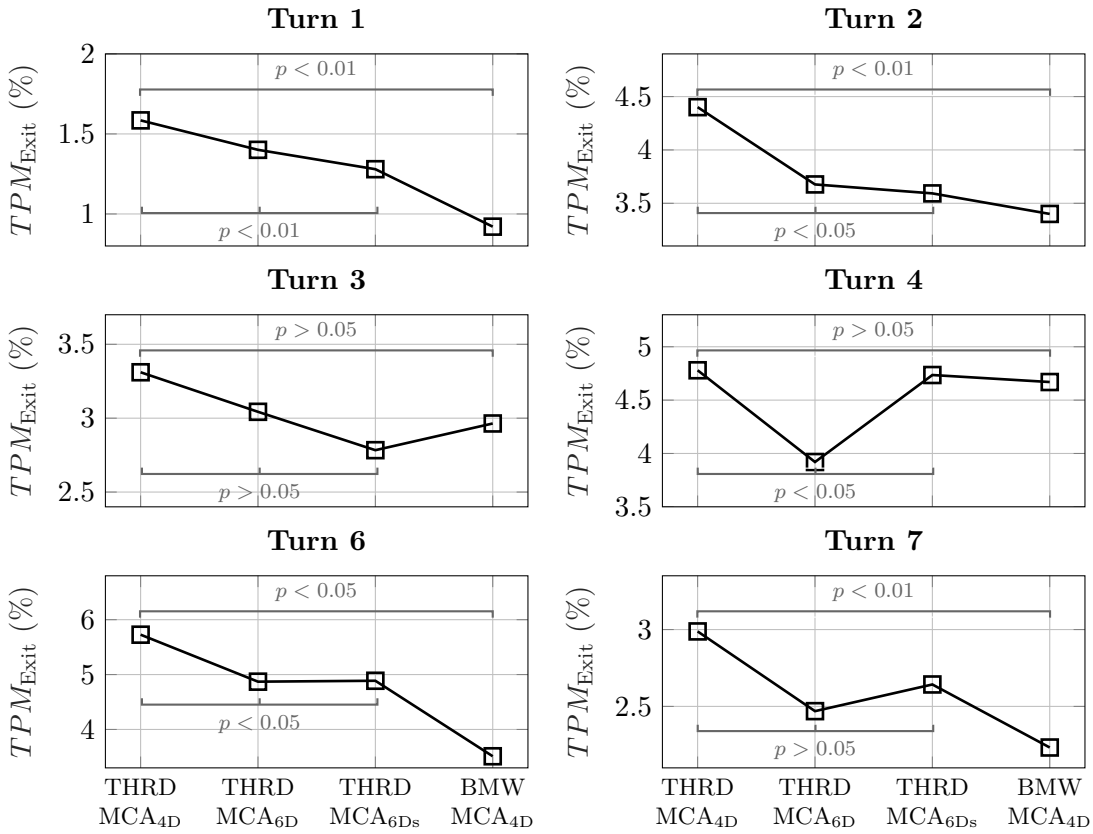

Figure 5.3.: Results of TPM_{Exit} combined for both drivers and separately for Turns T1, T2, T3, T4, T6 and T7 at the Hockenheimring race track.
The p values indicate the statistical significance of effects related to the independent variables MCA (three levels) and DiLS (two levels).

The TPM_{Exit} results including the respective data of both drivers on both race tracks show similar trends using MCA_{6D} and MCA_{6Ds}. For a profound understanding of this result, it is examined in Figure 5.3 for the Hockenheimring race track separately. Individual corners (numbering according to Figure 4.2(a)) are depicted with their respective TPM_{Exit} result. While MCA_{6D} leads to improved results consistently for all corners compared to MCA_{4D}, the effect of MCA_{6Ds} is corner dependent. In turns T1 to T3, MCA_{6Ds} further improves the results compared to MCA_{6D} and the effect is inverted for turns T4 and T7. Therefore, the similar score of TPM_{Exit} for both MCA_{6D} and MCA_{6Ds} in Figure 5.2 is a consequence of superimposed stochastic processes rather than a consistent similarity. However, the opposite is true for TPM_{Exit} of MCA_{4D} compared to MCA_{6D} and DiLS_{BMW} (MCA_{4D}) respectively.

Figures 5.2 and 5.3 both show that drivers can exploit more vehicle potential when perceiving additional surge and sway motion cues. When operating a vehicle close to its maximum capabilities, there is a risk of overestimating the vehicle's potential which may lead to an oversteer and ultimately, if drivers' can not anticipate this change of vehicle behaviour, to a spin. This is certainly relevant for driving simulation where drivers do not perceive the same motion cues as they would in the real car. Therefore, an overview of the cumulated number of spins N_{fail} with all configurations of DiL simulators and MCAs is provided by Figure 5.4. Each configuration is driven for 20 laps (familiarisation excluded) by both drivers per track which leads to a total of 40 laps considered for every plotted bar. Although both drivers operate the vehicle closer to its maximum capabilities with MCA_{6D} and MCA_{6Ds} compared to MCA_{4D} at $\text{DiLS}_{\text{THRD}}$, the cumulated number of spins is reduced by two thirds (Hockenheimring) and by half (TT Circuit Assen). The opposite is true at both tracks for DiLS_{BMW} where double and four-thirds of the spins in $\text{DiLS}_{\text{THRD}}$ (MCA_{4D}) occur. The trends are not race track dependent. Considering the results of TPM and N_{fail}, an increased ability to extract maximum vehicle capabilities with surge and sway MCs is confirmed and therefore H_{a1} is accepted.

5.1.2. Behavioural Validity

All results of the previous section are captured at OP3. Although this allows quantifying drivers' performance and indirectly vehicle state anticipation, there is only limited insight into how the drivers interact with the simulated vehicle. This aspect is covered by Table 5.2. The VQ method as proposed in section 2.4 is applied to the dataset of the DRIVEenvironment study. As driving styles are found to be distinct for racing drivers [109], both participants are examined separately. Therefore, Table 5.2 shows the results of one driver at the Assen race track. Firstly, the validity indicator (VI) is at its maximum for DiLS_{BMW} with a total value of 51%. This is equivalent to an increase of 16% compared to $\text{DiLS}_{\text{THRD}}$ when using the same MCA (MCA_{4D}). The impact of MCAs on the VI appears much smaller compared to the effect of DiLS environments. The results reveal an overall validity of $VI = 45.36\%$ and $VI = 44.18\%$ for MCA_{6D} and MCA_{6Ds} respectively which is equivalent to an increase of 3% and 0.5%.

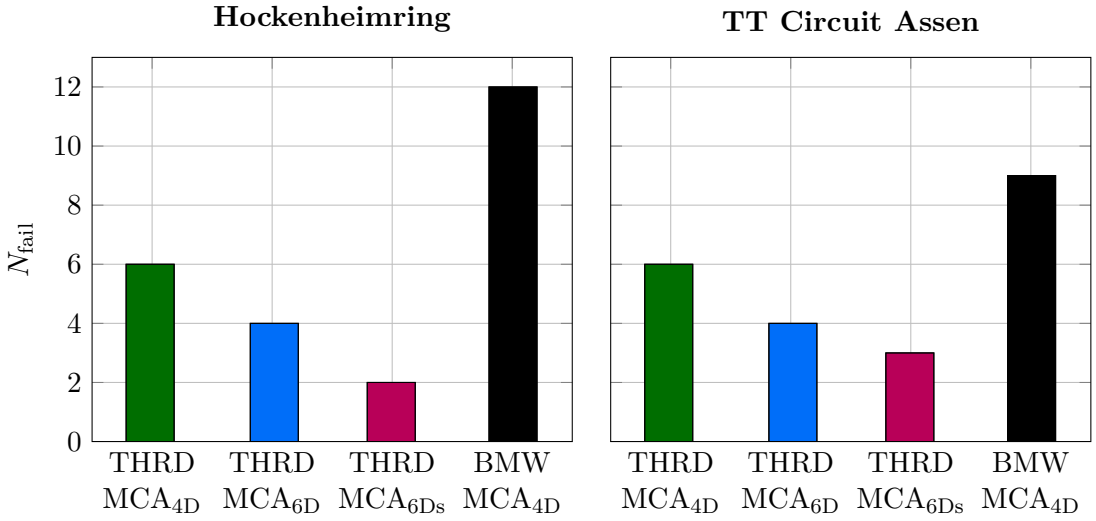

Figure 5.4.: Cumulated number of spins N_{fail} per race track.

Besides the overall VI, the Table includes subscales for throttle pedal interaction (VI_{Thr}), brake pedal interaction (VI_{Brk}), steering wheel interaction (VI_{Str}) and the relation of those three (VI_{Rlt}). The subscale VI_{Rlt} reveals an MCA dependent effect on the interplay of throttle, brake and steering activities. Taking DiLS$_{\text{THRD}}$ (MCA$_{4D}$) as a reference, the VI_{Rlt} score is reduced by 27.9% for MCA$_{6Ds}$ whereas a change of DiLS environment shows an increased score of 7.2%. The same trends at lower magnitude shows VI_{Thr}. Opposite to this, the six DoF MCAs increase the validity of the braking and steering subscales. However, the highest KPI results are achieved at DiLS$_{\text{BMW}}$ on all of the four subscales. Following these results, an effect of physical fidelity on behavioural validity is confirmed and hence H_{a3} is accepted. In contrast, the effect of the surge and sway MCs is not verified consistently which is why H_{a2} is rejected.

Table 5.2.: Validity quantification results for both DiLS and three MCAs.
Subscales indicate the effect within each degree of freedom represented by Throttle (VI_{Thr}), Brake (VI_{Brk}), Steering (VI_{Str}) and the temporal relation between those three (VI_{Rlt}). All VI values in (%) in the range of [0%, 100%].

Environment Settings		**Validity Quantification**		**Subscales**			
DiLS	**MCA**	VI	ΔVI	VI_{Thr}	VI_{Brk}	VI_{Str}	VI_{Rlt}
DiLS$_{\text{THRD}}$	MCA$_{4D}$	43.97	-	45.71	41.62	43.05	49.65
DiLS$_{\text{THRD}}$	MCA$_{6D}$	45.36	+3.2%	44.03	46.88	46.26	42.03
DiLS$_{\text{THRD}}$	MCA$_{6Ds}$	44.18	+0.04%	42.14	45.42	48.83	35.80
DiLS$_{\text{BMW}}$	MCA$_{4D}$	51.00	+16.0%	46.82	53.68	52.78	53.22

5.2. DRIVEmotion

This section firstly covers overall results of the DRIVEmotion experiment, followed by an examination of motion characteristics and motion intensity related effects individually. Positive and negative affects as well as mental workload of each participant are measured twice during the experimental procedure using the PANAS and NASA TLX questionnaires. After completing the familiarisation phase and after completing the main driving part of the experiment is when the repeated measures are conducted. The first questionnaires completed by the participants are referred to as 'pre-test' whereas the second ones are referred to as 'post-test'. Due to the within-subjects repeated measurements, the repeated measures t-test, also known as paired samples t-test, is applicable to test for significant effects.

Table 5.3 summarises the PANAS results for pre- and post-test. Overall, the positive subscale consistently obtains higher results than the negative subscale. This finding is independent of the participants' performance group affiliation. For the entirety of participants, the mean rating on the positive subscale increases from 40.45 in the pre-test up to 45 in the post-test. Similar to the observation made regarding the relation of positive and negative subscale within all groups, the effect between pre- and post-test appears independent of participants' performance group. However, for both pre- and post-test, medium and low performing subjects grade the positive subscale higher than participants of the high performing group. The negative subscale rating increases from high (pre 16.29, post 17.43) over medium (pre 19, post 20) to the low (pre 20.6, post 21.8) performing group and therefore shows inverse correlation to the performance categories.

Table 5.3.: PANAS results before and after the driving block of MCA variation including the paired t-test statistic t.

Group	**Subscale**	**N**	**Pre-test**		**Post-test**		**t**
			Mean	SD	Mean	SD	
Overall	Positive Subscale	27	40.45	4.93	45	5.28	33.10*
	Negative Subscale	27	19.48	5.40	20	5.18	17.46*
High Perfo	Positive Subscale	7	39.43	5.94	43.71	6.32	23.24*
	Negative Subscale	7	16.29	4.03	17.43	4.20	8*
Medium Perfo	Positive Subscale	11	41.44	4.39	45.67	4.72	15.20*
	Negative Subscale	11	19	6.89	20	6.89	inf*
Low Perfo	Positive Subscale	9	41.10	5.17	45.30	5.42	21*
	Negative Subscale	9	20.60	3.50	21.80	3.43	9*

*($p < 0.01$)

Another measure taken into account to analyse participants' evolution of mental constitution is based on the NASA TLX questionnaire. The results are listed in Table 5.4. As introduced in section 2.1.1.4, scores between 50 and 79 relate to experiments with a high workload. Hence the overall workload to complete the active driving tasks is rated to be high. However, there is a decrease in workload from pre- to post-test of at least 7% overall and in each performance group. What is more, inverse correlation occurs between mean workload results of the pre-test and the performance categories. Participants of the low performance group show the highest mean result of 65.50 whereas the subgroup of professional racing drivers relates to a mean workload of 48.33. Hence, for PRO drivers the task shows a 'somewhat high' workload only. Similar trends at an even higher magnitude are obtained in the post-test.

The last overall results applicable to this section are the ratings of AM and PRO drivers. Figure 5.5 depicts both the characteristic and intensity preferences. While PRO drivers preferred MCA_A at high intensity, AM drivers have no joint preference for the MCA characteristic. Nevertheless, MCA_C is the characteristic twelve AM drivers preferred, followed by eight participants preferring MCA_A and six participants chose MCA_B as their preference. Regarding the MCA intensity, there is a trend towards high intensity preferences. Medium and high intensity is preferred by ten and 14 participants respectively, whereas only two amateur drivers preferred low intensity. These findings yield a rejection of H_{a4} as the yaw characteristic preference is approximately uniformly distributed. The bias towards increased intensity preference is an indicator of a common preference. However, the biased distribution appears insufficient to accept H_{a5} at this stage. Taking these initial findings as a basis, the following subsections cover more detailed results related to MCA characteristics and intensity.

Table 5.4.: NASA TLX results before and after the driving block of MCA variation.

Group	**N**	**Pre-test**		**Post-test**		**t**
		Mean	SD	Mean	SD	
Overall	27	62.74	13.41	56.89	13.20	8.33*
High Perfo	7	56.67	15.56	50.36	15.38	8.41*
Medium Perfo	11	63.33	13.03	58.57	10.48	4.2*
Low Perfo	9	65.50	13.47	60.43	13.18	3.94*
PRO	2	48.33	21.21	41.43	18.18	-

*($p < 0.01$)

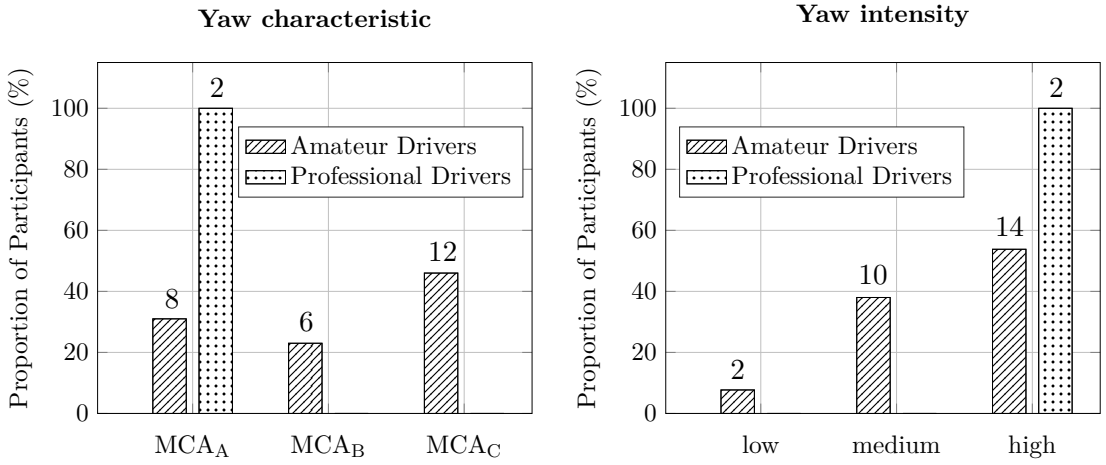

Figure 5.5.: Distribution of preferred MCA characteristics and MCA intensity for professional and amateur drivers.
The digits above the bars indicate the total number of participants who preferred the respective settings.

5.2.1. Motion Characteristic

The MCA preferences for the yaw motion's characteristic are displayed in Figure 5.5. For a deeper insight into the subjective decision making of each participant, the CQ (see section 4.3.3) results are examined. A representative result is depicted in Figure 5.6. The Figure includes participants who prefer $\mathrm{MCA_C}$ only and shows the difference between their ratings on $\mathrm{MCA_C}$ and $\mathrm{MCA_B}$. The uppermost plot reveals that there are only minor differences in workload experienced by the participants with a maximum of ± 1. In contrast, all but participant 31 rated $\mathrm{MCA_C}$ to result in a better feeling for the actual vehicle behaviour during cornering and higher predictability and consistency of the motion feedback. Furthermore, $\mathrm{MCA_C}$ leads to a presumed increase in driving performance for most participants of preference group C.

In terms of objective KPIs, t_{lap} and TPM results are examined in parallel. Figure 5.7 includes the lap time difference Δt_{Lap} of all participants relative to their mean lap time $\mu(t_{\mathrm{lap}})$ achieved during the experiment. A decrease in t_{lap} compared to $\mu(t_{\mathrm{lap}})$ corresponds to the negative half-plane. The Figure shows a correlation between the MCA characteristic preference and median lap times. Preference group A shows a median decrease of $\Delta t_{\mathrm{Lap}} = -0.57\,\mathrm{s}$ at $\mathrm{MCA_A}$ and an increase of $\Delta t_{\mathrm{Lap}} = 0.33\,\mathrm{s}$ and $\Delta t_{\mathrm{Lap}} = 0.51\,\mathrm{s}$ corresponding to $\mathrm{MCA_B}$ and $\mathrm{MCA_C}$ respectively. Group B and group C show similar trends regarding t_{lap} towards their preferred MCA characteristics. However, the results of TPM reveal a different effect. The overall TPM results depicted in the

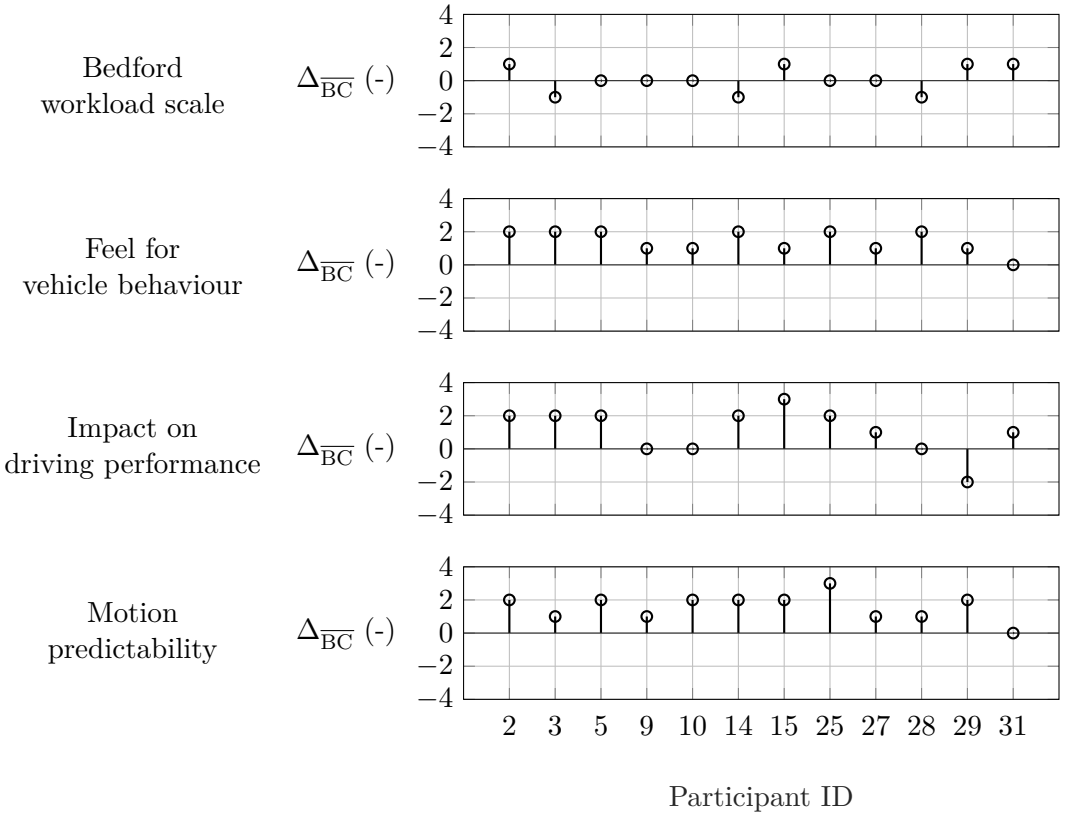

Figure 5.6.: Results of the cockpit questionnaire rating difference $\Delta_{\overline{BC}}$ for the comparison of MCA_B and MCA_C.
This Figure includes participants of the preference group C only and therefore provides insights into the subjective justification of participants' MCA characteristic preference.

lower row of Figure 5.7 show the lowest median results at MCA_A for all preference groups. Preference groups A and B show lower tire potential margins with MCA_A whereas MCA_B and MCA_C lead to results in the positive half-plane of ΔTPM_{All}. The effect is similar in preference group C, although less prominent.

Besides KPIs such as Δt_{Lap} and ΔTPM_{All} which both describe aspects of driving performance, the consistency of task completion is addressed. For that purpose, the mean number of spins $\mu(N_{fail})$ per participant and run is depicted in Figure 5.8. It is at its minimum of 0.85 with MCA_A followed by 1.11 with MCA_B and the maximum value of 1.42 corresponds to MCA_C. The combination of TPM and $\mu(N_{fail})$ demonstrates an improved vehicle control performance using MCA_A and hence H_{a6} is accepted.

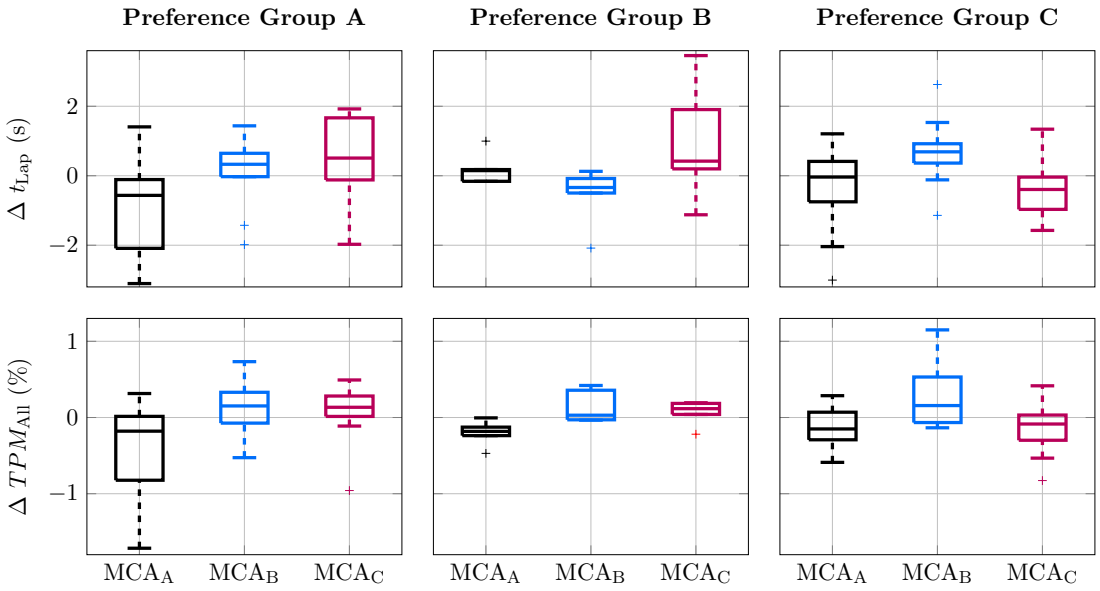

Figure 5.7.: Difference in lap time Δt_{Lap} and tire potential margin $\Delta TPM_{\mathrm{All}}$ individually for the three yaw characteristic preference groups.
The differences are relative to each participants' average result across MCA_{A}, MCA_{B} and MCA_{C}. For the results of Δt_{Lap}, no statistical significance is found in any of the preference groups. In contrast, $p < 0.05$ holds for the $\Delta TPM_{\mathrm{All}}$ results of all MCA levels across the three groups.

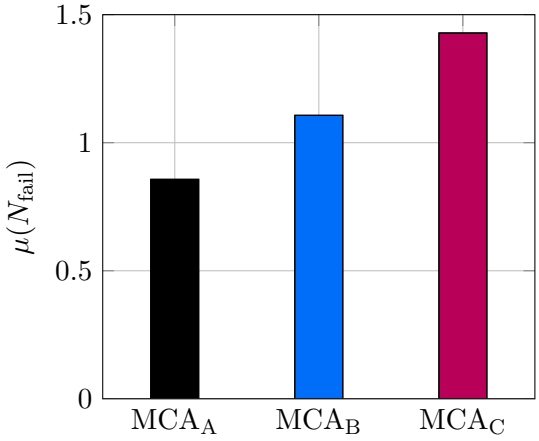

Figure 5.8.: Mean number of spins $\mu(N_{\mathrm{fail}})$ per participant and run in each MCA characteristic setting.

5.2.2. Motion Intensity

The intensity preference rating results (see Figure 5.5) show a subjective preference trend towards medium and high MCA intensity. Again, the comparative questionnaires allow a more detailed insight into how participants' preference is justified subjectively. Figure 5.9 compares the rating results of high versus medium intensity. Similar to the results related to MCA characteristics, there is no consistent impact on the Bedford workload scale. Seven out of 16 participants perceived no change at all which is indicated by $\Delta_{\overline{\text{HighMed}}} = 0$. For the residual nine participants, the effect is small and varying with regard to its sign. The most consistent results are related to participants' feeling for the simulated vehicle's behaviour. The high intensity option is rated to have no or a positive impact by all participants. Driving performance and motion predictability are both rated equally good or better at a higher intensity for all but two participants.

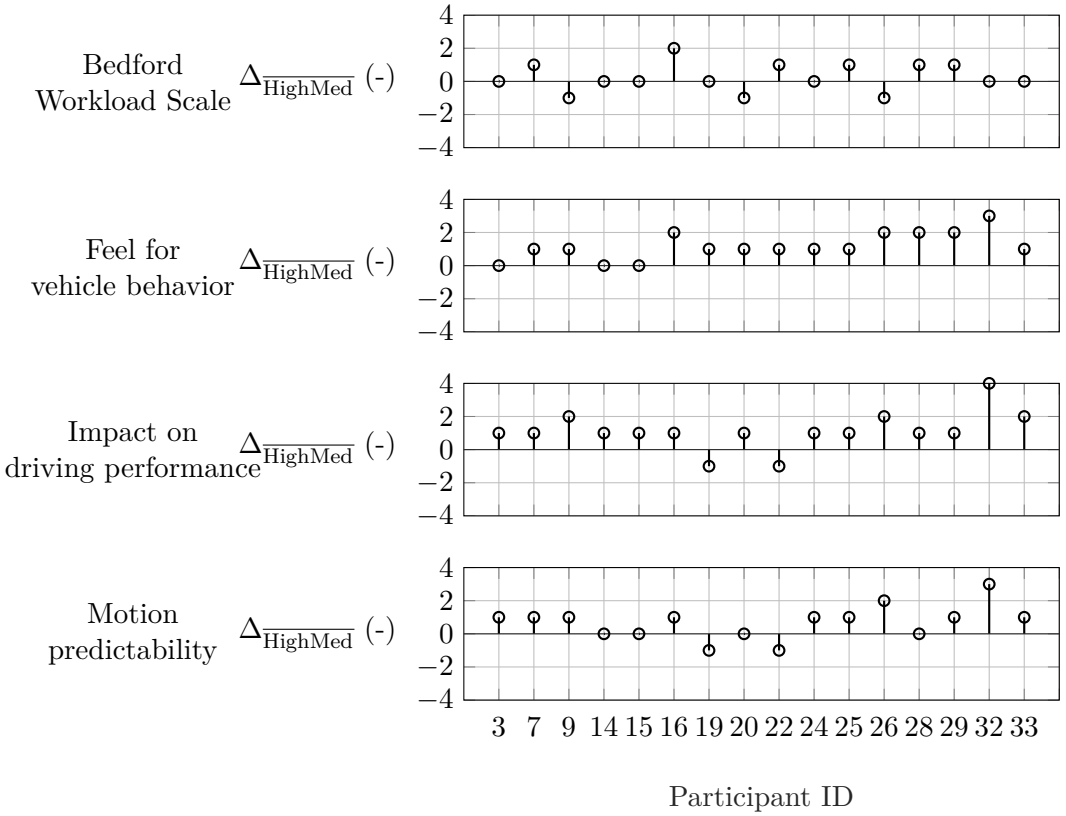

Figure 5.9.: Results of the cockpit questionnaire rating difference $\Delta_{\overline{\text{HighMed}}}$ for the comparison of high and medium intensity.
This Figure includes participants who preferred high intensity only and therefore provides insights into the subjective justification of participants' MCA intensity preference.

As the participants compare either high or low intensity to medium intensity which they are running for the MCA characteristic variation, the effects of high and low intensity are displayed relative to medium intensity in Figure 5.10. Thereby, low intensity increases the mean number of spins by 0.5 per participant and run whereas high intensity decreases the mean number of spins by -0.33.

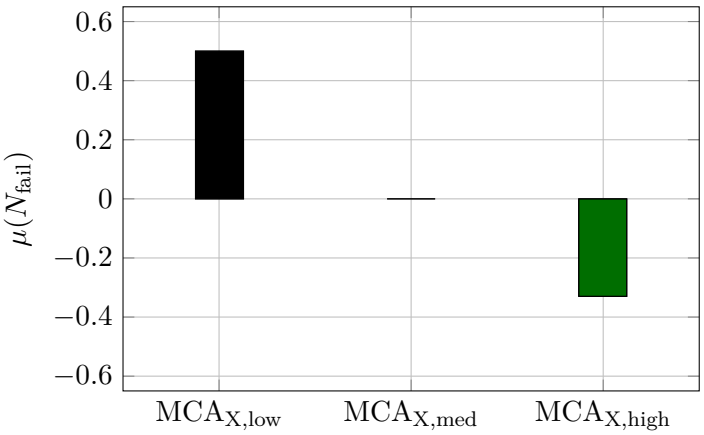

Figure 5.10.: Mean number of spins per participant and run for $\text{MCA}_{\text{X,low}}$ and $\text{MCA}_{\text{X,high}}$, relative to $\text{MCA}_{\text{X,med}}$.

6. Evaluation

This chapter discusses key findings by answering the research questions related to both experimental studies. Additionally, limitations are analysed and transferred to recommendations for future research.

The results show that surge, sway and yaw MCs affect professional racing drivers' vehicle state anticipation. The addition of particular surge and sway MCs leads to improved TPM results and a reduced failure rate by 50% (RQ_1). The effect size of MCs on this aspect is about half of the effect size observed between the two levels of physical fidelity. With regard to behavioural validity, the impact of physical fidelity as it appeared in the DRIVEenvironment study is found to be almost one order of magnitude higher (RQ_2). At the four DoF simulator, where no lateral and longitudinal acceleration cues are provided to the driver, an elimination of yaw rate signal components that correlate with the vehicle's horizontal accelerations is preferred by PRO drivers. As these preferences are supported by TPER and failure rate analyses, the MCs related to side slip angular velocity are confirmed to be relevant for near-limit vehicle state anticipation (RQ_3). AM drivers' yaw characteristic preferences are approximately uniformly distributed across the three tested yaw motion signal characteristics and do not correlate to the respective objective measures (RQ_5). Apart from the difference between PRO and AM drivers, no subjective preference dependency on driving skill could be confirmed (RQ_4). However, the objective measures identified MCA_A to yield the best driving performance regarding TPER and failure rate which is universally valid for all participant groups. A comparison of this finding to the preliminary analysis of MCA fidelity on the basis of CC_d, AD_d and DI_d (Table 3.3) reveals that the KPIs are inconclusive for the present use case. Overall, a manoeuvre dependency rather than skill or subjective preference dependency of MCs' relevance can be concluded.

6.1. Discussion

One aspect of the DRIVEmotion study is to test whether the relevance of certain yaw MCs is related to the use case of circuit racing and near-limit vehicle operation or related to a driver's level of skill. If the first statement holds, the results obtained with PRO drivers could apply to a wider range of participants and use cases. Despite the significant differences in yaw motion characteristics, the subjective preferences of AM drivers show no clear trend. With respect to yaw motion intensity a trend towards the increased intensity (+25%) is found. Knowing that the preferences of PRO racing drivers are closely aligned, although only two of them participated in this particular study, the question arises of

what the reason for the wide distribution of AM preferences is. One possibility is the workload which is rated high according to the NASA TLX questionnaires. The Bedford Scale further reveals that different MCA settings have little to no impact on mental workload which leads to the assumption that the workload was high due to the entire driving task itself, independent of the MCA settings. It is conceivable that the preference rankings are lacking precision due to the workload while driving. Another aspect that could influence the preference ratings is related to the AM drivers' ability to operate the race car somewhat close to its maximum capabilities. As $\mathrm{MCA_A}$ replicates the vehicle's side slip gradient, the motion feedback is very limited while driving in the vehicle's linear region. This driving style is comparable to what is expected on a rural road which relates to a different use case of DiL simulation. Although the intensity is compensated between the three parametrisations for near-limit vehicle operation, different driving styles are not considered. As a result, $\mathrm{MCA_C}$ provides yaw motion feedback above the vestibular perception threshold independent of the vehicle's operating region. Therefore, perceiving some feedback could be ranked higher than no feedback which in turn does not allow any statements regarding yaw motion characteristic preference.

As the results of TPER and failure rate reveal superior task completion performance with $\mathrm{MCA_A}$, the hypothesis on a use case dependency of relevant cues is not rejected. Another statement based on the DRIVEmotion study relates to the MCA quality indicators CC_d, AD_d and DI_d which are frequently used for road car DiLS applications. [54] As the results of TPER and failure rates suggest, $\mathrm{MCA_A}$ provides the most relevant MCs for the particular driving task despite being rated worst out of the three yaw characteristics with regard to the KPIs. Therefore, the application of these objective measures provides no added value for this use case as opposed to MCAs for urban driving scenarios. Instead of comparing vehicle yaw rate $\omega_{z,\mathrm{v}}$ and simulator motion platform yaw rate $\omega_{z,\mathrm{s}}$, the same methods could be applied to combinations of vehicle state related signals. Three exemplary derived vehicle signals are added to Table 5.1 for an explorative analysis using the DRIVEenvironment study results. Comparing the CC_d and TPER results, a correlation between improved TPB_All and TPM_All and the alignment of yaw and sway MCs ($\mathrm{d} \coloneqq \frac{\omega_z}{a_y}$) is identified. Due to its lacking sway MCs, a comparison of this alignment with $\mathrm{MCA_{4D}}$ is not feasible. It is worth noting that the CC_d with $\mathrm{d} \coloneqq \frac{\omega_z}{a_y}$ results in 0.33 and 0.24 for the MCAs $\mathrm{MCA_{6D}}$ and $\mathrm{MCA_{6Ds}}$ respectively and hence the correlation is more than twice as high compared to the CC_d of both factors individually. There, the correlation coefficient remains below 0.11. Furthermore, the CC_d with $\mathrm{d} \coloneqq a_y$ and $\mathrm{d} \coloneqq \omega_z$ are almost identical for both MCAs whereas the derived signal shows a remarkable difference of $\Delta CC_\mathrm{d} = 0.09$ ($\mathrm{d} \coloneqq \frac{\omega_z}{a_y}$). A separation of the results into entry-, mid- and exit-phase could further increase the KPIs' explanatory power. In combination with the TPER method, this should yield deeper insights into drivers' multisensory integration tasks while operating a vehicle close to its dynamic limits. This example is intended to serve as an inspiration for how the perceptual basis for near-limit vehicle state anticipation could be identified.

Furthermore, the DRIVEenvironment study reveals a dependency of behavioural validity on physical fidelity. In comparison, the impact of surge and sway MCs is small yet also positive. On the one hand, this finding implies a demand for high physical fidelity of a DiLS used for motorsport applications and hence generic chassis mock-ups appear unsuitable. On the other hand, the smaller effect size of MCs allows some room for MCA tuning targeted at drivers' maximum task completion performance. The results of behavioural validity quantification listed in Table 5.2 reveal an improvement in the braking and steering related subscales for the six DoF MCAs compared to the four DoF MCA at the same DiLS. By contrast, the throttle related measure VI_{Thr} decreases in the same comparison. Interestingly, the throttle application phase, which is closely aligned with the previously defined exit-phase, is where drivers benefit the most in terms of driving performance. It appears that drivers use the additional MCs to operate the vehicle closer to its maximum capabilities. By doing so, they adjust their driving style (i.e., throttle application) at the cost of behavioural validity. This emphasises the demand for continuous VQ analyses to identify such effects at an early stage and decide on the direction of further developments.

6.2. Limitations

Following the previous discussion, this section covers limitations of the proposed methods and results.

The comparability between $\mathrm{DiLS}_{\mathrm{BMW}}$- and $\mathrm{DiLS}_{\mathrm{THRD}}$-based results is subject to a few uncertainties. Despite identical tire, vehicle and track models, minimum lap times differ significantly. A post hoc analysis reveals varying driving lines at both DiLS. The off-track area is used as an advantage at $\mathrm{DiLS}_{\mathrm{BMW}}$ on the outside of some corner exits and the inside close to corners' apexes. This behaviour is a somewhat grey area of the racing series' sporting regulations and therefore acceptable to some extent. However, the behaviour is penalised at $\mathrm{DiLS}_{\mathrm{THRD}}$ which is the reason why the drivers choose a divergent trajectory. It is worth noting that track limits are predominantly respected in the reference data originating from track operation. In addition, the tire and vehicle models are running at 2 kHz at $\mathrm{DiLS}_{\mathrm{BMW}}$ whereas $\mathrm{DiLS}_{\mathrm{THRD}}$ uses an execution frequency of 1 kHz. Compared to the deviation of driving lines in both DiLS, the numerically caused differences in the vehicle model are negligible.

The current implementation of the TPER methodology is limited in two areas that relate to its accuracy and computational efficiency. The latter is irrelevant for the outcome of this work but affects the method's usability in day-to-day simulator operations. One possibility to overcome the latter is based on a machine learning approach as published by von Schleinitz et al. (2022) [103]. Another approach could be to reduce the sampling frequency at which the optimisation based algorithm operates. The results' accuracy is limited due to the assumption of static tire loads. As a consideration of their dependency on the maximised horizontal acceleration would yield higher computational cost, a

suitable trade-off must be found. The VQ methodology benefits from large datasets, as the metrics' probability distribution estimations become more precise. Thus, the method is well suited for a continuous DiLS evaluation using data from all sessions instead of dedicated experimental studies. Currently, there are no setup variations considered and the track reference data is obtained from the same race track and the same driver. While reference data from the same driver is mandatory due to their distinct driving styles, an investigation across several race tracks could sharpen the results. Therefore, the race track dependency of metric results should be examined and compared to the benefits of increased data availability.

In the experimental study DRIVEmotion, little agreement was found between subjective preferences and task completion performance. As a high workload was identified for the participants of the AM group, it could be argued that their ability to precise judging was impaired. For that reason, experienced drivers only should be considered for future studies in this context. As soon as findings are conclusive within a specialised group, an expansion to a wider group of drivers could be considered.

7. Summary

This chapter summarises the motivation and methodologies developed to gain insights on the interrelation of motion cues (MCs) and vehicle state anticipation in nonlinear vehicle dynamics. Furthermore, the most important results and implications are compiled.

Chapter 1 introduced the motivation which is closely related to regulations applied to most racing series. Driven by its potential to increase performance on track, driving simulation has evolved to an indispensable tool for race car drivers and engineers. However, it was found that only little research effort was dedicated to near-limit vehicle operation and its interaction with MCs. In this regard, a lack of knowledge on the relevance of MCs for vehicle state anticipation was identified and hence the motivation of working towards closing that gap was defined.

Chapter 2 firstly described methodical approaches to subjectively and objectively evaluate different aspects in driver in the loop (DiL) simulation. Methods aiming to rate fidelity, validity and task completion performance were reviewed. As most of them were considered unsuitable for nonlinear vehicle dynamics due to their lacking focus on the vehicle control level, two novel methods were proposed. The first method named tire potential exploitation rating (TPER) was introduced to quantify drivers' capabilities to exploit maximum vehicle capabilities in the driver in the loop simulator (DiLS). It relies on the availability of tire and vehicle models used for the simulation. These models are integrated into an optimisation framework to approximate maximum vehicle capabilities. Under consideration of vehicle-related constraints and its trajectory around the race track, the maximum attainable horizontal acceleration based on the tire potential exploitation is calculated in each time step. Thereby, a continuous performance indicator is obtained which allows separate evaluation of distinct cornering sections such as entry-, mid- and exit-phase. The second evaluation method aimed to quantify behavioural validity by analysing signals which describe driver-vehicle interaction on four distinct scales. Throttle pedal, brake pedal and steering wheel actuation as well as their temporal interrelation were described by 38 metrics from literature. A complexity reduction based on correlation analyses was conducted to describe each scale with reduced redundancies. Subsequently, track data was considered as a reference and the metrics were applied to both DiLS and track originated data. The resulting probability distributions were compared using the Hellinger distance metric and the distances were combined to one validity indicator for each subscale. Finally, the euclidean distance was calculated to further combine the four dimensions of the validity quantification under the assumption of orthogonality between the subscales. The result yields a validity indicator that is particularly suitable to analyse a racing driver's actions on the vehicle control level of the driving task.

Chapter 3 reviewed state of the art motion cueing algorithms (MCAs) based on classical washout filtering and numerical optimisation. The latter category focused on approaches using offline optimisation as well as model predictive control. Two reasons why optimisation-based approaches are rarely used in motorsport applications were identified. Firstly, closed-loop applicability is a mandatory requirement and secondly, the formulation of a suitable objective function remains unclear. This is due to the limited knowledge on the perceptual basis of drivers' near-limit vehicle control actions. To partially close that gap, the research questions and the simulator framework were compiled to a simple yet novel MCA. It is composed of a hybrid structure that combines a model-based yaw motion reference generator and a classical washout filter approach. An advantage of the proposed algorithm is its ease of use for vehicle dynamics engineers rather than control systems engineers. More important for the scope of this work, it allows separating the simulated vehicle's yaw rate into two components of distinct physical origin which is not possible using linear time-invariant filters. Likewise, the distinct signal components can be transferred and perceived by the driver with individual weightings. This characteristic facilitates the identification of which yaw MCs are most relevant for near-limit vehicle operation in a four degrees of freedom (DoF) simulator.

Chapter 4 reviewed DiL studies of related work with a focus on experimental study designs. As there is no common ground for best practice, the reviewed studies were classified according to open- and closed-loop driving manoeuvres, the independent variables of 'Environment', 'DiLS configuration', 'MCA', 'Driving task' and 'Subjects', as well as dependent variables. The compilation of reviewed studies and high-level research questions led to a demand for two experiments which were designed and conducted within this work. The first study was aiming to identify how racing drivers' near-limit vehicle operation is affected by different types of motion and non-motion related cues. In particular, the impact of additional surge and sway MCs is examined and the effect size is compared to the one of decreased physical fidelity. Therefore and to obtain a reference for benchmarking purposes, the experiment was carried out at two different DiL simulators using the same underlying vehicle and tire models and partially the same MCA. Furthermore, track data was considered to apply the validity quantification (VQ) methodology. Overall, the experiment was a four factorial design with the environments, drivers, MCAs and race tracks as independent variables. The second study was following the question of whether or to what extent results from studies with professional racing drivers are applicable to amateur drivers and vice versa. For that purpose, an experimental study was designed and conducted at the BMW M Motorsport DiLS. Two professional race car drivers and a total of 31 amateur drivers participated in the two-staged trial. All subjects were running different yaw MCA characteristics and intensities and finally identified a personal preference of both attributes. Those preferences were compared to objective measures such as the results from applying the TPER methodology.

Chapter 5 described the results of both studies. The first study revealed that additional surge and sway MCs increased the racing drivers' ability to exploit maximum vehicle capabilities by 12% overall and, at the same time, decreased the driving error probability

by up to 50%. In contrast, a clear impact of the additional surge and sway MCs' on behavioural validity in the sense of the VQ method could not be confirmed. Physical fidelity proved to have an impact on both behavioural validity and driving performance. The latter was found to be impacted statistically significant by the two levels of physical fidelity with $p < 0.01$. The validity indicator results were 16% higher at the DiLS of BMW M Motorsport compared to the third party DiLS. The second study revealed a non-conclusive subjective preference of yaw motion characteristic of amateur drivers. By contrast, professional racing drivers consistently selected the characteristic which eliminates the approximated steady state yaw rate. However, the TPER results revealed that all drivers, amateurs and professionals, extracted more vehicle potential during cornering with the professional drivers' preferred characteristic, independent of their subjective preference. With regard to yaw motion intensity preferences, an increase of 25% is preferred by most participants and objectively confirmed using the results of TPER and driving error detection.

Chapter 6 used the findings of chapter 5 to discuss the research questions:

- RQ_1: How do varying surge, sway and yaw MCs affect professional racing drivers' vehicle state anticipation?
- RQ_2: How significant is the effect compared to the impact of varying physical fidelity?
- RQ_3: Which yaw MCs are most relevant for vehicle state anticipation in a four DoF DiLS?
- RQ_4: Are drivers' preferences of yaw motion feedback depending on their experience and driving skills?
- RQ_5: Are subjective preferences supported by enhanced driving performance?

The subjective yaw characteristic preference was found to be closely aligned in the group of professional racing drivers but inconclusive for amateur drivers. However, as the same characteristic produced the best TPER results for all preference groups, these preferences were not supported by objective measures. The potential inability of precise judging could be related to the very high workload during the experiment as captured by the NASA TLX questionnaire. Therefore, it is concluded yet not confirmed that the relevance of certain MCs is use case dependent but not driver skill dependent. According to these findings, yaw MCs which correlate with horizontal accelerations are not supporting vehicle state anticipation in a four DoF DiLS. Therefore, their elimination from the yaw motion reference is recommendable. The DRIVEenvironment study revealed the importance of surge and sway MCs which significantly improved drivers' TPER results. Although the vehicle was operated closer to its maximum capabilities, the amount of driving errors (failures) was decreased by up to 50%. If the motion feedback provided by the different MCAs would be equally relevant for vehicle state anticipation, it could be assumed that the failure rate increases as the tire potential margin decreases. However, with the opposite being true, the presence of more relevant cues was concluded.

The novel methodologies and their proposed applications constitute an important step towards understanding drivers' vehicle state anticipation in a driving simulator. By quantifying the importance of both physical fidelity and motion cues, this work has demonstrated its high potential to contribute to a further identification and optimal replication of the most relevant motion cues for near-limit vehicle operation.

Publications of the Author

The following remarks provide an overview of the author's contribution to publications which are partially incorporated into this thesis:

- **Identification of Drivers' Controlled Stimuli in Nonlinear Vehicle Dynamics Driving Simulation [89]**
  TPER methodology conception, TPER software implementation support, DiLS study design, conduct and analysis, publication conceptualisation, writing original draft, writing review and editing.
- **Validity Quantification of Driver-In-The-Loop Simulation in Motorsport [91]**
  VQ methodology conception and software implementation, DiLS study design, conduct and analysis, publication conceptualisation, writing original draft, writing review and editing.
- **Investigations on Model Predictive Control Objectives for Motion Cueing Algorithms in Motorsport Driving Simulators [88]**
  MCA methodology conception and software implementation, simulation study design, conduct and analysis, publication conceptualisation, writing original draft, writing review and editing.
- **Replication of Near-Limit Lateral Vehicle Dynamics in a Four DOF Driving Simulator [90]**
  MCA methodology conception and software implementation, publication conceptualisation, writing original draft, writing review and editing.
- **Race Driver Evaluation at a Driving Simulator using a physical Model and a Machine Learning Approach [103]**
  Conceptualisation support, writing support original draft, review and editing, methodology support.

List of Equations

List of Figures

List of Tables

Bibliography

[1] C. C. Aggarwal, A. Hinneburg, and D. A. Keim. On the surprising behavior of distance metrics in high dimensional space. In Jan van den Bussche and Victor Vianu, editors, *Database Theory — ICDT 2001*, pages 420–434, Berlin, Heidelberg, 2001. Springer Berlin Heidelberg.

[2] A. Berthoz, W. Bles, H. H. Bulthoff, B. J. Correia Gracio, P. Feenstra, N. Filliard, R. Huhne, A. Kemeny, M. Mayrhofer, M. Mulder, H. G. Nusseck, P. Pretto, G. Reymond, R. Schlusselberger, J. Schwandtner, H. Teufel, B. Vailleau, M. M. van Paassen, M. Vidal, and M. Wentink. Motion scaling for high-performance driving simulators. *IEEE Transactions on Human-Machine Systems*, 43(3):265–276, 2013.

[3] A. Bhattacharyya. On a measure of divergence between two multinomial populations. *Sankhya: The Indian Journal of Statistics*, 7(4):401–406, Juli 1946.

[4] P. Biemelt, C. Link, S. Gausemeier, and A. Trächtler. A model-based online reference prediction strategy for model predictive motion cueing algorithms. *IFAC-PapersOnLine*, 53(2):6082–6088, 2020.

[5] G. J. Blaauw. Driving experience and task demands in simulator and instrumented car: A validation study. *Human factors*, 24(4):473–486, 1982.

[6] J. E. Bos and W. Bles. Theoretical considerations on canal-otolith interaction and an observer model. *Biological cybernetics*, 86(3):191–207, 2002.

[7] V. Branzi, L. Domenichini, and F. La Torre. Drivers' speed behaviour in real and simulated urban roads – a validation study. *Transportation Research Part F: Traffic Psychology and Behaviour*, 49:1–17, 2017.

[8] W. Brems. *Querdynamische Eigenschaftsbewertung in einem Fahrsimulator*. PhD thesis, Universität Stuttgart, Institut für Verbrennungsmotoren und Kraftfahrwesen, Wiesbaden, 2018.

[9] Z. Britton and Q. Arshad. Vestibular and multi-sensory influences upon self-motion perception and the consequences for human behavior. *Frontiers in neurology*, 10:63, 2019.

[10] L. Bruck, B. Haycock, and A. Emadi. A review of driving simulation technology and applications. *IEEE Open Journal of Vehicular Technology*, 2:1–16, 2021.

[11] M. Bruschetta, C. Cenedese, A. Beghi, and F. Maran. A motion cueing algorithm with look-ahead and driver characterization: Application to vertical car dynamics. *IEEE Transactions on Human-Machine Systems*, 48(1):6–16, 2018.

[12] M. Bruschetta, F. Maran, and A. Beghi. A nonlinear, mpc-based motion cueing algorithm for a high-performance, nine-dof dynamic simulator platform. *IEEE Transactions on Control Systems Technology*, 25(2):686–694, 2017.

[13] S. Casas, I. Coma, J. V. Riera, and M. Fernández. Motion-cuing algorithms: characterization of users' perception. *Human factors*, 57(1):144–162, 2015.

[14] S. Casas, R. Olanda, and N. Dey. Motion cueing algorithms: A review. *International Journal of Virtual and Augmented Reality*, 1(1):90–106, 2017.

[15] S. Casas-Yrurzum, C. Portales-Ricart, P. Morillo-Tena, and C. Cruz-Neira. On the objective evaluation of motion cueing in vehicle simulations. *IEEE Transactions on Intelligent Transportation Systems*, 22(5):3001–3013, 2021.

[16] M. R. Chalak Qazani, H. Asadi, M. Al-Ashmori, S. Mohamed, C. P. Lim, and S. Nahavandi. Time series prediction of driving motion scenarios using fuzzy neural networks: * motion signal prediction using fnns. In *2021 IEEE International Conference on Mechatronics (ICM)*, pages 1–6, 2021.

[17] D. Cleij, J. Venrooij, P. Pretto, M. Katliar, H. H. Bülthoff, Steffen, F. W. Hoffmeyer, and H.-P. Schöner. Comparison between filter- and optimization-based motion cueing algorithms for driving simulation. *Transportation Research Part F: Traffic Psychology and Behaviour*, 61:53–68, 2019.

[18] D. Cleij, J. Venrooij, P. Pretto, D. M. Pool, M. Mulder, and H. H. Bülthoff. Continuous rating of perceived visual-inertial motion incoherence during driving simulation. In H. Bülthoff, A. Kemeny, and P. Pretto, editors, *Proceedings of DSC 2015 Europe Driving Simulation Conference & Exhibition*, pages 191–198, Tübingen, 2015.

[19] D. Cleij, J. Venrooij, P. Pretto, D. M. Pool, M. Mulder, and H. H. Bulthoff. Continuous subjective rating of perceived motion incongruence during driving simulation. *IEEE Transactions on Human-Machine Systems*, 48(1):17–29, 2018.

[20] F. Colombet, Z. Fang, and A. Kemeny. Tilt thresholds for acceleration rendering in driving simulation. *SIMULATION*, 93(7):595–603, 2017.

[21] M. Dagdelen, G. Reymond, A. Kemeny, M. Bordier, and N. Maïzi. Model-based predictive motion cueing strategy for vehicle driving simulators. *Control Engineering Practice*, 17(9):995–1003, 2009.

[22] L. C. DePaoli and D. C. Sweeney. Further validation of the positive and negative affect schedule. *Journal of Social Behavior and Personality*, 15(4):561–568, 2000.

[23] E. Donges. Aspekte der aktiven sicherheit bei der führung von personenkraftwagen. *Automobil-Industrie*, (2):183–190, 1982.

[24] M. Eisend and A. Kuß. *Grundlagen empirischer Forschung*. Springer Fachmedien Wiesbaden, Wiesbaden, 2017.

[25] F. Ellensohn, J. Venrooij, M. Schwienbacher, and D. Rixen. Experimental evaluation of an optimization-based motion cueing algorithm. *Transportation Research Part F: Traffic Psychology and Behaviour*, 62:115–125, 2019.

[26] H. Elloumi, M. Bordier, and N. Maizi. Integrated model-based control with human perception models in driving simulation. In *Proceedings of IMACS International conference on Scientific Computation, Applied Mathematics and Simulation*, Paris, 2005.

[27] M. Ersoy and S. Gies. *Fahrwerkhandbuch: Grundlagen - Fahrdynamik - Fahrverhalten- Komponenten - Elektronische Systeme - Fahrerassistenz - Autonomes Fahren- Perspektiven.* ATZ / MTZ-Fachbuch. Springer Fachmedien Wiesbaden, Wiesbaden, 2017.

[28] Z. Fang and A. Kemeny. Explicit mpc motion cueing algorithm for real-time driving simulator. In *Proceedings of The 7th International Power Electronics and Motion Control Conference*, pages 874–878. IEEE, 02.06.2012 - 05.06.2012.

[29] Z. Fang and A. Kemeny. Review and prospects of renault's mpc based motion cueing algorithm for driving simulator. In *Proceedings of DSC 2014 Europe Driving Simulation Conference & Exhibition*, pages 23.1–23.9, 2014.

[30] F. Farroni, E. Rocca, A. Sakhnevych, and F. Timpone. Performance indices for motorsport drivers analysis. In Giuseppe Carbone and Alessandro Gasparetto, editors, *Advances in Italian Mechanism Science*, volume 68 of *Mechanisms and Machine Science*, pages 123–129. Springer International Publishing, Cham, 2019.

[31] Fédération Internationale de l'Automobile. 2018 Formula One Technical Regulations, December 2017. `https://www.fia.com/sites/default/files/1-2018_technical_regulations_2017-12-19_0.pdf`, visited on 2022-03-11.

[32] Ferreira McGrath, E. *Modeling and Monitoring of Otolith Organ Performance in U.S. Navy Operating Environments.* Blacksburg, Virginia, 2003.

[33] M. Fischer. *Motion-Cueing-Algorithmen für eine realitätsnahe Bewegungssimulation.* PhD thesis, Technische Universität Carolo-Wilhelmina zu Braunschweig, Fakultät für Maschinenbau, Braunschweig, 2009.

[34] D. L. Fisher. *Handbook of driving simulation for engineering, medicine, and psychology.* CRC Press, Boca Raton, 2011.

[35] N. J. I. Garrett and M. C. Best. Evaluation of a new body-sideslip-based driving simulator motion cueing algorithm. *Proceedings of the Institution of Mechanical Engineers, Part D: Journal of Automobile Engineering*, 226(11):1433–1444, 2012.

[36] M. Gemou. Transferability of driver speed and lateral deviation measurable performance from semi-dynamic driving simulator to real traffic conditions. *European Transport Research Review*, 5(4):217–233, 2013.

[37] L. Grabherr, K. Nicoucar, F. W. Mast, and D. M. Merfeld. Vestibular thresholds for yaw rotation about an earth-vertical axis as a function of frequency. *Experimental brain research*, 186(4):677–681, 2008.

[38] P. Grant and P. T. S. Lee. Motion-visual phase-error detection in a flight simulator. *Journal of Aircraft*, 44(3):927–935, 2007.

[39] P. Grant and L. Reid. Motion washout filter tuning - rules and requirements (expert systems flight simulators). In *Flight Simulation Technologies Conference*, pages 148–158, Reston, Virigina, 08071995. American Institute of Aeronautics and Astronautics.

[40] J. A. Groeger and G. Murphy. Driver performance under simulated and actual driving conditions: Validity and orthogonality. *Accident; analysis and prevention*, 143:105593, 2020.

[41] M. Grottoli, D. Cleij, P. Pretto, Y. Lemmens, R. Happee, and H. H. Bülthoff. Objective evaluation of prediction strategies for optimization-based motion cueing. *SIMULATION*, 95(8):707–724, 2019.

[42] S. G. Hart and L. E. Staveland. Development of nasa-tlx (task load index): Results of empirical and theoretical research. In *Human Mental Workload*, volume 52 of *Advances in Psychology*, pages 139–183. Elsevier, 1988.

[43] S. M. Highstein, R. R. Fay, and A. N. Popper. *The vestibular system*, volume 19 of *Springer handbook of auditory research*. Springer, New York and Berlin and Heidelberg, 2004.

[44] M. Hogerbrug, J. Venrooij, D. M. Pool, and M. Mulder. Simulator sickness ratings reduce with simulator motion when driven through urban environments. *Driving Simulation Conference Europe 2020 VR, Antibes*, 2020.

[45] R.J.A.W. Hosman and J. C. van der Vaart. *Vestibular models and thresholds of motion perception: Results of tests in a flight simulator*. Report, TU Delft, Department of Aerospace Engineering, Delft, 1978.

[46] J. A. Houck, R. J. Telban, and F. M. Cardullo. *Motion Cueing Algorithm Development: Human-Centered Linear and Nonlinear Approaches*. Report, State University of New York, Binghampton, New York, 2005.

[47] International Organization for Standardization. ISO 8855: Road vehicles - Vehicle dynamics and road-holding ability - Vocabulary, 2011.

[48] C. G. Irwin, J. A. Mollica, and B. Desbrow. Sensitive and reliable measures of driver performance in simulated motor-racing. *International journal of exercise science*, 12(6):971–978, 2019.

[49] R. N. Jazar. *Vehicle Dynamics*. Springer International Publishing, Cham, 2017.

[50] P. Jonik, A. R. Valente Pais, M. van Paassen, and M. Mulder. Phase coherence zones in flight simulation. In *AIAA Modeling and Simulation Technologies Conference*, page 11, Reston, Virigina, 08082011. American Institute of Aeronautics and Astronautics.

[51] Katliar, M. *Optimal Control of Motion Simulators*. PhD thesis, Albert-Ludwigs-Universität Freiburg, Faculty of Engineering, Department of Microsystems Engineering, Freiburg, 2020.

[52] R. S. Kennedy, N. E. Lane, K. S. Berbaum, and M. G. Lilienthal. Simulator sickness questionnaire: An enhanced method for quantifying simulator sickness. *The International Journal of Aviation Psychology*, 3(3):203–220, 1993.

[53] I. Koglbauer, K. W. Kallus, R. Braunstingl, and W. Boucsein. Recovery training in simulator improves performance and psychophysiological state of pilots during simulated and real visual flight rules flight. *The International Journal of Aviation Psychology*, 21(4):307–324, 2011.

[54] M.J.C. Kolff, J. Venrooij, D. M. Pool, and M. Mulder. Comparison of quality metrics between motion cueing algorithms in a virtual test environment. *Driving Simulation Conference Europe 2020 VR, Antibes*, 2020.

[55] A. B. Koyuncu, E. Ercelik, E. Comulada-Simpson, J. Venrooij, M. Kaboli, and A. Knoll. A novel approach to neural network-based motion cueing algorithm for a driving simulator. In *2020 IEEE Intelligent Vehicles Symposium (IV)*, pages 2118–2125. IEEE, 19.10.2020 - 13.11.2020.

[56] Kusachov, A. *Motion Perception and Tire Models for Winter Conditions in Driving Simulators*. PhD thesis, Gothenburg, Sweden, 2016.

[57] E. Kutluay and H. Winner. Validation of vehicle dynamics simulation models – a review. *Vehicle System Dynamics*, 52(2):186–200, 2014.

[58] P. R. Lakerveld, H. J. Damveld, D. M. Pool, K. van der El, M. M. van Paassen, and M. Mulder. The effects of yaw and sway motion cues in curve driving simulation. *IFAC-PapersOnLine*, 49(19):500–505, 2016.

[59] O. Lappi. The racer's mind-how core perceptual-cognitive expertise is reflected in deliberate practice procedures in professional motorsport. *Frontiers in psychology*, 9:1294, 2018.

[60] G. Markkula, R. Romano, A. H. Jamson, L. Pariota, A. Bean, and E. R. Boer. Using driver control models to understand and evaluate behavioral validity of driving simulators. *IEEE Transactions on Human-Machine Systems*, 48(6):592–603, 2018.

[61] G. Markkula, R. Romano, R. Waldram, O. Giles, C. Mole, and R. Wilkie. Modelling visual-vestibular integration and behavioural adaptation in the driving simulator. *Transportation Research Part F: Traffic Psychology and Behaviour*, 66:310–323, 2019.

[62] D. R. Mayhew, H. M. Simpson, K. M. Wood, L. Lonero, K. M. Clinton, and A. G. Johnson. On-road and simulated driving: concurrent and discriminant validation. *Journal of safety research*, 42(4):267–275, 2011.

[63] M. Mayrhofer, B. Langwallner, R. Schlüsselberger, W. Bles, and M. Wentink. An innovative optimal control approach for the next generation simulator motion platform desdemona. In *AIAA Modeling and Simulation Technologies Conference and Exhibit*, Reston, Virigina, 08202007. American Institute of Aeronautics and Astronautics.

[64] J. A. Michon. A critical view of driver behavior models: What do we know, what should we do? In Leonard Evans and Richard C. Schwing, editors, *Human Behavior and Traffic Safety*, pages 485–524. Springer US, Boston, MA, 1985.

[65] A. Mohammadi, H. Asadi, S. Mohamed, K. Nelson, and S. Nahavandi. Optimizing model predictive control horizons using genetic algorithm for motion cueing algorithm. *Expert Systems with Applications*, 92(4):73–81, 2018.

[66] S. Mudd. Assessment of the fidelity of dynamic flight simulators. *Human factors*, 10(4):351–358, 1968.

[67] S. Munir, M. Hovd, Z. Fang, S. Olaru, and A. Kemeny. Complexity reduction in motion cueing algorithm for the ultimate driving simulator. *IFAC-PapersOnLine*, 50(1):10729–10734, 2017.

[68] C. J. Nash, D. J. Cole, and R. S. Bigler. A review of human sensory dynamics for application to models of driver steering and speed control. *Biological cybernetics*, 110(2-3):91–116, 2016.

[69] M.-T. Nguyen, J. Pitz, W. Krantz, J. Neubeck, and J. Wiedemann. Subjective perception and evaluation of driving dynamics in the virtual test drive. *SAE International Journal of Vehicle Dynamics, Stability, and NVH*, 1(2):247–252, 2017.

[70] M. Olivari, P. Pretto, J. Venrooij, and H. H. Bülthoff. Defining the kinematic requirements for a theoretical driving simulator. *Transportation Research Part F: Traffic Psychology and Behaviour*, 61:5–15, 2019.

[71] C. C. Ormsby and L. R. Young. Integration of semicircular canal and otolith information for multisensory orientation stimuli. *Mathematical Biosciences*, 34(1-2):1–21, 1977.

[72] H. B. Pacejka and E. Bakker. The magic formula tyre model. *Vehicle System Dynamics*, 21(sup001):1–18, 1992.

[73] D.-A. Pham and D.-T. Nguyen. A novel motion cueing algorithm integrated multi-sensory system–vestibular and proprioceptive system. *Proceedings of the Institution of Mechanical Engineers, Part K: Journal of Multi-body Dynamics*, 49:146441931989535, 2019.

[74] D.-A. Pham and D.-T. Nguyen. False cue influence on motion cue quality for 10 motion cueing algorithms. *Science progress*, 104(3):368504211036857, 2021.

[75] J.-O. Pitz. *Vorausschauender Motion-Cueing-Algorithmus für den Stuttgarter Fahrsimulator*. PhD thesis, Universität Stuttgart, Institut für Verbrennungsmotoren und Kraftfahrwesen, Wiesbaden, 2017.

[76] N. A. Pouliot, C. M. Gosselin, and M. A. Nahon. Motion simulation capabilities of three-degree-of-freedom flight simulators. *Journal of Aircraft*, 35(1):9–17, 1998.

[77] U. Proske and S. C. Gandevia. The kinaesthetic senses. *The Journal of physiology*, 587(Pt 17):4139–4146, 2009.

[78] M. R. C. Qazani, H. Asadi, C. P. Lim, S. Mohamed, and S. Nahavandi. Prediction of motion simulator signals using time-series neural networks. *IEEE Transactions on Aerospace and Electronic Systems*, page 1, 2021.

[79] A. Ralescu and M. Minoh. Measuring proximity between heterogeneous data. In *2007 IEEE International Fuzzy Systems Conference*, pages 1–6. IEEE, 23.07.2007 - 26.07.2007.

[80] J. Rasmussen. Skills, rules, and knowledge; signals, signs, and symbols, and other distinctions in human performance models. *IEEE Transactions on Systems, Man, and Cybernetics*, SMC-13(3):257–266, 1983.

[81] G. Reymond and A. Kemeny. Motion cueing in the renault driving simulator. *Vehicle System Dynamics*, 34(4):249–259, 2000.

[82] rFpro. Digital road models, 2022. `https://www.rfpro.com/digital-road-models`, visited on 2022-03-11. Romsey, Hampshire.

[83] R. Romano, G. Markkula, E. Boer, H. Jamson, A. Bean, A. Tomlinson, A. Horrobin, and E. Sadraei. An objective assessment of the utility of a driving simulator for low mu testing. *Transportation Research Part F: Traffic Psychology and Behaviour*, 65:34–45, 2019.

[84] A. H. Roscoe. Assessing pilot workload in flight. *AGARD Conference Proceeings Flight Test. Techniques*, 1984.

[85] I. G. Salisbury and D. J. N. Limebeer. Optimal motion cueing for race cars. *IEEE Transactions on Control Systems Technology*, 24(1):200–215, 2016.

[86] I. G. Salisbury and D. J. N. Limebeer. Motion cueing in high-performance vehicle simulators. *Vehicle System Dynamics*, 55(6):1–27, 2017.

[87] Schmidt, S. F., Conrad, B. *Motion drive signals for piloted flight simulators*. Report, NASA, Washington D. C., USA, 1970.

[88] T. Schwarzhuber, M. Graf, and A. Eichberger. Investigations on model predictive control objectives for motion cueing algorithms in motorsport driving simulators. In *2021 IEEE Intelligent Vehicles Symposium (IV)*, pages 49–54, 2021.

[89] T. Schwarzhuber, J. von Schleinitz, H. Geiser, M. Graf, and A. Eichberger. Identification of drivers' controlled stimuli in nonlinear vehicle dynamics driving simulation. In *Proceedings of the Driving Simulation Conference 2020*, pages 45–52. 2020.

[90] T. Schwarzhuber, L. Wörle, M. Graf, and A. Eichberger. Replication of near-limit lateral vehicle dynamics in a four dof driving simulator. In *Proceedings of the Driving Simulation Conference 2021*. Driving Simulation Association, 2021.

[91] Schwarzhuber, T. and Wörle, L. and Graf, M. and Eichberger, A. Validity quantification of driver-in-the-loop simulation in motorsport. In *Proceedings of the FISITA 2020 Web Congress*. 2020.

[92] B. Schweizer and A. Sklar. Statistical metric spaces. *Pacific Journal of Math*, 10(1):313–334, 1960.

[93] SENSODRIVE GmbH. Senso-wheel ht, 2022. `https://www.sensodrive.de/produkte-leistungen/senso-wheel-ht.php`, visited on 2022-03-11. Weßling.

[94] K. Siebertz, D. van Bebber, and T. Hochkirchen. *Statistische Versuchsplanung*. Springer Berlin Heidelberg, Berlin, Heidelberg, 2017.

[95] P. D. Spyridakos, N. Merat, E. R. Boer, and G. M. Markkula. Behavioural validity of driving simulators for prototype hmi evaluation. *IET Intelligent Transport Systems*, 14(6):601–610, 2020.

[96] P. Stahl, B. Donmez, and G. A. Jamieson. Anticipation in driving: The role of experience in the efficacy of pre-event conflict cues. *IEEE Transactions on Human-Machine Systems*, 44(5):603–613, 2014.

[97] The Mathworks, Inc. Solver-based nonlinear optimization, 2022. `https://de.mathworks.com/help/optim/solver-based-nonlinear-optimization.html`, visited on 2022-03-17.

[98] D. Toffin, G. Reymond, A. Kemeny, and J. Droulez. Influence of steering wheel torque feedback in a dynamic driving simulator. In *DSC North America 2003*.

[99] M. Trzesniowski and P. Eder. *Datenanalyse, Abstimmung und Entwicklung*. Springer Fachmedien Wiesbaden, Wiesbaden, 2017.

[100] A. Väljamäe, P. Larsson, D. Västfjäll, and M. Kleiner. Travelling without moving: Auditory scene cues for translational self-motion. In *Meeting of the International Conference on Auditory Display*, Limerick, Ireland, 2005.

[101] T. D. van Leeuwen, D. Cleij, D. M. Pool, M. Mulder, and H. H. Bülthoff. Time-varying perceived motion mismatch due to motion scaling in curve driving simulation. *Transportation Research Part F: Traffic Psychology and Behaviour*, 61:84–92, 2019.

[102] J. Venrooij, P. Pretto, M. Katliar, S. Nooij, A. Nesti, M. Lächele, K. de Winkel, and D. Cleij. Perception-based motion cueing: validation in driving simulation. In H. Bülthoff, A. Kemeny, and P. Pretto, editors, *Proceedings of DSC 2015 Europe Driving Simulation Conference & Exhibition*, Tübingen, 2015.

[103] J. von Schleinitz, T. Schwarzhuber, L. Wörle, M. Graf, A. Eichberger2, W. Trutschnig, and A. Schröder. Race driver evaluation at a driving simulator using a physical model and a machine learning approach. 2022. arXiv:2201.12939.

[104] J. von Schleinitz, L. Wörle, M. Graf, A. Schroder, and W. Trutschnig. Analysis of race car drivers pedal interactions by means of supervised learning. In *2019 IEEE Intelligent Transportation Systems Conference (ITSC)*, pages 4152–4157. IEEE, 27.10.2019 - 30.10.2019.

[105] Y. Wang, B. Mehler, B. Reimer, V. Lammers, L. A. D'Ambrosio, and J. F. Coughlin. The validity of driving simulation for assessing differences between in-vehicle informational interfaces: A comparison with field testing. *Ergonomics*, 53(3):404–420, 2010.

[106] W. H. Warren. Self-motion: Visual perception and visual control. In *Perception of Space and Motion*, pages 263–325. Elsevier, 1995.

[107] D. Watson, L. A. Clark, and A. Tellegen. Development and validation of brief measures of positive and negative affect: The panas scales. *Journal of Personality and Social Psychology*, 54(6):1063–1070, 1988.

[108] L. Woerle, J. von Schleinitz, M. Graf, and A. Eichberger. Driver detection from objective criteria describing the driving style of race car drivers. In *2019 IEEE Intelligent Transportation Systems Conference (ITSC)*, pages 1198–1203. IEEE, 27.10.2019 - 30.10.2019.

[109] L. Wörle. *Objective Criteria for Driving Style in Motorsport*. PhD thesis, Graz University of Technology, Institute of Automotive Engineering, 2019.

[110] L. Wörle, M. Graf, and A. Eichberger. Objective metrics for control inputs of racecar drivers: F2018-vdy-050. In *Proceedings of FISITA 2018 World Automotive Congress*. 2018.

[111] R. A. Wynne, V. Beanland, and P. M. Salmon. Systematic review of driving simulator validation studies. *Safety Science*, 117:138–151, 2019.

[112] G. Zacharias. *Motion sensation dependence on visual and vestibular cues*. Massachusetts Institute of Technology, Massachusetts, 1977.

[113] Z. Zhang, Y. Asakawa, T. Imamura, and T. Miyake. Experiment design for measuring driver reaction time in driving situation. In *2013 IEEE International Conference on Systems, Man, and Cybernetics*, pages 3699–3703. IEEE, 13.10.2013 - 16.10.2013.

A. Appendix

A.1. Coordinate Systems of the Planar Two Track Model

For the TPER methodology, a planar two track vehicle model according to [49] is considered. The simplification for planar motion includes longitudinal, lateral and yaw motion, whereas heave, pitch and roll motion are neglected. Two coordinate systems are required for the mathematical description which are illustrated in Figure A.1. The origin C of the vehicle coordinate system $v(C, x, y, z)$ is located at the vehicle's CoG. The longitudinal and lateral axes x and y are parallel to the vehicle's longitudinal and lateral plane of symmetry which follows the definition of the ISO 8855 convention [47]. The vertical z-axis is pointing upward. For readability, all variables of the vehicle model without any prefix subscript relate to the vehicle coordinate system. The four local tire coordinate systems $t(P, {}_tx, {}_ty, {}_tz)$ are described by the axes ${}_tx$, ${}_ty$, ${}_tz$. Figure A.1 shows the local coordinate system exemplary for the front left tire. As pitch and roll motion,

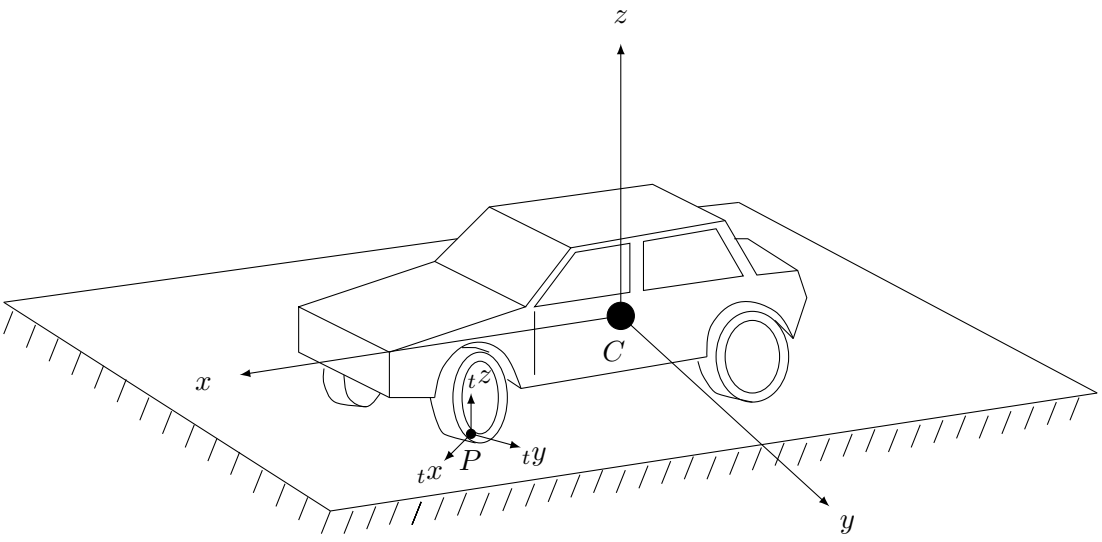

Figure A.1.: Vehicle coordinate system and an exemplary tire coordinate system (front left) used for the planar two track model of the TPER methodology.
The vehicle coordinate system $v(C, x, y, z)$ follows the ISO 8855 convention [47]. The z- and ${}_tz$-axes are parallel and the tire coordinate system $t(P, x, y, z)$ is rotated around the vertical axis by the steered tire angle δ_i.

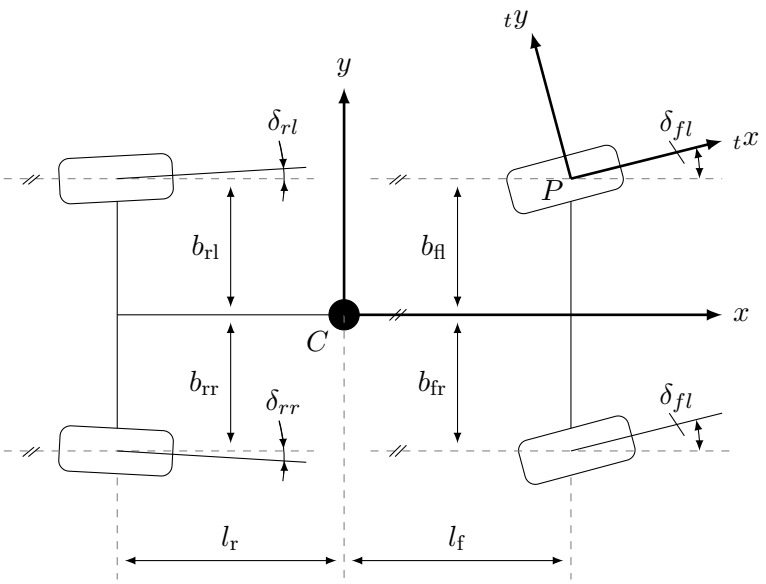

Figure A.2.: Two track vehicle model including the vehicle coordinate system and the exemplary local front left tire coordinate system.

and implicitly road inclination, are neglected, the vertical axes z and $_t z$ are perpendicular to the road plane. The $_t x$-axis is defined by the intersection of the road plane and the wheel plane. Therefore, the $_t x$ and $_t y$ axes are rotated by the steered wheel angle δ_i with respect to x and y. The origin of the tire coordinate system is located at the assumed single contact point P between road and tire model. A two-dimensional representation of the coordinate systems is integrated into the two track model illustration of Figure A.2.

The differential equations of motion for the reduced order vehicle model in the vehicle coordinate system are

$$m \cdot (\dot{v}_x \ + \ \omega_z v_y) \ = \ \sum_{i=1}^{4} F_{x,i} \ + \ F_{x,\mathrm{Ext}}, \tag{A.1}$$

$$m \cdot (\dot{v}_y \ + \ \omega_z v_x) \ = \ \sum_{i=1}^{4} F_{y,i} \ + \ F_{y,\mathrm{Ext}}, \tag{A.2}$$

$$J_{\mathrm{zz}} \cdot \dot{\omega}_z \ = \ \sum_{i=1}^{4} l_{\mathrm{i}} \cdot F_{y,i} \ - \ \sum_{i=1}^{4} b_{\mathrm{i}} \cdot F_{x,i} \ + \ \sum_{i=1}^{4} M_{z,i}, \tag{A.3}$$

with index $i \in \{1(\mathrm{fl}),\ 2(\mathrm{fr}),\ 3(\mathrm{rl}),\ 4(\mathrm{rr})\}$ denoting the respective wheel. The half track widths b_i and the distances from the CoG to the front and rear axle, l_f and l_r, are shown in Figure A.2. The tires' self-aligning torques are denoted by $M_{z,i}$. The variables $F_{x,\mathrm{Ext}}$ and $F_{y,\mathrm{Ext}}$ describe the sum of external forces translated into one single force acting

on the vehicle's CoG parallel to the x- and y-axes. The forces at each tire $F_{x,i}$, $F_{y,i}$ in the vehicle fixed coordinate frame are obtained using the transformation matrix $\boldsymbol{R}_{vt}$ according to

$$\begin{bmatrix} F_{x,i} \\ F_{y,i} \\ M_{z,i} \end{bmatrix} = \underbrace{\begin{bmatrix} \cos\delta_i & -\sin\delta_i & 0 \\ \sin\delta_i & \cos\delta_i & 0 \\ 0 & 0 & 1 \end{bmatrix}}_{\boldsymbol{R}_{vt}} \cdot \begin{bmatrix} {}_tF_{x,i} \\ {}_tF_{y,i} \\ {}_tM_{z,i} \end{bmatrix}. \tag{A.4}$$

The transformation depends on the tire steering angles δ_i which result from the superposition of driver's steering wheel actuation and the respective toe angles. Hence, δ_i is applicable for the front and rear wheels despite considering vehicles with front axle steering only.

A.2. High-Level Validity Quantification of the Vehicle Model

The vehicle model validation follows a hierarchical approach, where model parameters are first identified and validated on component and subsystem level using test bench experiments. One such subsystem is devoted to tire dynamics which are modelled using Pacejka's Magic Formula. As the particular area of interest relates to nonlinear vehicle dynamics, the tire characteristics are identified for the full range of feasible longitudinal and lateral slips, camber angles and tire loads. The validation on subsystem level requires additional experimental test bench data in order to compare the physical and the modelled subsystem outputs for a predefined input sequence using objective validation metrics. In the particular case of tire dynamics, the resulting longitudinal and lateral tire forces ${}_tF_{x,i}$ and ${}_tF_{y,i}$ are analysed. After completing the subsystem validation, the full vehicle model (top level of the hierarchical validation approach) is considered. While the subsystem validation is based on open-loop manoeuvres, where pre-defined excitations are passed to the model and the physical instance of the subsystem, the high-level validation is based on closed-loop manoeuvres. An exemplary comparison of the track (real vehicle) and DiLS originated data is depicted in Figure A.3. It shows an overlay of longitudinal vehicle velocity v_x, longitudinal acceleration a_x and lateral acceleration a_y. The transient behaviour of all three signals appear very accurate, whereas deviations are visible for maximum velocities and minimum braking accelerations. Such qualitative comparisons are supplemented using validation metrics which aim to capture characteristics of the relevant use case. In this regard, Table A.1 shows exemplary metrics and lists the related results for the data of Figure A.3.

Table A.1.: Exemplary results of the high-level vehicle model validation metrics. The values relate to one lap at the Hockenheimring race track.
Metrics show relative errors between DiL simulator and race track originated data.
Numbering of consecutive corners T1 - T9 follows the definition of Figure A.3.

Metric	Description	T1	T2	T3	T4	T5	T6	T7	T8	T9	Mean
$e^{\mathrm{rel}}_{v_{\min}}$	relative error of minimum cornering speed	0.01	0.11	0.22	0.01	0.01	0.01	0.09	0.01	0.01	0.01
$e^{\mathrm{rel}}_{a_{x,\min}}$	relative error of maximum long. deceleration	0.33	0.15	0.05	0.01	0.17	0.29	0.07	0.38	0.01	0.15
$e^{\mathrm{rel}}_{a_{x,\max}}$	relative error of maximum long. acceleration	0.17	0.01	0.02	0.09	0.13	0.02	0.01	0.01	0.11	0.02
$e^{\mathrm{rel}}_{a_{y,\max}}$	relative error of maximum lateral acceleration	0.01	0.02	0.01	0.01	0.06	0.02	0.07	0.19	0.01	0.02

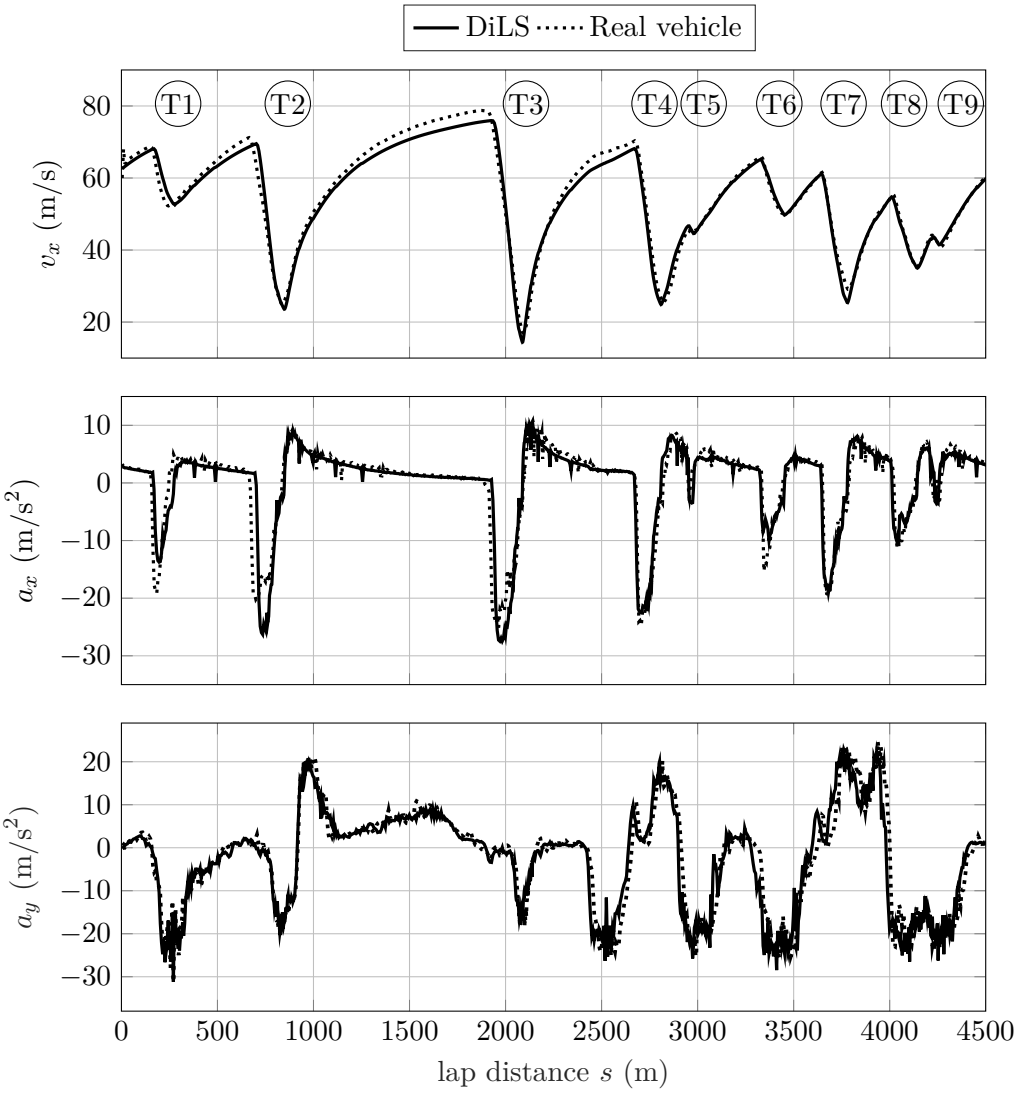

Figure A.3.: Data overlay of DiLS and on-track results for a qualitative evaluation of vehicle model validity.
The three rows from top to bottom show the longitudinal velocity v_x, longitudinal acceleration a_x and lateral acceleration a_y profiles for one full lap.

The mean relative error of minimum cornering speeds $e^{\text{rel}}_{v_{\text{min}}}$ is at 1%, the mean relative error of maximum longitudinal acceleration $e^{\text{rel}}_{a_{x,\text{max}}}$ is 2% and the same value applies to the mean relative error of maximum lateral acceleration $e^{\text{rel}}_{a_{y,\text{max}}}$. The mean relative error of maximum deceleration $e^{\text{rel}}_{a_{x,\text{min}}}$ is one order of magnitude higher and results in 15%. It is worth noting that this closed loop approach introduces some uncertainty as the effects of vehicle model, track model and driver behaviour are not completely separable.

A.3. Motion System Transfer Characteristics

The transfer characteristics of both DiL simulators used for the DRIVEenvironment study are identified according to Figure A.4. The respective degrees of freedom are compared with regard to magnitude and phase characteristics. The results devoted to the BMW M Motorsport driving simulator $\mathrm{DiLS_{BMW}}$ are obtained from a system identification study which is based on frequency and amplitude sweeps of the motion demand signals. The system's response is captured using inertial measurement units and the measurement and transfer delay is identified and compensated post hoc. This procedure is not conducted at the third party driving simulator $\mathrm{DiLS_{THRD}}$. Therefore, the transfer characteristics are estimated using the motion demands from normal simulator operation and the respective measurements of an inertial measurement unit directly. As a result, the characteristics of $\mathrm{DiLS_{THRD}}$ are considered as an approximation whereas the characteristics of $\mathrm{DiLS_{BMW}}$ are identified robustly.

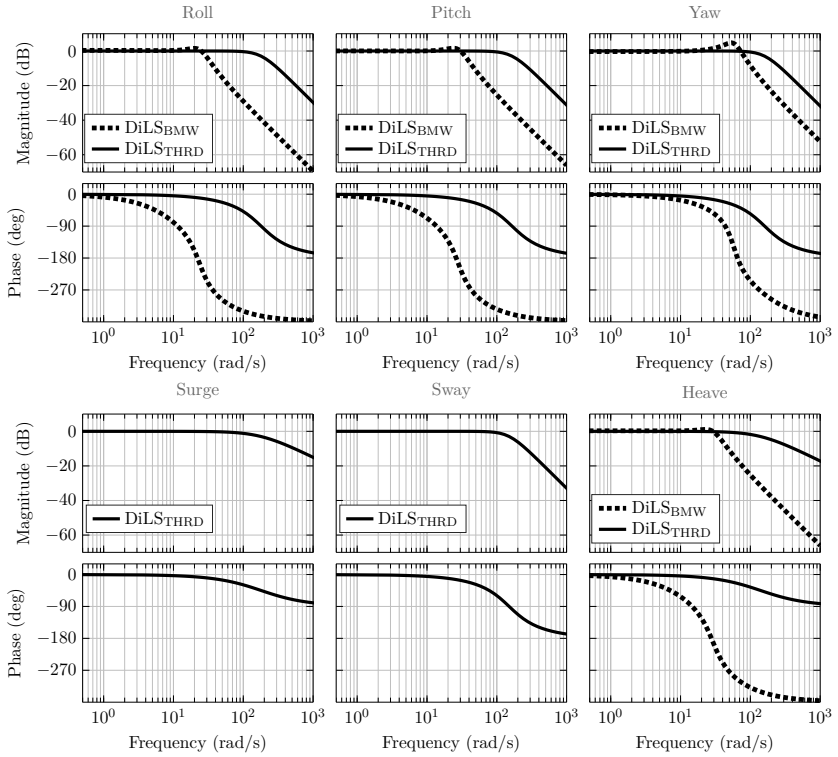

Figure A.4.: Comparison of $\mathrm{DiLS_{BMW}}$ and $\mathrm{DiLS_{THRD}}$ frequency response characteristics for each degree of freedom individually.

A.4. Technical Specifications of the Joysys ChronoCord Device

TECHNISCHE DATEN

Typenbezeichnung:	ChronoCord
Betriebsart:	Dauerbetrieb
Schutzart	Batteriebetrieb
Betriebsdauer	typ. 60h (mind. 40h)
Anwendungsteil	Typ BF, von Erde isoliert
Speichermedium	ChronoCord Micro-SD Karte 4 GB
Interne Abtastrate zur Berechnung der Herzratenvariabilität	8000 Samples pro Sekunde
Speicherrate EKG	In Schritten einstellbar bis 8000 Samples pro Sekunde
Elektroden	Ag/AgCl Elektroden mit Standard Druckknopf-Anschlüssen gemäß ANSI / AAMI Standard EC 12

Umweltbedingungen

Betrieb:	
Umgebungstemperatur	0 ... +45 °C
Feuchtigkeit	Max. 95% rH nicht kondensierend
Transport:	
Umgebungstemperatur	-20 ... +60 °C
Feuchtigkeit	Max. 95% rH nicht kondensierend
Lagerung:	
Umgebungstemperatur	-20 ... +60 °C
Feuchtigkeit	Max. 95% rH nicht kondensierend

Abmessungen, Gewicht

Länge x Breite x Höhe:	71 x 56 x 18 mm
Gewicht (ohne Batterie):	ca. 60g

KONTAKT / IMPRESSUM

Hersteller, Inverkehrbringer und Herausgeber	Human Research Institut für Gesundheitstechnologie und Präventionsforschung GmbH Franz-Pichler-Straße 30 A-8160 Weiz Geschäftsführer: ao.Univ.-Prof. Dr. Maximilian Moser Internet: www.humanesearch.at e-mail: office@humanresearch.at Tel: +43 (0) 3172 44111-0
Technischer Service:	Human Research Service Center e-mail: office@humanresearch.at Tel: +43 (0) 3172 44111-20

21

Figure A.5.: Technical specifications of the Joysys ChronoCord device.